

**Characterization and Control of Quantum Dynamics:  
Computational Methodology Developments and NMR Demonstrations**

विद्या वाचस्पति की  
उपाधि की अपेक्षाओं की आंशिक पूर्ति में प्रस्तुत शोध प्रबंध

A thesis submitted in partial fulfillment of the requirements of the degree of Doctor of  
Philosophy

द्वारा / By  
प्रिया बत्रा/  
Priya Batra

पंजीकरण सं. / Registration No.:  
20162032

शोध प्रबंध पर्यवेक्षक / Thesis Supervisor:  
प्रो. टी एस महेश/  
Prof. T S Mahesh



भारतीय विज्ञान शिक्षा एवं अनुसंधान संस्थान पुणे  
INDIAN INSTITUTE OF SCIENCE EDUCATION AND RESEARCH PUNE

2023



# Certificate

---

Certified that the work incorporated in the thesis entitled “**Characterization and Control of Quantum Dynamics: Computational Methodology Developments and NMR Demonstrations**” submitted by **Priya Batra** was carried out by the candidate, under my supervision. The work presented here or any part of it has not been included in any other thesis submitted previously for the award of any degree or diploma from any other university or institution.

Date: January 12, 2024



Prof. T.S. Mahesh

(Supervisor)



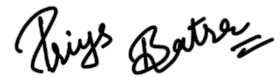


# Declaration

---

I declare that this written submission represents my ideas in my own words and where others ideas have been included, I have adequately cited and referenced the original sources. I also declare that I have adhered to all principles of academic honesty and integrity and have not misrepresented or fabricated or falsified any idea/data/fact/source in my submission. I understand that violation of the above will be cause for disciplinary action by the Institute and can also evoke penal action from the sources which have thus not been properly cited or from whom proper permission has not been taken when needed.

Date: January 12, 2024



Priya Batra  
(20162032)



*To my grandparents*



# Acknowledgments

---

In life, the only constant is change. As a student in the integrated PhD program, I spent some of the prime years of my life at IISER. My experiences at IISER brought about significant transformations, both positive and negative. However, a bunch of people stayed with me through thick and thin, laughed with me on good days and provided solace during the bad ones. I'm truly grateful to all of them.

Foremost among those to whom I owe gratitude is my supervisor, Prof. T S Mahesh. This thesis would not have reached completion without his unwavering support, extensive knowledge, and even his occasional touch of sarcasm. There is much to be gleaned from his approach, and I aspire to embody the same calmness he consistently exudes. Prof. Mahesh adeptly demonstrated the art of balancing work and personal life, offering clever insights into coding and displaying a thorough understanding of the subject that made collaboration with him all the more enjoyable. His anecdotes, ranging from travels to personal experiences and mythologies, were not only insightful but are memories I will forever cherish.

I extend my appreciation to my RAC members, Prof. Santhanam and Dr. Sreejith, for their patient evaluation of my research and consistent provision of valuable suggestions. Prof. Santhanam's kindness and Dr. Sreejith's dedication served as a perpetual source of inspiration.

As an IPhD student, I completed my coursework at IISER. A Hindi medium girl stepping out to explore the world, I encountered professors who significantly eased my academic journey. In particular, I extend my sincere thanks to Suneeta vardharajan for one of the best course at IISER, Prof. Deepak Dhar for always being available and motivating us to excel.

The journey through the PhD process was lengthy and involved substantial paperwork. I am thankful for the support of the physics office team, Prabhakar sir and Dhanashree mam, who were always willing to simplify tasks and assist with the workload. Their random smiles throughout the day created a comforting environment. My gratitude also extends to Sayalee Damle, Ranjan Sahu, and Tushar sir from academics for their support during this journey. Additionally, I appreciate the efforts of the housekeeping staff at IISER Pune, whose generosity in assisting us did not go

unnoticed. My special thanks to CCD and MDP for providing the daily dose to all tired faces.

A significant portion of my PhD journey unfolded within the confines of my office space. I owe a debt of gratitude to both my past and present labmates who shared in this expedition with me. These individuals provided not just a workspace but a sanctuary for camaraderie, especially during our "chai pe charcha" or tea time discussions, where connections were forged. Deepak, with his coding expertise and patient ear, was a constant support, attentively listening to all my challenges. Soham, my collaborator and a reliable academic confidant, Krithika, the epitome of kindness and my go-to person for both personal and professional sharing, and my cricket-mate with whom I shared much more, all hold a special place in my heart. Dr. Rupak, Jitendra, Arijit, Harshant, Conan, and Deepesh, I express my gratitude for your companionship and our discussions spanning topics from quantum information to philosophy. Guiding Abhinav during his semester project was a delightful experience, adding a layer of joy to our discussions. I thank Vishal and Hari for providing me the companionship in the lab in the later years of my PhD. To each one of you, thank you sincerely.

I owe immense gratitude to my friends and family, and though the list is extensive, I appreciate your patience. Throughout this journey, I forged numerous friendships and connections. Special thanks to my IPhD'16 batchmates, Diptabrata Paul, Debarshi Mitra, and Akash Mukherjee. The camaraderie forged in our small batch made every experience, from late-night assignments and gossip sessions to discussions on various aspects of life, truly enjoyable. Unexpectedly, I found a vibrant community in the BS-MS group – Danish, Anwesh, Vrushali, Yogesh, Shravya, Steenu, Poornima, Sayan, Wadikur, Bhaskar, Nishant, and Shruthi – who welcomed me into their lives with genuine warmth, blurring the lines between PhD and BS-MS.

As I got to know the PhD'17 and IPhD'17 batches, Sneha emerged as a cherished friend who introduced me to a wonderful group of individuals. I never had to think twice before telling her anything. My tea partner, Korean food and drama explorer and the best person to discuss life. Sarvottam, a chatterbox always laughing on his not so funny jokes; Anupam, my own piece of comfort; Vrinda, a kind-hearted and fellow explorer; Gokul, a bond that only words can describe with his bad Hindi; Sushant, a motivator and party partner; Navita, Chetna, Umashankar, Pranav, all of them welcomed me with open hearts. Returning to campus during the pandemic was challenging, and everything felt grim. However, my coincidental conversation with Rayan

helped me get back on track. He stayed there, motivated me, shared the best music, made the best pasta and taught me to work hard while enjoying life. As time progressed, I got a chance to reintroduce with Saurabh (whom we all fondly call ‘Pants’ or ‘Pant’), a friend who never shied away from helping me, consoling me, laughing with me, watching movies with me, making the best breakfast, and accompanying me on all outings or usual dinners; he made my IISER life possible in the hardest of times. He has been a friend that everyone deserves to have. His company introduced me to Dhruv and Lovleen. I’m thankful to them for all the small talk, laughs, get-together and good times. During my time in the department, I met Sakil, who also kept me company during random events of daily life. My neighbours, Akanksha, Pragati and Pooja, became my friends in the later years of my PhD. They made my hostel life homely, and it felt like a warm hug. Especially Pooja, she became my lunch partner, my go-to person to talk and a friend that I always want to keep by my side.

Some of my friends who weren’t in IISER also helped me keep afloat. Priyanka, my childhood friend and gossip partner, was always there. I enjoyed all the long conversations with my college friends Mahaveer Thalor, Mohit Mudgal, and Jitesh.

One thing that I always missed in IISER was good food after having mess food. However, some people made sure to have the scrumptious homemade food. First, Anuradha Aunty, thanks to Danish for introducing me to her, who invited me for numerous lunches and dinners and fed me the best food. I can’t thank her enough for making me feel at home whenever I meet her. She has been so kind and loving towards me. Another person who always sent her homemade snacks and sweets was Vani Mam. Her dosas and vadas were yum; every festival was incomplete without her food. I thank her for all the delectable eats.

It would not have been possible without the support of my family. First and foremost, my parents have always been so proud of me and motivated me to continue. I can not thank my other parents, ‘Badi maa’ and ‘Bade Papa’, who always had my back. Growing up in a joint family and receiving love and care in various forms shaped me into the human being I am today. I always enjoyed my cousins’ laughs and love towards me, my stress busters, and everything. I am grateful to find friends in my family. The smiles of younger nephews and nieces and the bad sense of humor of elder ones always kept me going. I couldn’t have survived COVID without their video call every night. Last but not least, I couldn’t be more grateful to have my siblings,

Riya and Samir, by my side. Even though they are younger than me, they understand me truly. They made me laugh during my bad times and even more during good times. I reconnected with them during COVID, and I should thank the universe for that. They are my confidante, money-spenders, and the best part of my life.

Some non-person objects were also handy during the completion of my PhD. First, the funding from PMRF enabled me to live a comfortable life without worrying about any financial constraints. It helped me in visiting the conferences and workshops in India and abroad. Secondly, K-Dramas and P-Dramas might sound absurd, but they helped me stay afloat. I always went back to them whenever I felt low. Above all, this thesis would only have taken this shape with the help of IISER Pune. I'm grateful for providing such a diverse environment, fun and kind people, all the essential facilities and a safe environment. I developed myself in every way possible here in past years, truly and wholeheartedly. Thank you to All!

With all the gratitude,

Priya



# Abstract

---

Characterization and control in quantum dynamics are paramount for the emerging field of quantum technologies. In the realm of quantum mechanics, the Schrödinger equation or Von-Neumann equation governs quantum evolution. However, efficiently characterizing the final state and determining external parameters or controls remains challenging, necessitating the development of advanced computational methodologies. This thesis focuses on developing and demonstrating innovative computational approaches for efficient characterization and control of quantum dynamics. The first key aspect involves the application of a machine-learning algorithm known as the recommender system (RS). In this context, RS is utilized to estimate changes in quantum correlations following unitary or nonunitary evolution. Remarkably, RS demonstrates the capability to estimate quantities that are challenging to compute or lack analytical expressions. The subsequent discussion revolves around three distinct developments within the control framework and their demonstration using Nuclear Magnetic Resonance (NMR) experiments. Firstly, the thesis delves into RS-expedited quantum control optimization, where the machine learning algorithm efficiently populates a sparse table of quantum controls. Secondly, the concept of ‘push-pull quantum control’ is introduced, leveraging a target operator alongside a set of orthogonal operators to generate robust control sequences effectively. Lastly, implementing a Physics-informed neural network for solving the time-dependent Schrödinger equation is explained, highlighting its advantages, particularly avoiding prior discretization of the parameter space. These methodologies are demonstrated to be versatile and applicable across different physical hardware, signifying their crucial role in the unfolding landscape of quantum technologies.



# Synopsis

---

In this thesis, we report the advancement of computational methods and their NMR demonstrations for the characterization and control of quantum dynamics. The thesis is divided into six chapters, each briefly reviewed below.

## **Chapter 1 – Introduction**

This chapter introduces the basic terminology and concepts of quantum information processing, starting from qubits, dynamics, measurements and correlations. We then explain the experimental quantum information by giving an overview of the NMR test bed and its usage for quantum information processing. We then describe quantum control and summarize some famous quantum control algorithms. We conclude this chapter with the primitive ideas of machine learning and unfold the workings of a neural network.

## **Chapter 2 – Efficient Characterization of Quantum Evolutions via a Recommender System**

Characterization of a quantum system is important to infer any information about the dynamics. It can be done using the correlations or fidelity of the final state. However, it becomes difficult to calculate quantum correlations, especially discord, which has no analytical expression. This chapter uses a machine learning algorithm recommender system to characterize the dynamics. Here, we choose (i) quantum correlations quantified by measures such as entropy, negativity, or discord and (ii) state-fidelity. Using quantum registers with up to 10 qubits, we demonstrate that an RS can efficiently characterize unitary and non-unitary evolutions. After conducting a detailed performance analysis of the RS in two qubits, we show that it can distinguish a clean database of quantum correlations from a noisy or a fake one. Moreover, we find that the RS brings a significant computational advantage for building a large database of quantum discord, for which no simple closed-form expression exists. Also, RS can efficiently characterize systems undergoing non-unitary evolutions in terms of quantum discord reduction and state fidelity. Finally, we utilize RS to construct discord phase space in a nonlinear quantum system.

### **Chapter 3 – Recommender System Expedited Quantum Control Optimization**

In this chapter, we extend the use of RS to speed up the quantum control protocol. In the quantum control problem, each iteration of a numerical optimization algorithm typically involves evaluating many parameters, such as gradients or fidelities, which can be tabulated as a rating matrix. We establish that RS can rapidly and accurately predict elements of such a sparse rating matrix. Using this approach, we expedite a gradient ascent-based quantum control optimization, namely GRAPE, and demonstrate the faster construction of a two-qubit CNOT gate in registers with up to 8 qubits. We also describe and implement the enhancement of the computational speed of a hybrid algorithm involving simulated annealing and gradient ascent. Moreover, the faster construction of three-qubit Toffoli gates further confirmed the applicability of RS in larger registers.

### **Chapter 4 – Push-Pull Optimization of Quantum Controls**

The convergence of control algorithms is a quintessential feature for better quantum gates. In this chapter, we propose an objective function that incorporates not only the target operator but also a set of its orthogonal operators, whose combined influences lead to an efficient exploration of the parameter space, faster convergence, and extraction of superior solutions. As we call it, the *push-pull* optimization can be adopted in various quantum control scenarios. We describe adopting it to a gradient-based and a variational principle-based approaches. Numerical analysis of quantum registers with up to seven qubits reveals significant benefits of push-pull optimization. Finally, we describe applying the push-pull optimization to prepare a long-lived singlet-order in a two-qubit system using NMR techniques.

### **Chapter 5 – Physics Informed Neural Network for Robust Quantum Controls**

Machine learning is becoming increasingly integral across various domains. In this context, we present a novel approach utilizing a Physics Informed Neural Network for constructing quantum gates. Our focus is on creating a two-qubit CNOT gate and a protocol for state-to-state transfer, specifically designing a pulse to prepare a long-lived singlet state (LLS). These sequences are implemented on Nuclear Magnetic Resonance (NMR) platforms to assess the effectiveness of the algorithm. On the other hand, the significance of geometric quantum computation lies in

its inherent robustness against certain types of parameter noise. Therefore, it becomes imperative to devise innovative algorithms for generating geometric quantum gates applicable to diverse quantum platforms. Our study highlights the robust nature of the one-qubit phase gate when compared to the conventional hard pulse approach. This comparison sheds light on the algorithm's resilience, a critical aspect for the development of practical quantum computing solutions.



# List of Publications

---

1. Deepesh Khushwani, **Priya Batra**, VR Krithika, and T. S. Mahesh, *Selective Wigner phase space tomography and its application for studying quantum chaos*, [arXiv:2310.08307](https://arxiv.org/abs/2310.08307).
2. Abhinav Suresh, Vishal Varma, **Priya Batra**, and T. S. Mahesh, *Counterdiabatic driving for long-lived singlet state preparation*, [The Journal of Chemical Physics](https://doi.org/10.1063/1.5071070), 159(2):024202, 07 (2023).
3. **Priya Batra** and M. Harshanth Ram and T.S. Mahesh, *Recommender system expedited quantum control optimization*, [Physics Open](https://doi.org/10.1063/1.5071070), page 100127, 2022 [Chapter 3].
4. TS Mahesh, **Priya Batra**, and M Harshanth Ram, *Quantum optimal control: Practical aspects and diverse methods*, [Journal of the Indian Institute of Science](https://doi.org/10.1063/1.5071070), pages 1-17, 2022.
5. M. Harshanth Ram, V. R. Krithika, **Priya Batra**, and T. S. Mahesh, *Robust Quantum Control using Hybrid Pulse Engineering*, [Phys. Rev. A](https://doi.org/10.1103/PhysRevA.105.042437) 105, 042437 (2022).
6. **Priya Batra**, Anukriti Singh, and T. S. Mahesh, *Efficient Characterization of Quantum Evolutions via a Recommender System*, [Quantum](https://doi.org/10.1103/PhysRevX.5.051044), 5, 598 (2021) [Chapter 2].
7. Soham Pal, **Priya Batra**, Tanjung Krisnanda, Tomasz Paterek, and T. S. Mahesh, *Experimental localisation of quantum entanglement through monitored classical mediator*, [Quantum](https://doi.org/10.1103/PhysRevX.5.041044), 5, 478 2021.
8. **Priya Batra**, V. R. Krithika, and T. S. Mahesh, *Push-Pull Optimization of Quantum Controls*, [Phys. Rev. Research](https://doi.org/10.1103/PhysRevResearch.2.013314) 2, 013314 (2020) [Chapter 4].





# Contents

<b>Certificate</b>	<b>i</b>
<b>Declaration</b>	<b>iii</b>
<b>Acknowledgments</b>	<b>vii</b>
<b>Abstract</b>	<b>xi</b>
<b>Synopsis</b>	<b>xiii</b>
<b>List of Publications</b>	<b>xvii</b>
<b>1 Introduction</b>	<b>1</b>
1.1 Quantum Information . . . . .	2
1.1.1 Qubit . . . . .	3
1.1.2 Density matrix . . . . .	4
1.1.3 Quantum dynamics . . . . .	5
1.1.4 Open Quantum System . . . . .	6
1.1.5 Quantum Gates . . . . .	8
1.1.6 Quantum measurement . . . . .	9
1.1.7 Quantum Correlations . . . . .	10
1.1.7.1 Entanglement . . . . .	11
1.1.7.2 Discord . . . . .	14
1.1.8 Quantum Fidelity . . . . .	15
1.2 Experimental Quantum information . . . . .	17

1.2.1	Nuclear magnetic resonance (NMR) test bed . . . . .	18
1.2.1.1	NMR spin . . . . .	18
1.2.1.2	Chemical shift . . . . .	19
1.2.1.3	Interacting spins . . . . .	20
1.2.1.4	Spin manipulation . . . . .	22
1.2.1.5	Relaxation . . . . .	23
1.2.2	NMR quantum information processing . . . . .	25
1.2.2.1	Quantum gates . . . . .	25
1.2.2.2	State initialization . . . . .	28
1.2.2.3	Measurement . . . . .	28
1.2.2.4	Decoherence time . . . . .	29
1.3	Quantum Control . . . . .	29
1.3.1	Quantum optimal control theory (QOCT) . . . . .	31
1.3.2	Quantum control algorithms . . . . .	34
1.4	Machine learning . . . . .	36
1.5	Characterization and control of quantum dynamics . . . . .	40
<b>2</b>	<b>Efficient Characterization of Quantum Evolutions via a Recommender System</b>	<b>43</b>
2.1	Introduction . . . . .	43
2.1.1	Objectives . . . . .	44
2.2	Recommender system via matrix factorization . . . . .	45
2.3	Adapting the recommender system . . . . .	47
2.4	Rating unitary evolutions . . . . .	50
2.4.1	Rating the Werner state . . . . .	50
2.4.2	Dependence on the dimensions of database and latent vector . . . . .	51
2.4.3	Identifying noisy database . . . . .	53
2.4.4	Computational Time . . . . .	54
2.4.5	Predicting state fidelity . . . . .	55
2.4.6	Identifying local and nonlocal operators: . . . . .	55
2.4.7	Scaling to larger registers . . . . .	57
2.5	Rating nonunitary evolutions . . . . .	57

2.6	Construction of quantum phase space . . . . .	60
2.7	Summary and outlook . . . . .	62
<b>3</b>	<b>Recommender System Expedited Quantum Control Optimization</b>	<b>65</b>
3.1	Introduction . . . . .	66
3.1.1	Objectives . . . . .	67
3.2	Quantum Control Optimization . . . . .	68
3.2.1	Gradient Ascent Pulse Engineering (GRAPE) . . . . .	69
3.2.2	Simulated Annealing (SA) . . . . .	70
3.3	Recommender System (RS) . . . . .	71
3.4	RS enhanced GRAPE and SAGRAPE . . . . .	73
3.4.1	RS expedited GRAPE (RSGRAPE) . . . . .	74
3.4.2	RS expedited SAGRAPE (RSSAGRAPE) . . . . .	78
3.5	Summary and outlook . . . . .	82
<b>4</b>	<b>Push-Pull Optimization of Quantum Controls</b>	<b>85</b>
4.1	Introduction . . . . .	85
4.1.1	Objectives . . . . .	86
4.2	The optimization problem . . . . .	86
4.2.1	GRAPE optimization . . . . .	88
4.2.2	Krotov optimization . . . . .	89
4.3	Numerical analysis . . . . .	90
4.3.1	Rapid parameter search in push-pull approach . . . . .	93
4.3.2	Push-weight . . . . .	93
4.4	NMR experiments . . . . .	94
4.5	Summary and outlook . . . . .	97
<b>5</b>	<b>Physics-Informed Neural Network for Robust Quantum Control</b>	<b>99</b>
5.1	Introduction . . . . .	99
5.1.1	Objectives . . . . .	101
5.2	Physics-informed neural networks (PINNs) . . . . .	101
5.3	State to state transfer . . . . .	103

5.3.1	Preparation of long-lived singlet state in NMR . . . . .	104
5.3.2	Effect of noise on singlet state preparation . . . . .	106
5.3.3	Unitary synthesis . . . . .	107
5.4	Geometric quantum gates . . . . .	109
5.5	Summary and outlook . . . . .	111
	<b>Thesis Summary</b>	<b>116</b>
	<b>References</b>	<b>118</b>

# CHAPTER 1

---

## Introduction

---

**To feel absolutely right is the beginning of the end** – *Albert Camus*

The allure of science lies in its ability to unveil the mysteries that enshroud our immediate surroundings and the distant realms of the cosmos. Physicists have pioneered tools to learn about atoms as well as stars. As Galileo articulates, “All truths are easy to understand once they are discovered; the point is to discover them”. The development of quantitative laws, coupled with experimental findings, led to the emergence of Physics as a distinct subject, showcasing a rich history marked by remarkable progress. Newton’s discovery of laws of classical mechanics [1] has an impact even in the modern world centuries later. However, Newton’s law could not explain systems with extreme conditions, such as particles moving with the speed of light, length scales comparable to atomic radius or smaller and high energy systems. Einstein’s “Theory of Special Relativity” explained the dynamics of particles moving near the speed of light [2], and quantum mechanics became the basis for understanding the atomic and subatomic particles giving rise to Modern Physics. Today, the framework of quantum mechanics is an integral part of numerous sub-branches of physics. Some of the hallmarks of early quantum mechanics include explanation of black-body radiation [3], photoelectric effect [4], Bohr’s hydrogen atom model [5], and Stern-Gerlach experiment [6–8]. In 1923, Louis de Broglie introduced the principle of wave-particle duality, according to which a particle can have particle and wave behavior [9]. The further advances unfolded with the mathematical formulation of quantum mechanics, which encompasses *Matrix Mechanics* by Werner Heisenberg, Max Born and Pascual Jordan [10] and *Wave Mechanics* by Erwin Schrödinger [11]. It was additionally interpreted or understood in light of the contributions of David Hilbert, Paul Dirac, and John von Neumann. Following the success of quantum mechanics, its impact extended to various scientific disciplines, including information science, chemistry, and others. As information science and quantum mechanics started coming together, it gave rise

to whole new field of quantum information and computation [12]. It started to progress with the work of Bell on entanglement [13], concept of quantum Turing machine by David Duestch [14] and later the development of Shor's [15] and Grover's [16] algorithm paved a way to build quantum algorithms for quantum advantage. Schrödinger's equation or Von-Neumann equation has been the governing dynamical equations for quantum system. Thus, the primary focus of this thesis revolves around understanding some of the key aspects such as characterization and control of quantum dynamics, an important paradigm of quantum information. The thesis commences by elucidating the fundamental concepts of quantum information and computation in the following section.

## 1.1 Quantum Information

Information, the amount of surprise, is an abstract concept. Information theory makes beautiful use of this abstractness to study its quantification, storage and communication [17]. In the realm of classical information processing, transistors have laid the foundation for practical realizations [18]. With the discovery of transistors, classical computers became powerful, making information storage and processing easier. In the classical case, the basic unit of information is called *bit*, which possesses binary values such as 0 or 1. Classical computers manipulate these bits and produce outputs in the form of bits as well. Despite the remarkable success of classical computers, certain problems remained unsolvable within their computational framework. In 1981, when Richard Feynman stated, "Nature isn't classical, dammit, and if you want to make a simulation of nature, you'd better make it quantum mechanical, and by golly it's a wonderful problem, because it doesn't look so easy" prompted people to seriously think about the possibility of quantum systems and their processing on a quantum level [19]. This incited the whole field of *quantum information processing (QIP)*, which is today not only limited to simulations but expands to computation, communication, sensing, and more. It has gained massive success over the last 2-3 decades, with tech giants investing a hefty sum for building a quantum computer [20–22]. Now, we proceed to delineate the basic terminology employed in quantum information processing.

### 1.1.1 Qubit

Quantum bit or *qubit* is the fundamental unit of information in quantum mechanics. Unlike bits, qubits can have values 0 and 1 simultaneously with certain probabilities owing to the rule of superposition in quantum mechanics. The state of a qubit, also called the wave vector of a quantum particle, represented with a column vector is given by

$$|\psi\rangle = \alpha |0\rangle + \beta |1\rangle. \quad (1.1)$$

Here  $\alpha$  and  $\beta$  are complex number with identity  $|\alpha|^2 + |\beta|^2 = 1$ .  $|\alpha|^2$  and  $|\beta|^2$  are called the probabilities of being in state  $|0\rangle$  and  $|1\rangle$  respectively. The adjoint of state  $|\psi\rangle$  is a row vector  $\langle\psi| = \alpha^* \langle 0| + \beta^* \langle 1|$  where  $\alpha^*$  and  $\beta^*$  are the complex conjugate of  $\alpha$  and  $\beta$ . In the lexicon of quantum mechanics,  $|\psi\rangle$  and  $\langle\psi|$  are called ket and bra vector, respectively.

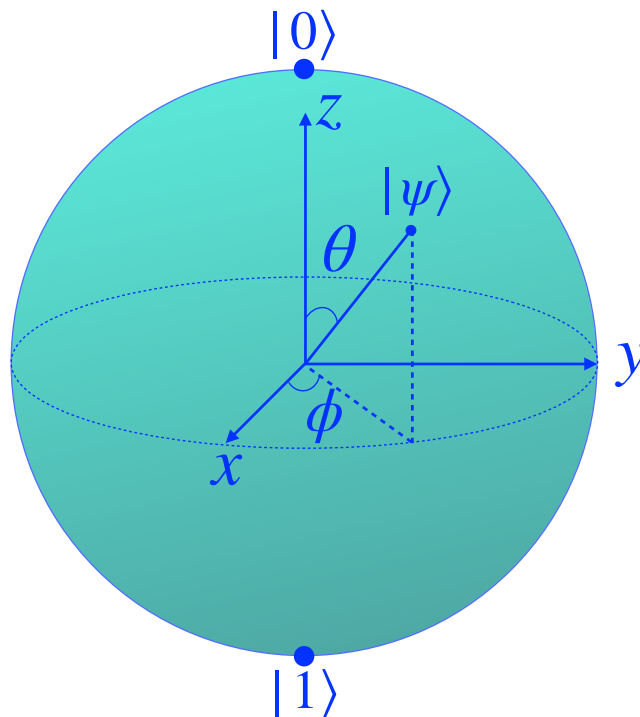


**Figure 1.1:** Qubit representation on a 3D Bloch sphere

Geometrically, a qubit state is depicted as a vector on a 3D Bloch sphere, as shown in fig. 1.1. A general state on a Bloch sphere is written using polar angle  $\theta$  and azimuthal angle  $\phi$  as

$$|\psi\rangle = \cos\frac{\theta}{2}|0\rangle + e^{i\phi}\sin\frac{\theta}{2}|1\rangle. \quad (1.2)$$

The point on the north pole with  $\theta = 0^\circ$  is assigned to the  $|0\rangle$  state while point on the south pole with  $\theta = 180^\circ$  is assigned to the  $|1\rangle$  state. The point on  $x$ -axis with  $\theta = 90^\circ$  and  $\phi = 0^\circ$  represents the superposition state  $\frac{|0\rangle+|1\rangle}{\sqrt{2}}$ .

Physically, a qubit can be realized in a two-level system. Here,  $|0\rangle$  and  $|1\rangle$  represent the ground and excited state of the two-level system, respectively. There are multiple candidates for the physical realization of the two-level system, for example, nuclear spins in nuclear magnetic resonance [23], electron spins in defect centers and quantum dots [24, 25], hyperfine levels in trapped ions [26], charge, current or energy in cooper pairs of superconductors [27], the polarization of light in Photonic setup [28], Rydberg atoms [29], etc.

## 1.1.2 Density matrix

A density matrix is a more general way of describing the state of a quantum system. The wave function approach is suitable for a pure state but inadequate for a mixed state. The density matrix of a general state is given by

$$\rho = \sum_{i=1}^m p_i |\psi_i\rangle \langle \psi_i|,$$

with probability  $p_i$  of being in state  $|\psi_i\rangle$ . The density matrix's diagonal and off-diagonal elements are called populations and coherences, respectively. It satisfies the following properties:

- $\rho$  is a Hermitian matrix, i.e.  $\rho^\dagger = \rho$ .
- Since probabilities must be normalized, i.e.  $\text{Tr}[\rho] = 1$ .
- $\rho$  is a positive semi-definite matrix, i.e. all eigenvalues are non-negative.

The states can be classified as either pure or mixed depending on the following features:



<p>Pure state</p> <ul style="list-style-type: none"> <li>• <math>m = 1, \rho =  \psi_1\rangle \langle \psi_1 </math></li> <li>• Purity, <math>\text{Tr} [\rho^2] = 1</math></li> <li>• Idempotent, <math>\rho = \rho^2</math></li> <li>• Lies on the surface of Bloch sphere</li> </ul>	<p>Mixed state</p> <p><math>m &gt; 1, \rho = \sum_{i=1}^m p_i  \psi_i\rangle \langle \psi_i </math></p> <p><math>\text{Tr} [\rho^2] &lt; 1</math></p> <p><math>\rho \neq \rho^2</math></p> <p>Lies inside Bloch sphere</p>
---	--

### 1.1.3 Quantum dynamics

According to Schrödinger equation, the Hamiltonian operator  $H$  controls the dynamics of a quantum state. The expectation value of  $H$  quantifies the total energy of a quantum mechanical system. Like classical mechanics, Hamiltonian has two terms, one corresponding to kinetic energy and the other to potential energy. For a general system, Hamiltonian  $H$  takes the following form

$$H = \frac{P^2}{2m} + V, \quad (1.3)$$

where  $P$  is the momentum operator,  $V$  is the potential term, and  $m$  is the mass of particle. The given Hamiltonian governs the dynamics of particle in the potential  $V$ . The evolution of a pure quantum state  $|\psi(t)\rangle$  under time-dependent Hamiltonian  $H(t)$  in a closed system is governed by Schrödinger equation

$$\frac{d|\psi(t)\rangle}{dt} = -\frac{i}{\hbar} H(t) |\psi(t)\rangle. \quad (1.4)$$

The solution of the above equation in a time interval of 0 and T is given by

$$U(T) = \mathcal{T} \exp \left( \int_0^T -\frac{i}{\hbar} H(t) dt \right), \quad (1.5)$$

where  $\mathcal{T}$  stands for Dyson time ordering operator. The Schrödinger equation can alternatively be expressed in the Heisenberg picture as the evolution of the unitary operator  $U(t)$

$$\frac{dU(t)}{dt} = -\frac{i}{\hbar} H(t) U(t). \quad (1.6)$$

The alternative way of depicting the quantum evolution of a general quantum state with density matrix  $\rho(t)$  in a closed system is given by the Liouville-von Neumann equation

$$\frac{d\rho(t)}{dt} = -\frac{i}{\hbar} [H(t), \rho(t)]. \quad (1.7)$$

### 1.1.4 Open Quantum System

In practical situations, no system is ideal and constantly interacts with its surroundings. For an open system, the total Hamiltonian  $H$  can be expressed as the sum of the system Hamiltonian  $H_S$ , bath Hamiltonian  $H_B$  and system-bath interaction  $H_{SB}$  [30, 31]

$$H = H_S + H_B + H_{SB}. \quad (1.8)$$

The evolution of total density matrix  $\rho(t)$  under the Hamiltonian  $H$  is given as

$$\rho(t) = U(t) \rho(0) U^\dagger(t), \quad (1.9)$$

with unitary operator of the form  $U(t) = e^{-iHt}$ . The bath operator at the initial time with the eigenvalues  $\lambda_\alpha$  and orthonormal basis vectors  $\{|\alpha\rangle\}$  can be decomposed as

$$\rho_B(0) = \sum_{\alpha} \lambda_{\alpha} |\alpha\rangle \langle\alpha|. \quad (1.10)$$

The system density matrix can be obtained by partially tracing the total density matrix  $\rho(t)$  over bath degrees of freedom

$$\begin{aligned} \rho_S(t) &= \text{Tr}_B [\rho(t)] \\ \rho_S(t) &= \text{Tr}_B [U(t) \rho(0) U^\dagger(t)] \\ \rho_S(t) &= \sum_{\beta} \langle\beta| U(t) \rho(0) U^\dagger(t) |\beta\rangle, \end{aligned} \quad (1.11)$$

where  $|\beta\rangle$  are the eigenvectors for bath operator. Starting with the assumption that system and bath are uncorrelated at initial time, such that

$$\rho(0) = \rho_S(0) \otimes \rho_B(0). \quad (1.12)$$

Based on the above assumption, the system state can be simplified as

$$\begin{aligned} \rho_S(t) &= \sum_{\beta} \langle \beta | U(t) (\rho_S(0) \otimes \rho_B(0)) U^\dagger(t) | \beta \rangle \\ \rho_S(t) &= \sum_{\beta} \langle \beta | U(t) (\rho_S(0) \otimes \sum_{\alpha} \lambda_{\alpha} |\alpha\rangle \langle \alpha|) U^\dagger(t) | \beta \rangle \\ \rho_S(t) &= \sum_{\beta \alpha} (\sqrt{\lambda_{\alpha}} \langle \beta | U(t) |\alpha\rangle_B) \rho_S(0) (\sqrt{\lambda_{\alpha}} \langle \alpha | U^\dagger(t) | \beta \rangle_B) \\ \rho_S(t) &= \sum_{\beta \alpha} K_{\beta\alpha}(t) \rho_S(0) K_{\beta\alpha}^\dagger(t). \end{aligned} \quad (1.13)$$

Here  $\{K_{\beta\alpha}\}$  are called Kraus operators having the following form

$$K_{\beta\alpha}(t) = \sqrt{\lambda_{\alpha}} \langle \beta | U(t) |\alpha\rangle_B. \quad (1.14)$$

The equation 1.13 is called the Kraus operator-sum representation for the evolution of the system density matrix. Kraus operators follow the condition

$$\sum_{\beta \alpha} K_{\beta\alpha}^\dagger(t) K_{\beta\alpha}(t) = \mathbb{1}_S \quad (1.15)$$

The alternative way to define the evolution of the system density matrix  $\rho_S(t)$  is given using the Gorini-Kossakowski-Sudarshan-Lindblad (GKSL) equation [32]

$$\frac{d\rho_S(t)}{dt} = -\frac{i}{\hbar} [H_S(t), \rho_S(t)] + \mathcal{L}(\rho_S), \quad (1.16)$$

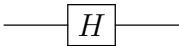
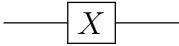
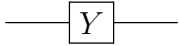


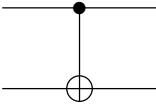
where  $\mathcal{L}$  is called *Lindbladian* operator having the form

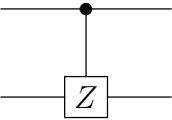
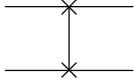
$$\mathcal{L}(\rho_S) = \sum_n \gamma_n \left( V_n \rho_S V_n^\dagger - \frac{1}{2} \left( \rho_S V_n^\dagger V_n + V_n^\dagger V_n \rho_S \right) \right). \quad (1.17)$$

Here  $V_n$  and  $\gamma_n$  represent the jump operators and damping rates for the dissipative part of dynamics.

### 1.1.5 Quantum Gates

Logic gates are an integral part of the circuit model of computation. In classical computers, gates like AND, OR, NOT, etc, are routinely used for processing. These gates together implement a set of instructions for the bits to generate the desired output. Similar to classical computation, various single- and multi-qubit gates operating on qubits constitute quantum circuits. These gates are unitary operators of dimension  $2^n$  where  $n$  is the number of qubits. Some of the basic gates in quantum computation are as follows:

Gate	Circuit representation	Matrix representation
Hadamard		$\frac{1}{\sqrt{2}} \begin{bmatrix} 1 & 1 \\ 1 & -1 \end{bmatrix}$
X Gate		$\begin{bmatrix} 0 & 1 \\ 1 & 0 \end{bmatrix}$
Y gate		$\begin{bmatrix} 0 & -i \\ i & 0 \end{bmatrix}$
Z gate		$\begin{bmatrix} 1 & 0 \\ 0 & -1 \end{bmatrix}$
Phase gate		$\begin{bmatrix} 1 & 0 \\ 0 & e^{i\phi} \end{bmatrix}$
CNOT gate		$\begin{bmatrix} 1 & 0 & 0 & 0 \\ 0 & 1 & 0 & 0 \\ 0 & 0 & 0 & 1 \\ 0 & 0 & 1 & 0 \end{bmatrix}$

CZ gate		$\begin{bmatrix} 1 & 0 & 0 & 0 \\ 0 & 1 & 0 & 0 \\ 0 & 0 & 1 & 0 \\ 0 & 0 & 0 & -1 \end{bmatrix}$
Swap gate		$\begin{bmatrix} 1 & 0 & 0 & 0 \\ 0 & 0 & 1 & 0 \\ 0 & 1 & 0 & 0 \\ 0 & 0 & 0 & 1 \end{bmatrix}$

### 1.1.6 Quantum measurement

The revelation of physical information necessitates a measurement in both classical and quantum systems. In the quantum realm, linear operators defined on the Hilbert space, also called observables, are measurable properties of the physical system. The spectral decomposition of an observable  $A$  is written as [33]

$$A = \sum_n n P_n.$$

Here  $n$  are eigenvalues of observable  $A$  and  $P_n$  are projectors defined onto eigenvectors  $\{a_1, a_2, \dots, a_n\}$  of observable  $A$  as  $P_n = |a_n\rangle \langle a_n|$ . Projectors form a complete set and thus satisfy the identity relation  $\sum_n P_n = 1$ . The measurement probability  $p$  of getting eigenvalue  $n$  for a general state  $|\psi\rangle$  is given by Born rule

$$p(n) = \|P_n |\psi\rangle\|_2 = \langle \psi | P_n | \psi \rangle, \tag{1.18}$$

where the identity for projectors  $P_n^2 = P_n$  has been employed and  $\|A\|_2 \equiv \sqrt{A^\dagger A}$  is the two-norm. Thus, the post-measurement state would be

$$|\psi\rangle \rightarrow \frac{P_n |\psi\rangle}{\|P_n |\psi\rangle\|_2}. \quad (1.19)$$

The expectation value of observable  $A$  is expressed as

$$\langle A \rangle = \sum_n n \langle \psi | P_n | \psi \rangle = \sum_n n p(n).$$

These are also called *Projective measurements*.

However, there is another set of generalized measurements known as *Positive Operator Valued Measure (POVM)*, defined as the decomposition of identity into  $m$  operators, i.e.

$$\sum_m M_m^\dagger M_m = \mathbb{1},$$

where  $M_m$  are called Kraus operators as defined in 1.1.4. The probability  $p(m)$  of getting outcome  $m$  on density matrix  $\rho$  is given as

$$p(m) = \text{Tr}[Q_m \rho],$$

where  $Q_m = M_m^\dagger M_m$ . If  $\rho$  depicts a pure state  $\rho = |\psi\rangle \langle \psi|$  then probability reduces to

$$p(m) = \langle \psi | M_m^\dagger M_m | \psi \rangle,$$

which is equivalent to projective measurement as shown in equation 1.18.

### 1.1.7 Quantum Correlations

When quantum systems interact, information exchange occurs, giving rise to quantum correlations. Physically, the amount of correlations is quantified aiding measurements. The crucial distinction between classical and quantum systems lies in the fact that, ideally, measurements on a classical system do not disturb its state, whereas measurements do disrupt the state of a quantum

system. Quantum coherence, a consequence of quantum superposition, is a necessary condition for the existence of quantum correlations [34, 35]. These quantum correlations serve as valuable resources for a range of quantum technologies [36]. In the subsequent sections, we will delve into the comprehensive description of two fundamental correlations: entanglement and discord.

### 1.1.7.1 Entanglement

Entanglement is the property of two or more quantum particles where the state of one particle can't be described without the knowledge of others. For two parties, Alice (A) and Bob (B), pictorially the entanglement can be shown as fig 1.2. A measurement on any part of the entangled

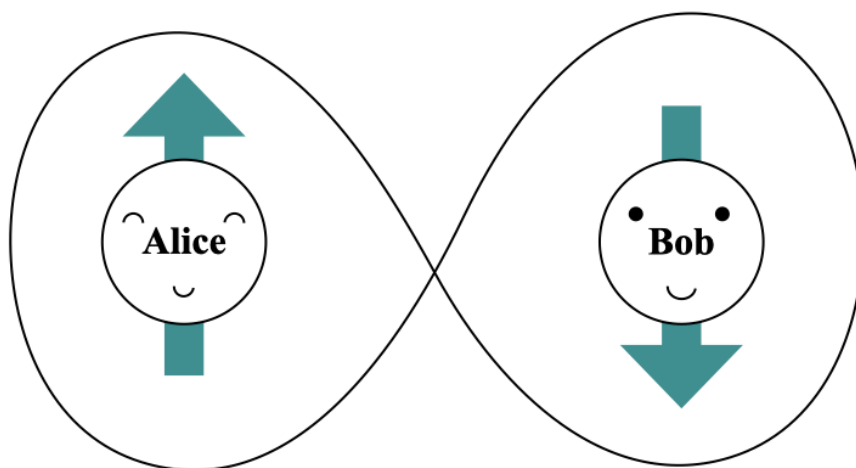


**Figure 1.2:** Pictorial representation of entanglement

state collapses the whole state. Before the formulation of quantum mechanics, it was believed that every physical theory should follow locality, realism and experimenter's free will. However, in 1935, the famous paper of Einstein, Podolsky and Rosen argued that quantum mechanics is an incomplete physical theory as it does not obey local realism [37]. This was famously called the EPR paradox and was troubling physicists for a few decades. EPR paradox was resolved in 1964 with the work of John Bell using a stroke of pen [13]. Bell's theorem proves the maximum amount of correlation that any theory can possess, obeying local realism. Consider a thought

experiment in which A and B, located at a distance, receive one particle each from Charlie (C), who prepares two particles by some means. A and B can perform two possible measurements each for two different physical properties. Let's define the physical properties using operators  $A_0$  or  $A_1$  for A and  $B_0$  or  $B_1$  for B. The measurement outcome for each property is binary, giving value  $+1$  or  $-1$ . Now, A and B make one measurement each. After repeating the experiment a large number of times and by taking the average over trials, the expectation value of observables is given by Bell's inequality

$$\langle A_0 B_0 \rangle + \langle A_0 B_1 \rangle + \langle A_1 B_0 \rangle - \langle A_1 B_1 \rangle \leq 2, \quad (1.20)$$

where the angle bracket denotes the average. Equation 1.20 is also called CHSH inequality [38]. Four famous two-qubit states, called Bell state, show the maximum amount of quantum entanglement. These states are written as

$$\begin{aligned} |\phi^\pm\rangle &= \frac{1}{\sqrt{2}} [ |00\rangle \pm |11\rangle ] \\ |\psi^\pm\rangle &= \frac{1}{\sqrt{2}} [ |01\rangle \pm |10\rangle ]. \end{aligned} \quad (1.21)$$

However, quantum mechanics can violate Bell or CHSH inequality if C prepares the initial state as one of the Bell states shown in equation 1.21. C then passes one qubit to A and another to B where A has Pauli matrices  $\sigma_z$  and  $\sigma_x$  while Bob possess  $-(\sigma_x + \sigma_z)/\sqrt{2}$  and  $(\sigma_x - \sigma_z)/\sqrt{2}$  as two of the possible measurements. After calculating the expectation value for pair of observables as shown in equation 1.20, the equation is modified as

$$\langle A_0 B_0 \rangle + \langle A_0 B_1 \rangle + \langle A_1 B_0 \rangle - \langle A_1 B_1 \rangle = 2\sqrt{2}, \quad (1.22)$$

which exceeds the bound achieved earlier, obeying local realism theory. This is the maximum amount of correlation value for pair of observables, also known as Tsirelson bound [39]. Soon after Bell's paper, John Clauser and Stuart Freedman performed the Bell test in the laboratory [40], which was made more stringent by Alain Aspect and collaborators [41]. Additionally, Anton Zeilinger utilized Bell states to experimentally carry out quantum teleportation [42]. Recently, the trio of Aspect, Clauser, and Zeilinger was awarded the 2022 Nobel Prize in Physics [43, 44].



Despite the theoretical progress, quantifying entanglement has been a non-trivial task for a general quantum state. There have been some successful attempts in the same direction. For a bipartite case, Peres [45] gave the *Positive Partial Transpose (PPT)* criteria according to which a state  $\rho_{AB}$  is separable if the partial transposed matrix  $\rho_{AB}^\Gamma$  is a positive operator. It is a necessary and sufficient condition for the separability of  $2 \otimes 2$  and  $2 \otimes 3$  cases. Some fundamental tools called *entanglement witness* show the separability of quantum states. However, only very few witnesses can measure the amount of entanglement in a quantum state, also called *entanglement measure*. The postulate for a measure was given by Bennett et al. [46] based on local operation and classical communication (LOCC) monotone, according to which, “Entanglement cannot increase under local operations and classical communication.” Here we discuss some entanglement measures for a bipartite case [47]. One of them being entanglement entropy defined for a pure bipartite state  $\rho_{AB}$  as

$$S(\rho_A) = -\text{Tr}[\rho_A \log \rho_A] = -\text{Tr}[\rho_B \log \rho_B] = S(\rho_B), \quad (1.23)$$

where  $\rho_A$  ( $\rho_B$ ) represents the density matrix of subsystem A (B) after partial trace. It is worth noticing that entanglement entropy is symmetric with respect to partition. A more generalized way of quantifying entanglement for state  $\rho$  is called negativity, given by

$$\mathcal{N}(\rho) = \log_2 \|\rho^\Gamma\|_1, \quad (1.24)$$

where  $\rho^\Gamma$  denotes the partial transpose of state  $\rho$  and  $\|A\|_1 \equiv \text{Tr}[\sqrt{A^\dagger A}]$  is the trace-norm or one-norm. There are a few other measures which can be used for entanglement quantification. A distance-based measure called *relative entropy of entanglement* is defined as

$$S(\rho|\sigma) = \text{Tr}[\rho(\log_2 \rho - \log_2 \sigma)], \quad (1.25)$$

where  $\sigma$  is the nearest separable state. Another measure for the two-qubit pure state  $\rho$  called *concurrence* based on convex roof measure is given as

$$\mathcal{C}(\rho) = \sqrt{2(1 - \text{Tr}[\rho_A^2])} = \sqrt{2(1 - \text{Tr}[\rho_B^2])}, \quad (1.26)$$

where  $\rho_A$  ( $\rho_B$ ) is the reduced density matrix of state  $\rho$  for subsystem  $A$  ( $B$ ).

### 1.1.7.2 Discord

Discord was first introduced by Ollivier and Zurek in their seminal paper in 2001 [48]. In naive terms, it shows the loss of information due to state measurement. It is considered a more general form of measuring quantum correlation, i.e., states with zero entanglement but non-zero discord exist. First, we need to understand the origin of discord to quantify the amount of discord [49, 50].

Let us take the example of two parties,  $A$  and  $B$ , which share mutual information as shown in 1.3. One can calculate mutual information in two ways

$$H(A : B) = H(A) + H(B) - H(A, B), \tag{1.27}$$

$$H(A : B) = H(A) - H(A|B) = H(B) - H(B|A), \tag{1.28}$$

where  $H$  denotes the entropy.

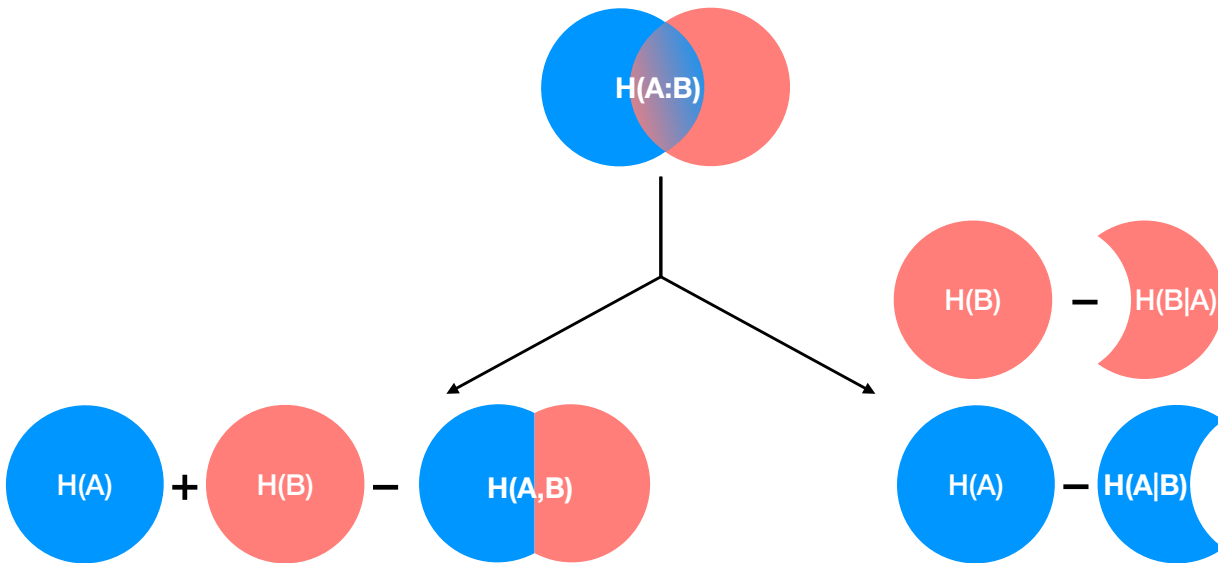


**Figure 1.3:** Ways of calculating mutual information

Classically, these two ways are equivalent; however, in quantum mechanics, they differ. The problem arises due to the second definition, which involves the knowledge of other subsystems.

To do so, one performs the measurement, and the outcome depends on the measurement basis. We can rewrite the mutual information in terms of Von-Neumann entropy

$$I(\rho) = S(\rho_A) + S(\rho_B) - S(\rho) \quad (1.29)$$

$$J_A(\rho) = S(\rho_B) - S(\rho_B|\rho_A)$$

$$J_B(\rho) = S(\rho_A) - S(\rho_A|\rho_B). \quad (1.30)$$

The difference between these two types of mutual information provides discord while maximizing  $J$  over all measurement basis states,

$$D_A(\rho) = I(\rho) - \max_{\{\Pi_j^A\}} J_{\Pi_j^A}(\rho) \quad (1.31)$$

$$D_B(\rho) = I(\rho) - \max_{\{\Pi_j^B\}} J_{\Pi_j^B}(\rho). \quad (1.32)$$

Generally, discord is not a symmetrical quantity, i.e.  $D_A(\rho) \neq D_B(\rho)$ . Due to the maximization involved, discord calculation is an NP-hard problem [51]. There doesn't exist any analytical formula for it.

### 1.1.8 Quantum Fidelity

The quantification of distance between two quantum operators is a useful tool. It has many applications in quantum information, such as characterizing the final state in experiments and quantifying entanglement [52]. One of commonly used measure *trace distance* between operators  $A$  and  $B$  is defined as

$$T(\rho, \sigma) = \frac{1}{2} \|A - B\|_1, \quad (1.33)$$

where  $\|A\|_1 \equiv \text{Tr}[\sqrt{A^\dagger A}]$  is the trace-norm or one-norm. The closeness between two unitary operators  $U_1$  and  $U_2$  can be given in terms of distance as

$$\begin{aligned} \|U_1 - U_2\|_1^2 &= \text{Tr}[(U_1 - U_2)^\dagger (U_1 - U_2)] \\ &= \text{Tr}[U_1^\dagger U_1 + U_2^\dagger U_2 - U_1^\dagger U_2 - U_2^\dagger U_1] \\ &= 2 - 2 \text{Re} \left( \text{Tr} [U_1^\dagger U_2] \right) = 2 - 2 \text{Re}(\langle U_1 | U_2 \rangle), \end{aligned} \quad (1.34)$$

where identity for unitary matrices  $U^\dagger U = \mathbb{1}$  has been exploited. The minimization of distance, in turn, implies the maximization of second term, also known as Frobenius inner product. Thus, the *Operator fidelity* between two operators is defined as

$$\begin{aligned} F_1(U_1, U_2) &= -\text{Re}(\langle U_1 | U_2 \rangle) \\ &\text{or} \\ F_2(U_1, U_2) &= |\langle U_1 | U_2 \rangle|^2, \end{aligned} \quad (1.35)$$

where the second expression is accurate up to a global phase, which is generally the requirement in practical cases.

*State fidelity* representing the degree of closeness between a pair of pure state  $\rho = |\psi\rangle\langle\psi|$  and  $\sigma = |\phi\rangle\langle\phi|$  can be defined as the transition probability [53]

$$F(|\psi\rangle\langle\psi|, |\phi\rangle\langle\phi|) = |\langle\phi|\psi\rangle|^2. \quad (1.36)$$

However, defining the fidelity for a general mixed state is more complex. The above expression was further generalized implicitly by the same authors, also known as Schumacher's fidelity [53]

$$F(\rho, |\psi\rangle\langle\psi|) = \langle\psi|\rho|\psi\rangle. \quad (1.37)$$

For a pair of general states  $\rho$  and  $\sigma$ , fidelity takes the following form

$$F(\rho, \sigma) = \langle\rho|\sigma\rangle = \text{Tr}(\rho\sigma). \quad (1.38)$$

Another extensively used measure in literature is Uhlman-Josza fidelity, which is applicable to general states and is expressed as [54, 55]

$$F_{\text{UJ}}(\rho, \sigma) = \left( \text{Tr} \sqrt{\sqrt{\rho} \sigma \sqrt{\rho}} \right)^2. \quad (1.39)$$

It reduces to equation 1.36 for a pair of pure states and to equation 1.37 for a pair of pure and mixed states. It is crucial to observe that all measures of operator and state fidelity are symmetric.

## 1.2 Experimental Quantum information

There has been tremendous progress in the experimental architectures for quantum information processing in the last few decades. Till date, we have several noisy intermediate-scale quantum (NISQ) devices, each having their strengths [56, 57]. Many tech giants like Google and IBM are investing in practical quantum computers, and small startups are also emerging rapidly [20–22]. Although there is no winner at the moment, the race to build a fault-tolerant quantum computer is on. We have multiple platforms for successful implementation of quantum processes, for example, nuclear magnetic resonance [23, 58], superconducting qubits [27, 59], photonic computers [60–62], Nitrogen-vacancy center or defect center [63, 64], ion trap [26, 65], neutral atoms [28, 66], Rydberg atoms [29, 67], and quantum dots [25, 68]. DiVincenzo described five criteria to realize a universal quantum computer given as [69]

1. Logical qubit scalability.
2. Initialization in a simple, easy-to-prepare state.
3. Long coherence times.
4. Universal set of gates.
5. Easy qubit targeted measurement ability.

In this thesis, we have employed NMR as our test bed to implement control algorithms. Initially, we will provide an overview of the fundamentals of NMR and subsequently demonstrate its application for quantum control algorithms.

## 1.2.1 Nuclear magnetic resonance (NMR) test bed

NMR has a long history of successful advancements and bagging of two Nobel Prizes [70]. The hardware is advanced, and the system is robust, thus making it the optimal candidate for performing quantum information tasks. The initial applications of NMR for quantum information processing were exhibited by Gershenfeld et al. for bringing forward the idea of multi-pulsed NMR to quantum computing [71], Cory et al. for ensemble quantum computing [72] and Nielsen et al. for teleportation [73]. After that, it gained the momenta, and various quantum information tasks have been performed [23]. Here, we will now explain the quintessentials of NMR [74, 75].

### 1.2.1.1 NMR spin

As the name implies, NMR relies on the nuclear spins of atoms, which possess the spin angular momentum operator  $\mathbf{I}$ . The eigenvalues of  $\mathbf{I}^2$  are given by  $I(I + 1)\hbar$ , where  $I$  represents the spin number. Based on nucleons' configuration, system can have spin  $I = 1/2, 3/2, \dots$ . For a single spin- $I$  of gyromagnetic ratio  $\gamma$  having magnetic moment  $\boldsymbol{\mu} = \hbar\gamma\mathbf{I}$  under magnetic field  $\mathbf{B}$ , the corresponding Hamiltonian  $H_0$  is

$$H_0 = -\boldsymbol{\mu} \cdot \mathbf{B} = -\hbar\gamma \mathbf{I} \cdot \mathbf{B}.$$

For magnetic field  $\mathbf{B}$  in the  $\hat{z}$ -direction with strength  $B_z$ , aforementioned Hamiltonian is reformulated as follows

$$H_0 = -\hbar\gamma I_z B_z = \hbar\omega_0 I_z, \tag{1.40}$$

with  $\omega_0 = -\gamma B_z$  being the Larmour frequency of the nuclei. It is of the order of  $10^1 - 10^2$  MHz based on the nuclei for magnetic fields of few tesla. The energy is contingent on the orientation of the magnetic moment, attaining a minimum when the magnetic field is parallel to it and a maximum when the field is anti-parallel to it for the positive value of  $\gamma$ . Conversely, for the negative value of  $\gamma$ , the relationship is reversed [74, 75].

The Zeeman Hamiltonian 1.40 has the eigenvalues  $E_m = -m\hbar\omega_0$  where  $m$  is the quantum number having  $2I + 1$  discrete values  $m = -I, -I + 1, \dots, I - 1, I$ . We take the example of

spin-1/2 nuclei, which form a two-level system with  $m = \pm 1/2$ .

### 1.2.1.2 Chemical shift

In a molecule, nuclei of the same species might experience different magnetic fields due to the distinctive local electronic environment. This effect is also known as nuclear shielding. With a good approximation, the induced field on  $j^{th}$  spin due to an electronic cloud can be considered linearly dependent on the external magnetic field, such that [74, 75]

$$\mathbf{B}_j^{\text{induced}} = \delta_j \mathbf{B}, \quad (1.41)$$

where  $\delta_j$  is the chemical shift tensor. For the secular approximation where chemical shift is weak compare to Zeeman interaction, the chemical shift Hamiltonian is given by

$$\begin{aligned} H_j^{\text{CS}} &= -\boldsymbol{\mu}_j \cdot \mathbf{B}_j^{\text{induced}} \\ &= -\boldsymbol{\mu}_j \cdot (\delta_j \mathbf{B}) \\ &= -\hbar \gamma_j \delta_{j,zz}(\theta, \phi) B_z I_{j,z}. \end{aligned} \quad (1.42)$$

Here the term  $\delta_{j,zz}(\theta, \phi)$  depends on the orientation of molecule and it takes the following form

$$\delta_{j,zz}(\theta, \phi) = \delta_{j,11} \sin^2 \theta \cos^2 \phi + \delta_{j,22} \sin^2 \theta \sin^2 \phi + \delta_{j,33} \cos^2 \theta, \quad (1.43)$$

where  $\delta_{11}, \delta_{22}, \delta_{33}$  denotes the principal values of the chemical shift tensor. In an isotropic liquid sample, molecules do tumbling motion, and time-averaged isotropic value of chemical shift tensor reduces to the form

$$\delta_j = \frac{1}{3}(\delta_{j,11} + \delta_{j,22} + \delta_{j,33}). \quad (1.44)$$

The total Hamiltonian for  $j^{\text{th}}$  spin due to static field and induced field is

$$\begin{aligned} H_0 &= -\hbar \gamma_j I_{j,z} (B_z + \delta_j B_z) \\ &= \hbar \omega_{j,0} I_{j,z} (1 + \delta_j) \\ &= \hbar I_z \omega_j, \end{aligned} \tag{1.45}$$

where each spin has a chemical shifted Larmour frequency defined as  $\omega_j = \omega_{j,0}(1 + \delta_j)$ .

### 1.2.1.3 Interacting spins

In a molecule, there can be more than one species of nuclear spins. If the spins are of same species then the molecular system is called *homonuclear system* while for spins of different species, it is called *heteronuclear system*. The interaction between these spins can be of multiple types such as [74, 75],

- Direct dipole-dipole coupling  $\mathcal{D}$ .
- Indirect spin-spin coupling  $\mathcal{J}$ .

Nuclear spins with quantum number  $> 1/2$  have asymmetric charge distribution resulting in electric quadruple interaction. However in this thesis, we have only worked with spin-1/2 nuclei, hence it is not discussed here.

Direct dipole-dipole coupling is rather easier to understand. Each spin in the magnetic field behaves like a tiny magnet with a dipolar moment. The magnetic fields of spins interact with each other and couple through that. The corresponding Hamiltonian with the dipole-dipole coupling  $\mathcal{D}$  is

$$H^{DD} = \sum_{i < j} \mathbf{I}_i \cdot \mathcal{D}_{ij} \cdot \mathbf{I}_j, \tag{1.46}$$

where  $\mathcal{D}_{ij}$  is the dipole-dipole interaction tensor. In the high-field, the secular approximation can be employed giving rise to reduced Hamiltonian of the form

$$H^{DD} = \sum_{i < j} d_{ij} (3 I_{iz} I_{jz} - \mathbf{I}_i \cdot \mathbf{I}_j), \tag{1.47}$$



where  $d_{ij} = \frac{b_{ij}}{2}(3 \cos^2 \theta_{ij} - 1)$  is the secular dipole-dipole constant with  $b_{ij} = -\frac{\mu_0 \gamma_i \gamma_j \hbar}{4\pi r_{ij}^3}$  and  $\theta_{ij}$  being the angle between vector of magnitude  $r_{ij}$  joining the spins and external magnetic field vector. For heteronuclear case, secular dipole-dipole Hamiltonian can further be reduced to the following expression

$$H^{DD} = \sum_{i < j} 2 d_{ij} I_{iz} I_{jz}. \quad (1.48)$$

It is clear from 1.47 that the dipole-dipole Hamiltonian depend on the molecule orientation. However, in an isotropic liquid sample, molecules keep moving around without having any particular direction; thus, the time-averaged Hamiltonian vanishes.

On the other hand, even in the absence of dipolar-dipolar coupling, spins still show a non-zero interaction. It is primarily attributed to bonding electrons between spins, resulting in an intramolecular effect. Since it does not originate because of vector fields, motional averaging leaves it unaffected. The Hamiltonian due to  $\mathcal{J}$ -coupling is given by

$$H^J = \sum_{i < j} 2\pi \mathbf{I}_i \cdot \mathcal{J}_{ij} \cdot \mathbf{I}_j, \quad (1.49)$$

where  $\mathcal{J}_{ij}$  is  $\mathcal{J}$ -coupling tensor. In an isotropic liquid due to rapid tumbling, similar to chemical shift, the averaged  $\mathcal{J}$ -coupling becomes  $\mathcal{J}_{ij}$  having the form  $\mathcal{J}_{ij} = \frac{1}{3}(\mathcal{J}_{ij,xx} + \mathcal{J}_{ij,yy} + \mathcal{J}_{ij,zz})$ . Thus, the modified Hamiltonian takes the following form

$$H^J = \sum_{i < j} 2\pi \mathcal{J}_{ij} \mathbf{I}_i \cdot \mathbf{I}_j. \quad (1.50)$$

The secular  $\mathcal{J}$ -coupling Hamiltonian satisfying the condition  $2\pi |\mathcal{J}_{ij}| \ll |\omega_i - \omega_j|$  have two different forms based on the type of nuclei interaction. For a homonuclear system, the secular Hamiltonian remains similar to equation 1.50; however, for a heteronuclear case, the secular Hamiltonian can be expressed as

$$H^J = \sum_{i < j} 2\pi \mathcal{J}_{ij} I_{iz} I_{jz}. \quad (1.51)$$

$\mathcal{J}$ -coupling contributes to the total energy based on the sign of coupling and polarization of spins.

The energy increases for a positive value of coupling and parallel spin, while for opposite spins, energy decreases. On the other hand, for negative  $\mathcal{J}$ -coupling, energy increases for opposite spin polarization and decreases for parallel spin polarization. In this thesis, we have only used liquid sample thus only  $\mathcal{J}$ -coupling is present. The total Hamiltonian for a system of spins inclusive of  $\mathcal{J}$ -coupling is

$$H = \sum_i \omega_i I_{iz} + \sum_{i < j} 2\pi \mathcal{J}_{ij} \mathbf{I}_i \cdot \mathbf{I}_j. \quad (1.52)$$

#### 1.2.1.4 Spin manipulation

As explained in section 1.2.1.1, energy levels of the spins under high static magnetic field split due to the Zeeman effect. For a field of 11.7 T, the Larmour frequency of  $^1H$  nucleus corresponds to 500 MHz, falling within the radio frequency (RF) range. Consequently, these spins can be coherently controlled using RF fields. The magnetic field  $\mathbf{B}^{\text{RF}}$  generated through RF waves is small compared to the static field. The effect of this weak field onto spin states gets accumulated over time if the direction of magnetic field is resonant with spin precession. The effective Hamiltonian due to the RF field along the transverse direction is given by [74, 75]

$$\begin{aligned} H^{\text{RF}}(t) &= -\boldsymbol{\mu} \cdot \mathbf{B}^{\text{RF}} \\ &= -\hbar \gamma B_1 \cos(\omega_{\text{ref}} t + \phi_p) I_x, \end{aligned} \quad (1.53)$$

where  $B_1$  is amplitude of the field while  $\omega_{\text{ref}}$  and  $\phi_p$  represent the oscillation frequency and initial phase respectively. A linearly oscillating field can be imagined as two components of the same frequency but rotating in opposite directions. Thus, we can recast the magnetic field generated from RF pulses into two rotating components, namely *resonant* and *non-resonant* field

$$\begin{aligned} B^{\text{res}}(t) &= \frac{1}{2} B_1 \left\{ \cos(\omega_{\text{ref}} t + \phi_p) \hat{e}_x + \sin(\omega_{\text{ref}} t + \phi_p) \hat{e}_y \right\} \\ B^{\text{non-res}}(t) &= \frac{1}{2} B_1 \left\{ \cos(\omega_{\text{ref}} t + \phi_p) \hat{e}_x - \sin(\omega_{\text{ref}} t + \phi_p) \hat{e}_y \right\}, \end{aligned} \quad (1.54)$$

where  $\hat{e}_x$  and  $\hat{e}_y$  are unit vectors in  $x$ - and  $y$ -direction, respectively. The resonant field precesses in the direction of the spin and gets coupled, while non-resonant component leaves it unaffected.

By ignoring the non-resonant component, the total transverse RF field Hamiltonian is given by

$$H^{\text{RF}}(t) = -\frac{1}{2} \hbar \gamma B_1 \left\{ \cos(\omega_{\text{ref}} t + \phi_p) I_x + \sin(\omega_{\text{ref}} t + \phi_p) I_y \right\} \quad (1.55)$$

with  $\omega_p = -\frac{\gamma B_1}{2}$  representing the maximum RF field amplitude. The time dependence of RF field can be removed by going into a rotating frame precessing with frequency  $\omega^{\text{ref}}$  about  $z$ -axis achieving the time-independent Hamiltonian

$$\begin{aligned} H^r &= \mathcal{R}^{-1} H^{\text{RF}}(t) \mathcal{R}, & \mathcal{R} &= \exp(-i\omega_{\text{ref}} I_z t) \\ &= \omega_p \hbar (\cos \phi_p I_x + \sin \phi_p I_y). \end{aligned} \quad (1.56)$$

In the rotating frame, the precession frequency is also modified as  $\Omega = \omega - \omega_{\text{ref}}$ , representing the difference between Larmor frequency and rotating frame frequency, referred as *offset*. The effective field in the rotating frame is given by

$$B^{\text{eff}} = B_1 (\cos \phi_p \hat{e}_x + \sin \phi_p \hat{e}_y) - \frac{\Omega}{\gamma} \hat{e}_z, \quad (1.57)$$

where precession around the effective field  $B^{\text{eff}}$  is characterized using *nutation frequency* having the form  $\omega_{\text{nut}} = -\gamma B^{\text{eff}}$ . The effective Hamiltonian takes the following form in rotating frame

$$H^{\text{eff}} = \Omega \hbar I_z + \omega_p \hbar (\cos \phi_p I_x + \sin \phi_p I_y), \quad (1.58)$$

which reduces to equation 1.56 for the *on-resonant case*, i.e.  $\omega = \omega_{\text{ref}}$ . Following this, nutation frequency  $\omega_{\text{nut}}$  also takes the form of  $\omega_p$ . From now onward, we will assume  $\hbar = 1$ .

### 1.2.1.5 Relaxation

Like all natural systems, a quantum system goes to equilibrium after a specific duration. However, it starts losing entanglement and superposition, some of the essential properties for computation as it relaxes. Therefore, it is essential to characterize the relaxation time such that all computation takes place before relaxation. In NMR, relaxation is majorly of two types [74, 75].

- **Longitudinal relaxation ( $T_1$ )** : After any perturbation to longitudinal magnetization ( $M_z$ ),

it goes back to its original position in the  $z$ -direction influenced by static field. When the magnetization becomes 63% of the initial value ( $M_0$ ), the time constant is called  $T_1$  relaxation time. A schematic for the magnetization recovery has been shown in figure 1.4. The process is also known as thermal relaxation or spin-lattice relaxation due to spin transferring energy to the environment and going to thermal equilibrium. The revival of longitudinal magnetization is written as

$$M_z(t) = M_0 (1 - e^{-t/T_1}). \quad (1.59)$$

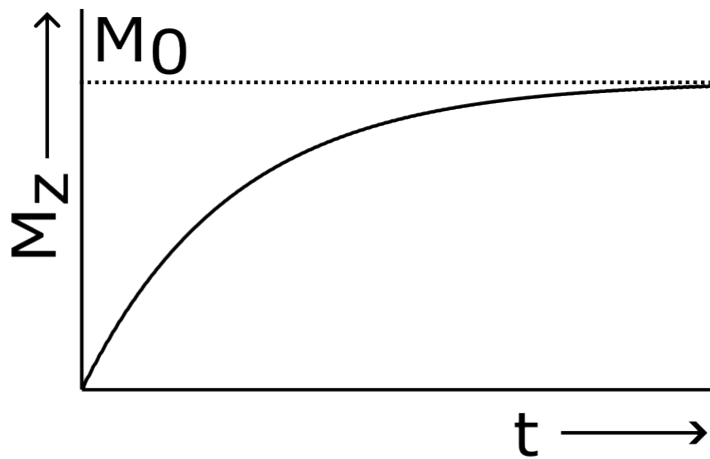


**Figure 1.4:** Revival of longitudinal magnetization with time

- **Transverse relaxation ( $T_2$ ):** The transverse component of magnetic field ( $M_{xy}$ ), perpendicular to static field  $B_0$ , decays with time constant  $T_2$ . During this time, a spin starts to dephase and coherence decays. The process is also known as decoherence or spin-spin relaxation as the spin experiences a local magnetic field from nearby spins in addition to static field  $B_0$ . The decay of magnetization can be shown using a schematic in figure 1.5 and mathematically given by

$$M_{xy}(t) = M_{xy}(0) e^{-t/T_2}. \quad (1.60)$$

Typically  $T_1$  is of the order of seconds while  $T_2$  is of the order of 100 ms. Hence,  $T_2$  sets an

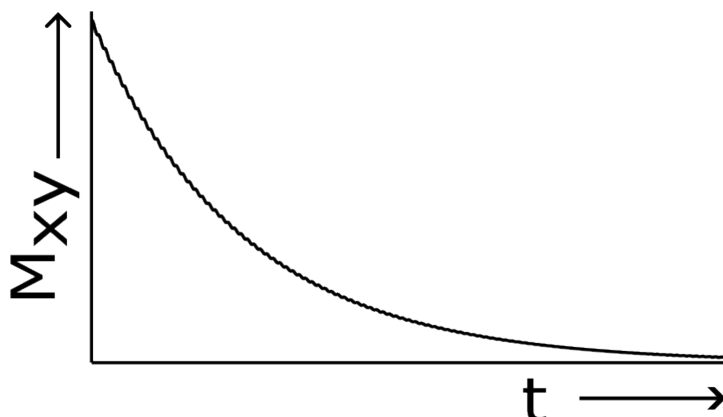


**Figure 1.5:** Decay of transverse magnetization with time

initial bound on the computation time. These times vary from nuclei to nuclei and molecule to molecule.

## 1.2.2 NMR quantum information processing

Nuclear spins in high magnetic fields form a two-level system, naturally making it a suitable candidate for qubits. These qubits can be manipulated using the external RF field as explained in the above section 1.2.1.4. Nonetheless, some ingredients are needed explicitly for quantum computation [23]. We will explain them one by one as given below.

### 1.2.2.1 Quantum gates

In the gate model of computation, quantum gates are essential. These gates are implemented utilizing the internal Hamiltonian of the molecular system in conjunction with the external RF field. We require a set of one-qubit and two-qubit gates to have a universal set of gates.

**Single-qubit gates:** Single-qubit gates are fundamentally rotations in a 3-dimensional space. Any single qubit gate can be executed with the help of a set of Pauli matrices and an identity matrix. Single-qubit gates like NOT, Hadamard etc. are realized using RF pulses. As explained in 1.2.1.4, an on-resonant  $x$ -pulse of angle  $\theta$  is achieved by applying RF Hamiltonian with initial phase being  $\phi_p = 0^\circ$  for a time duration  $\tau$  such that pulse angle  $\theta = \omega_p \tau$ . Similarly, we need

to change the initial phase to  $\phi_p = 90^\circ$  for rotation in the  $y$ -direction. The rotation operator for  $x$ -pulse with rotation angle  $\theta$  is given as

$$\mathcal{R}_x(\theta) = \exp(-i\theta I_x), \quad (1.61)$$

which is essentially a NOT gate for an angle  $\pi$

$$\mathcal{R}_x(\pi) = \exp(-i\pi I_x) = -i \begin{bmatrix} 0 & 1 \\ 1 & 0 \end{bmatrix}. \quad (1.62)$$

As  $-i$  represents the global phase and is not detectable, we can safely ignore it. We can obtain the Hadamard gate by a sequence of two pulses given by

$$\begin{aligned} \mathcal{R}_x(\pi)\mathcal{R}_y(\pi/2) &= \exp(-i\pi I_x) \exp(-iI_y\pi/2) \\ &= \frac{-i}{\sqrt{2}} \begin{bmatrix} 1 & 1 \\ 1 & -1 \end{bmatrix}, \end{aligned} \quad (1.63)$$

which depicts the Hadamard matrix along with undetectable global phase. A rotation about  $z$ -axis with an angle  $\theta$  is equivalent to phase shift gate. It can be achieved with a  $y$ -pulse of angle  $\theta$  sandwiched between  $x$ -pulses as follows:

$$\begin{aligned} \mathcal{R}_z(\theta) &= \mathcal{R}_{-x}(\pi/2)\mathcal{R}_y(\theta)\mathcal{R}_x(\pi/2) \\ &= \exp(i\pi/2 I_x) \exp(-i\theta I_y) \exp(-i\pi/2 I_x) \\ &= \exp(-i\theta/2) \begin{bmatrix} 1 & 0 \\ 0 & e^{i\theta} \end{bmatrix}. \end{aligned} \quad (1.64)$$

Thus, we can attain any single-qubit gate by appropriately choosing the rotation angle and phase to design a sequence of pulse.

**Multi-qubit gates:** Along with Pauli operators, a 2-qubit CNOT gate results in a universal set. We realize the multi-qubit gates by using the  $\mathcal{J}$ -coupling as explained in section 1.2.1.3. The

evolution of a pair of spin with  $\mathcal{J}$ -coupling for time  $t$  results in the following unitary

$$H_J = 2\pi \mathcal{J} \mathbf{I}_1 \cdot \mathbf{I}_2, \quad (1.65)$$

$$U_J = \exp(-iH_J t) = \exp(-i 2\pi \mathcal{J} t \mathbf{I}_1 \cdot \mathbf{I}_2). \quad (1.66)$$

Using the product operator formalism [76], starting from the state  $\rho$ , the final state at time  $\tau$  after applying the operator  $\alpha\hat{O}$  is given as

$$\rho \rightarrow \cos(\alpha\tau)\rho + \sin(\alpha\tau)[\hat{O}, \rho], \quad (1.67)$$

where  $[\hat{O}, \rho]$  represent the commutator between operator  $\hat{O}$  and initial state  $\rho$ . For a weakly coupled system, the Hamiltonian reduces as described in equation 1.51 and the corresponding unitary is

$$U_J = \exp(-iH_J t) = \exp(-i 2\pi \mathcal{J} t I_{1z} I_{2z}). \quad (1.68)$$

At time  $t = 0$ , we start with density matrix  $I_{1x}$ , then the matrix after time  $t = \tau$  would be:

$$I_{1x} \xrightarrow[\tau]{2\pi \mathcal{J} t I_{1z} I_{2z}} \cos(\pi \mathcal{J} \tau)(I_{1x}) + \sin(\pi \mathcal{J} \tau) 2I_{y1} I_{z2}, \quad (1.69)$$

which is a correlated matrix between two qubits. Thus we can convert an uncorrelated density matrix to correlated form using  $\mathcal{J}$  evolution. A very popular 2-qubit CNOT gate can be realized using the pulse sequence given as

$$U_{\text{CNOT}} = \left(\frac{\pi}{2}\right)_{-y}^2 \left(\frac{\pi}{2}\right)_{-z}^{1,2} \frac{\tau}{2} (\pi)_y^{1,2} \frac{\tau}{2} (\pi)_y^1 \left(\frac{\pi}{2}\right)_{-y}^2, \quad (1.70)$$

with  $\tau = \frac{1}{2\mathcal{J}}$ . Using the RF pulses and  $\mathcal{J}$ -evolution, we can implement various gates. We can also realize the multi-qubit gates using the techniques of quantum optimal control, which has been discussed in sufficient detail in the later section.

### 1.2.2.2 State initialization

Engineering a pure state is ubiquitous in many quantum computing problems. Since the equilibrium state in NMR is a thermal state that corresponds to Boltzmann distribution at room temperature, given as

$$\rho_{\text{thermal}} = \frac{\mathbb{1}}{2^N} + \sum_i \epsilon_i I_{iz}, \quad (1.71)$$

where  $\epsilon_i = \frac{\gamma_i B_z}{N k_B T} \sim 10^{-5}$  is called the purity of the system. The first part of the thermal density matrix remains invariant under unitary evolution, while the second part changes. In many tasks, one wants to start with a pure state. However purity being quite a small factor in NMR, either one needs very high magnetic field or very small temperature. In NMR, we use a pseudo-pure state (PPS) [71, 77], which corresponds to a significant population difference between a ground state and excited states and is isomorphic to a pure state. Thus, the extra population works as a pure state signature while the rest acts as a background without any observable magnetization. The density matrix for PPS is given by

$$\rho_{\text{PPS}} = (1 - \epsilon) \frac{\mathbb{1}}{2^N} + \epsilon \rho_{\text{pure}}. \quad (1.72)$$

### 1.2.2.3 Measurement

Measurement is an essential aspect of practical quantum devices. In NMR, we observe magnetization of spins with respect to time. Due to inherent relaxation, the time domain signal of magnetization decays, which is called free induction decay (FID). After doing the Fourier transform of FID, we get the corresponding peaks in the frequency domain. Since, we have coils in  $xy$ -plane, we can only observe the corresponding magnetization given by

$$M(t) = \text{Tr}[\rho(t)(\sigma_x + i\sigma_y)]. \quad (1.73)$$

To find a full-density matrix at any given time, one must perform quantum state tomography (QST), where each element must be measured separately.



### 1.2.2.4 Decoherence time

As mentioned in the section above 1.2.1.5, we defined the two primary sources of errors given by relaxation time  $T_1$  and  $T_2$ .  $T_2$  is generally defined as a decoherence time for single spin coherence and decoherence times for a multiqubit systems can differ. However, it gives a rough estimate of the time, which is in the order of seconds for liquid states sample, while each hard pulse for single-qubit and 2-qubit gate is in milliseconds. Thus, it is possible to implement reasonable deep circuits in NMR.

A schematic of NMR is shown in figure 1.6. In the thesis, we have explored the usage of NMR to carry out quantum control protocols. In the next section, we explain the basics of quantum

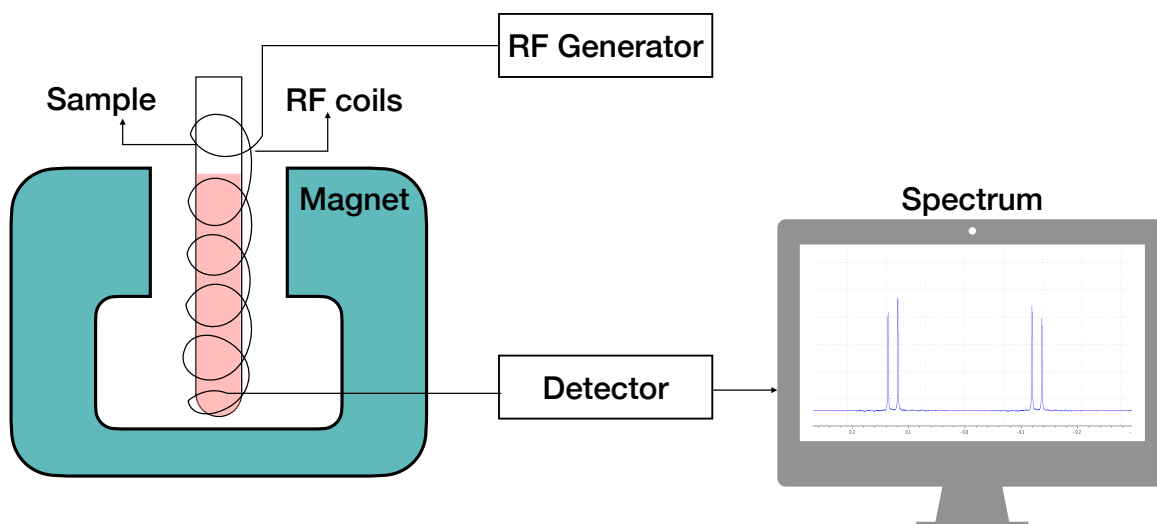


**Figure 1.6:** A schematic of NMR system

control and describe some of the most commonly used algorithms.

## 1.3 Quantum Control

Control theory provides a way to control a dynamic system efficiently while minimizing resources. It has seen tremendous progress over the years in various fields of science and engineering [78–81]. It has been used in engineering for aircraft cruise control, robotics, etc. [82]. Various

scientific sub-branches, including molecular dynamics [83] and physical chemistry [84, 85], incorporate control theory to manipulate and understand dynamic systems.

Optimal control can be divided into problem classes such as open or closed loop control, numerical or geometric optimal control, the Pontryagin maximum principle (PMP) or the Hamilton-Jacobi-Bellmann (HJB) approach, etc. In the closed-loop control, new controls are calculated based on the feedback, while open-loop control deals with prior optimization of controls before applying them to a physical system. In the other class, numerical or geometric optimal control deals with the type of algorithms used in optimization, such as a geodesic approach for geometric control and a gradient-based approach for numerical control. PMP or HJB provides conditions for the optimality of the dynamical equation. PMP provides a necessary condition for extremum solution along the trajectory, while HJB provides a necessary and sufficient condition for finding the optimum of a dynamical system. However, it is generally rather difficult to solve the HJB equation numerically.

As quantum mechanics became more popular and influential in many fields of Physics and Chemistry, the control of quantum systems became more ubiquitous, giving rise to the field of quantum control theory (QCT). There are various ways of controlling quantum systems, but they can be divided into the following parts.

- **Quantum optimal control theory (QOCT):** QOCT is the most widely used class of techniques for controlling quantum systems. As the name suggests, it tries to find the optimal strategies to control a quantum system for tasks such as unitary evolution, state-to-state transfer, etc. The fundamental principles of these techniques are based on numerical optimization algorithms. There has been significant progress in using optimization algorithms such as gradient-based methods, variational principle-based methods, metaheuristic algorithms, etc., for quantum control [86–90]. We will discuss them in detail subsequently.
- **Lyapunov-based control:** These control methods are based on the Lyapunov function invented by Aleksandr Lyapunov [91] and used for finding the stability of a dynamical equation. Control-Lyapunov functions are an extension of ordinary Lyapunov functions where we try to find controls which drive the system's state to the lowest energy state asymptotically [92]. For the Lyapunov function  $V$ , we want to find controls such that  $\dot{V} \leq 0$  corresponding to the Lyapunov stable region. P. Vettori [93] as well as Symeon

Grivopoulos and Bassam Bamieh [94] used it for quantum control in the context of state transfer. Consequently, it was used in experiments and theoretical approaches [95–97]. There have been proposals for advanced versions of Lyapunov-based control, which deals with specific problems of the scheme, such as reduction in total evolution time [98, 99].

- **Incoherent control:** The usual control approaches consider the system’s Hamiltonian evolution pertaining to coherent control. However, there are some tasks, for example, different spectra for initial and final states, same target state for different initial states, etc., where coherent controls have limited advantage. In such a case, we exploit incoherent controls (non-unitary dynamics) using environment [100, 101].

### 1.3.1 Quantum optimal control theory (QOCT)

In this thesis, we are mainly going to use QOCT. Let us consider a quantum mechanical system with a drift/constant Hamiltonian  $H_0$ , and the system is being controlled using external electromagnetic fields governed by time-dependent Hamiltonian  $H_c(t)$ . A general structure of the total Hamiltonian  $H(t)$  is

$$\begin{aligned} H(t) &= H_0 + H_c(t) \\ &= H_0 + \sum_{k=1}^M u_k(t) H_k. \end{aligned} \quad (1.74)$$

Here  $u_k(t)$  are time-dependent controls,  $H_k$  are the corresponding control Hamiltonians, and  $M$  is the number of qubits. The task of quantum control is to achieve a desired unitary or target state. In a closed system, the evolution is governed by Schrödinger equation 1.6 or 1.7. We can divide the control problem based on the target into two types:

- **Unitary transformation (UT):** In this, the goal is to achieve a desired unitary  $U_f$  under which the evolution of quantum system is taking place governed by equation 1.6. The fidelity between target unitary  $U_f$  and simulated unitary  $U_s$  as explained in equation 1.35 is defined as

$$F_u(U_f, U_s) = |\langle U_f | U_s \rangle|^2 = \left| \text{Tr} \left( U_f^\dagger U_s \right) \right|^2. \quad (1.75)$$

- **State-to-state transfer (s2s):** Starting from an initial quantum state  $\rho_0$  to reach to the final desired state  $\rho_f$  under the evolution 1.7. We can define the state fidelity between target state  $\rho_f$  and simulated state  $\rho_s$  as described in equation 1.38

$$F_s(\rho_f, \rho_s) = \langle \rho_f | \rho_s \rangle = \text{Tr}(\rho_f \rho_s), \quad (1.76)$$

However, it is convenient to use the slightly modified form of fidelity, also called correlation, for the traceless part of the density matrix, which takes into account purity [102]

$$F_c(\rho_f, \rho_s) = \frac{\text{Tr}(\rho_f \rho_s)}{\sqrt{\text{Tr}(\rho_f^2) \text{Tr}(\rho_s^2)}}. \quad (1.77)$$

Unitary transformation is more general as it doesn't take into account the state of the system and can be applied to any initial state irrespective of optimization procedure. However, the state-to-state transfer is more restrictive and can only be applied to a particular pair of initial and target states used in optimization.

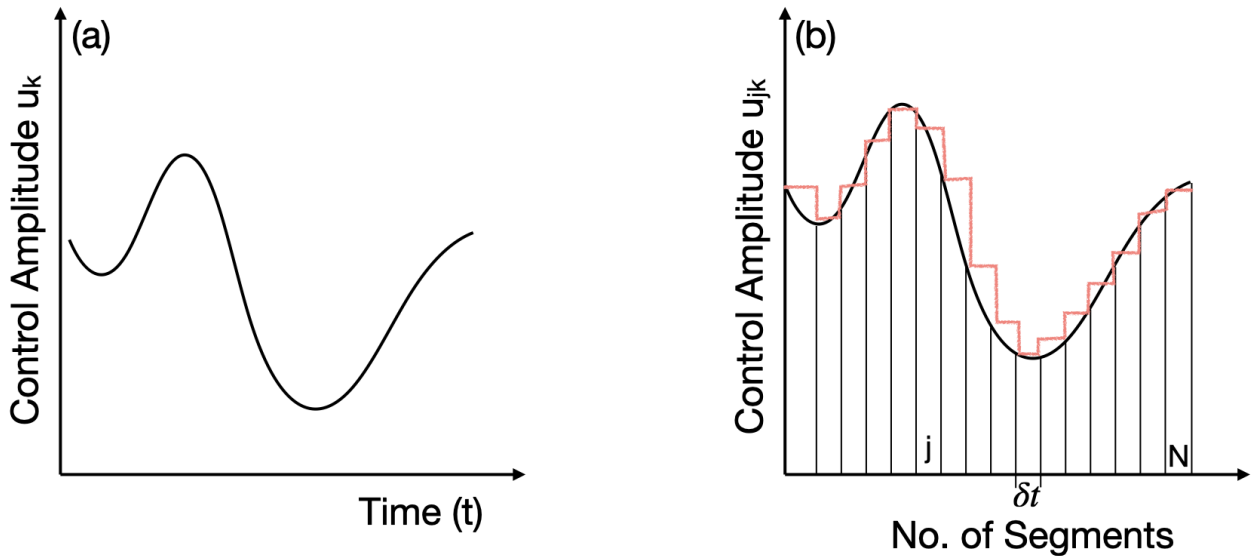


**Figure 1.7:** (a) Control amplitude vs time (b) Division of control amplitude into  $N$  segments each of  $\delta t$  time interval with amplitude  $u_{jk}$  for  $j^{th}$  segment (red curve represent the control amplitude after piecewise constant approximation).

One example of control amplitude vs time is shown in 1.7 (a). As our Hamiltonian 1.74 is time-dependent, solving the time-dependent Schrödinger equation is not a straightforward task. Given this, we resort to the piece-wise constant approximation. It is a widely used approximation, simultaneously being practical and advantageous. We divide the controls  $u_k(t)$  into  $N$  constant segments, each of the same time duration  $\delta t$  as shown in 1.7 (b). After the piece-wise constant approximation, the Hamiltonian for  $j^{\text{th}}$  segment is

$$H_j = H_0 + \sum_{k=1}^M u_{jk} H_k. \quad (1.78)$$

Due to the removal of time dependency, it becomes much easier to solve the above equation. The corresponding unitary for  $j^{\text{th}}$  segment is

$$U_j = \exp(-i H_j \delta t). \quad (1.79)$$

As a consequence, the total unitary  $U(T)$  after a time duration of  $T$  is written as the product of different segments unitaries time-ordered from 1 to  $N$

$$U(T) = U_N U_{N-1} \cdots U_2 U_1. \quad (1.80)$$

To simulate a unitary, we find control amplitudes  $u_{jk}$  followed by the control Hamiltonians  $H_j$ . We employ numerical optimization techniques and some machine learning optimization protocols for this. To this end, we look for an optimization function that would be an important ingredient for the algorithm. We choose unitary or state fidelity as described in 1.75 and 1.76, respectively. Along with maximizing the fidelity, we also wish to minimize the resources. For electromagnetic fields, total power is a resource to be minimized. In general, time is another parameter to be minimized. Thus, we formulate our final optimization function with fidelity and power consumption

$$J = F - \lambda_k \sum_{k=1}^M \sum_{j=1}^N u_{jk}^2, \quad (1.81)$$

here  $\lambda_k$  is called the penalty parameter. Using an optimization algorithm, we aim to maximize the function  $J$  or minimize  $\tilde{J} = 1 - J$ . The following section describes some of the most used

and famous quantum control algorithms.

### 1.3.2 Quantum control algorithms

In the last few decades, ample research has been done to advance quantum control algorithms. The first mathematical formulation of time optimal controls in coherent spectroscopy was shown by Khaneja et al. in their seminal paper [103]. It was a geometric approach with shortest paths lying on certain coset space. At the same time, people started looking at other geometric approaches, such as Pontryagin's maximum principle for finding optimal protocol for population transfer [104] as well as time optimal control [105]. From a different perspective, Fortunato et al. [102] developed strongly modulated pulses based on a direct numerical search algorithm called the Nelder-Mead simplex search. With this, numerical methods ushered in; however, a systematic and practical algorithm still needed to be developed. As a heuristic algorithm, Nelder-Mead suffered from a convergence problem and found it challenging to scale to higher qubits.

The formulation of a gradient-based method called Gradient Ascent Pulse Engineering (GRAPE) proposed by Khaneja et al. [106] attained immediate popularity for a general quantum control problem. The power of the GRAPE algorithm lies in straightforward analytical form of gradients. There have been many variants of the GRAPE algorithm to tackle specific issues. Some of the famous incorporations to enhance the convergence of GRAPE protocol are conjugate gradients [107], quasi-Newton BFGS method [108], Newton-Raphson method [109], push-pull algorithm [110], etc.

V. F. Krotov developed a variational principle-based optimization method [111] utilizing a Lagrange multiplier to have unconstrained optimization functional. Due to its global nature, it is expected to have better convergence. It was first used for optimal control of spin systems in NMR and dynamic nuclear polarization in 2008 by Maximov et al. [112]. Later, it was also used for spatial-selective pulses in magnetic resonance imaging [113].

Along with the Nelder-Mead simplex search, there are other direct search or heuristic algorithms. One of them is simulated annealing (SA), which has been used for solving quantum circuit transformation problems [114], optimizing quantum circuits for simultaneous dense protocol [115], and preparing high fidelity quantum controls [116]. Another famous class consists of evolutionary algorithms inspired by biological evolution. Genetic algorithms based on the ingre-

dients of biological evolution, such as recombination and mutation, have been used for quantum optimal control of qutrits [117], generating unitary and nonunitary quantum controls [118], and for preparing singlet order in an 11-qubit register [119], etc. Differential evolution using the same principles of evolution yet based on vector differences has also been used for gate control [117] and control of open quantum system [120].

Chopped Random Basis Optimization (CRAB) was first developed for control of time-dependent density matrix renormalization group (DMRG) simulations [121] and was later generalized for other quantum processes [122]. In this, we expand the controls in functional space basis such as Fourier space, Lagrange polynomials, etc. It has two distinct features: first, the function basis space is truncated at a finite dimension, and second, the corresponding basis functions are randomized to improve convergence. In recent years, there have been many applications of the CRAB algorithm, e.g. bandwidth-limited pulses [123], control of Bose-Einstein condensates [124], robust adiabatic population transfer in Nitrogen vacancy center [125], etc.

Gradient optimization of analytical controls (GOAT) is another gradient-based algorithm in which the gradients are calculated analytically. Analytical gradients make the algorithm flexible, accurate and practical [126].

As machine learning became prevalent in many areas of life, it also followed the advancement of ML-based control algorithms. Most of these algorithms rely on reinforcement learning (RL) based methods; however, other methods have also been used. RL gained fame after winning the Go game against a world champion [127]. It tries to find the best optimal strategy to move in the parameter space based on its history without requiring external training data as input. It was used for control of non-integrable many-body system [128], universal robust quantum control [129], quantum gate control [130], state preparation [131] etc. Some other methods, e.g. deep learning, have also been employed for robust quantum control [125]. Recently, some work displayed the usage of Physics-informed neural network (PINN) to solve quantum control problems via solving Schrödinger equation [132] and Markovian open system dynamics [133]. Another subset of ML algorithms called differential programming has also been employed for tasks like eigenstate preparation [134] and control of the quantum thermal machine [135].

Various hybrid algorithms have used the strength of two or more control algorithms. A combination of GRAPE and Krotov algorithm utilizes the simplicity and speed of GRAPE algorithm

at initial times while the monotonic convergent behaviour of Krotov at later times [136]. Eitan et al. combined Krotov and quasi-Newton method for accelerated convergence [137]. A merger of heuristic algorithm SA and GRAPE, namely SAGRAPE, uses the structural form of gradients while trying to explore a broader parameter space [116]. Machine learning algorithms such as differential programming and CRAB algorithm for speeding up of magnon transport [138] as well as recommender system along with GRAPE and SAGRAPE have been used for expediting the original algorithms for unitary synthesis in large quantum systems [139]. A summary of different control algorithms is presented in table 1.2.

Algorithm	Features	Drawbacks
Strongly modulated pulses	First numerical algorithm, adaptable	Computationally resource heavy, convergence issue, scaling problem
GRAPE	Easy gradient formula, numerically efficient	Get stuck in local minima, sensitive to initial guess
Krotov	Monotonically convergent	Convolutated updates, higher computational resources
Simulated annealing	Heuristic, local minima escape	Scaling up, slow
Evolutionary algorithm	Adaptable, global search	Slow, computationally expensive
CRAB	Functional space control expansion, flexibility in optimization routine	Sensitivity to chosen model
GOAT	Analytical controls	Sensitivity to chosen model
RL	Local optima overcome, improved convergence	Difficult to implement
PINN	Takes information of underlying physical model	Needs more research
Hybrid	Simultaneous advantage of two or more methods	Enhanced complexity, fine-tuning of various parameters

**Table 1.2:** A summary of different control algorithms

## 1.4 Machine learning

Machine learning is a branch of computer science that tries to use data and algorithms to mimic how humans behave. It is based on the human brain structure where thousands of neurons contin-



uously talk to each other [140]. The basic machine learning algorithms are based on the regression principle and try to predict the future outcome. With the invention of better storage devices and enhanced computational power, these methods have been routinely used in academia and industry for the last few years [141].

There are some terms like machine learning (ML), neural network (NN), and deep neural network (DNN) which are used interchangeably quite a lot. Although all these are branches of artificial intelligence (AI), we can consider machine learning as a branch of AI, NN as a branch of ML and DNN as a branch of NN [142].

ML deals with all algorithms used to model the datasets. These models can be further used for the prediction of future outcomes. The early algorithms in the field of ML include linear regression [143], principal component analysis [144], decision trees [145] etc. We can mainly divide ML into three classes:

1. **Supervised learning:** This ML model type connects input and output via a particular mathematical function by finding the underlying data pattern. In this class, there are specific labels assigned to outputs. It is the primary form of ML, yet it is convenient and practical.
2. **Unsupervised learning:** If no labels are associated with outputs, it is more difficult to predict the outcome. However, unsupervised learning-based methods can be helpful in this regard.
3. **Reinforcement learning:** This differs from the above two as it does not need any data to learn the underlying model. It is based on trial and error, such that it gets rewarded for each excellent step and punished for a bad one. Thus, it learns from its previous history only.

However, as computers' storage capacity and computational power increased, the ML subgroup called NN became more prevalent. The neurons in NN are called artificial neurons; the network is the artificial neural network (ANN). The basic structure of a neural network is shown in figure 1.8 having an input layer, a hidden layer and an output layer.

In NN, there are three primary components: the input layer needed to encode the input data, the hidden layer for processing and the output layer that reveals the outcome. If NN has more than one hidden layer, it is called a deep neural network (DNN). Each layer has multiple neurons based on the dataset available. Each neuron would connect with other neurons in the same or next

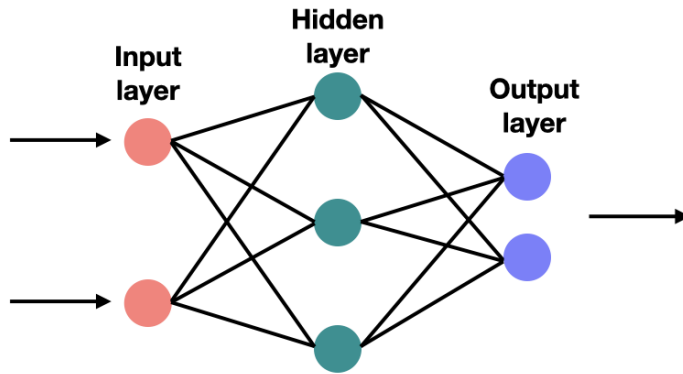


Figure 1.8: Neural network

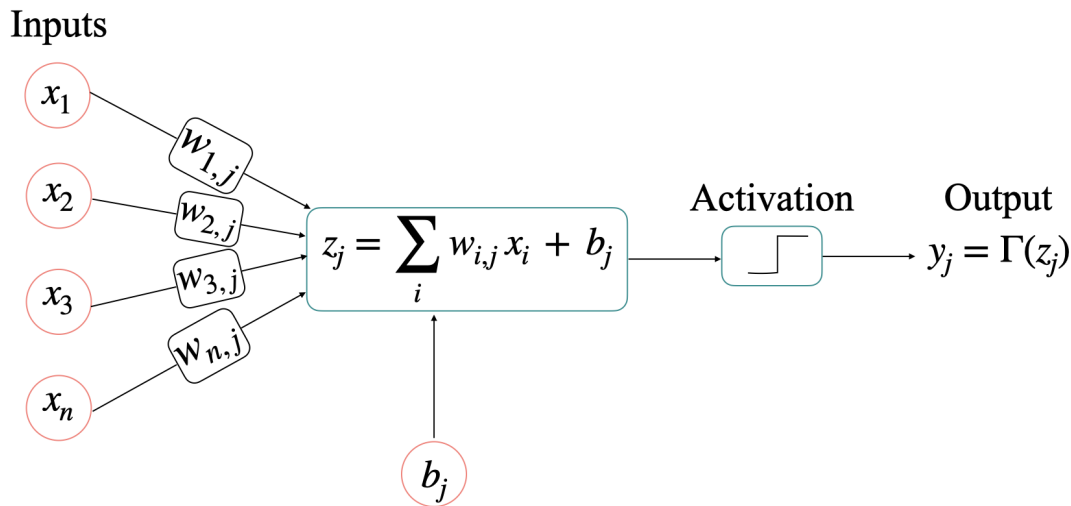
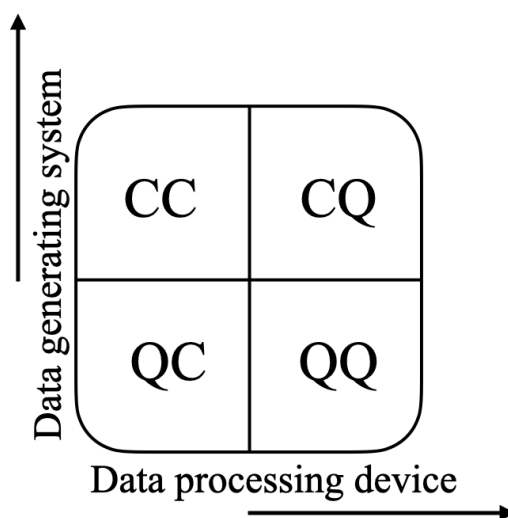


Figure 1.9: Mathematical processing of a neural network where  $x_i$  are inputs,  $w_{i,j}$  are the weights,  $b_j$  are bias, and  $y_j$  are output.

layer. The strength of these connections can be defined via weights  $w_{ij}$ , thus forming a matrix  $W$ . Each neuron has a constant value called bias  $b_i$ , which helps make the model more general and accurate. Bias does not depend on the previous layer but is a somewhat independent quantity to adjust the origin of the activation function. The activation functions, e.g. sigmoid, hyperbolic tangent, ReLu, etc., are generally non-linear function, which takes the sum of weights multiplied input and bias, a linear function as argument. After applying these functions, the output of a neuron becomes the non-linear function, which is more general and helps us better model the



**Figure 1.10:** Classification based on data type and processing device.

data [146]. Thus, a NN is considered a universal function approximator with the appropriate number of neurons and layers. We use this property in one of the problems described in 5. The processing of a neuron is shown in 1.9.

In recent years, there has been rapid progress in the intersection of quantum mechanics and machine learning. There are four types of possibilities we can have, as shown in 1.10

1. Classical data with a classical information processing device (CC, upper left), such as image recognition and computer vision using deep neural network [147], have gained adequate recognition.
2. Quantum data with classical devices (QC, bottom left) has made a big impact in the last few years. Since quantum data increases exponentially with qubit size, finding the optimal algorithms and showing the advantage became easier. The most prominent examples include quantum phase transition [148], quantum state tomography [149], ground state reconstruction of a quantum Hamiltonian [150], controlling the quantum dynamics [128] etc.
3. Classical data with quantum devices (CQ, upper right) uses classical data but processes it on quantum devices such as boson samplers, quantum computers, etc. The primary examples include handwriting recognition on a 4-qubit NMR system using quantum support vector

machine [151], robust binary classification using quantum adiabatic optimization [152], a quantum algorithm for well-known recommender systems [153], etc.

4. Quantum data with the quantum device (QQ, bottom right) has been advantageous in simulating the quantum Hamiltonian on a programmable quantum simulator, also called digital quantum computation [154–156]. Some other examples of the QQ section include quantum Hamiltonian learning using quantum algorithms [157, 158], state tomography using quantum Boltzmann machines [159], quantum convolutional neural network [160], etc.

ML has impacted all areas of quantum information and quantum mechanics. Here in this thesis, we specifically deal with quantum data processed on classical devices. We utilize specific ML algorithms and show their use cases with quantum data, especially in quantum characterization and control.

## 1.5 Characterization and control of quantum dynamics

Introduction to dynamical equations is crucial as they underlie the behavior of diverse physical systems, spanning classical mechanics, social behavior, economic dynamics, and chemical reaction dynamics. The quantum realm introduces challenges, where the Schrödinger equation or Von-Neumann equation governs system behavior, necessitating efficient characterization and control of quantum dynamics. The involvement of operators in quantum mechanics adds complexity, making rapid evolution assessment a non-trivial task.

Addressing the challenges in quantum dynamics, this thesis focuses on the development of computational methodologies for both characterizing and controlling quantum systems. We employ a recommender system, a machine learning algorithm, in the characterization phase to predict quantum correlation for unitary and non-unitary evolution. This contributes to an efficient understanding of quantum dynamics.

In the realm of quantum control problems, applying classical control theory directly is not straightforward. Therefore, specific control theories tailored for quantum evolution are essential. Mathematical tools and an NMR test bed are utilized as experimental setups to develop and validate new control protocols for addressing specific issues in quantum control algorithms.

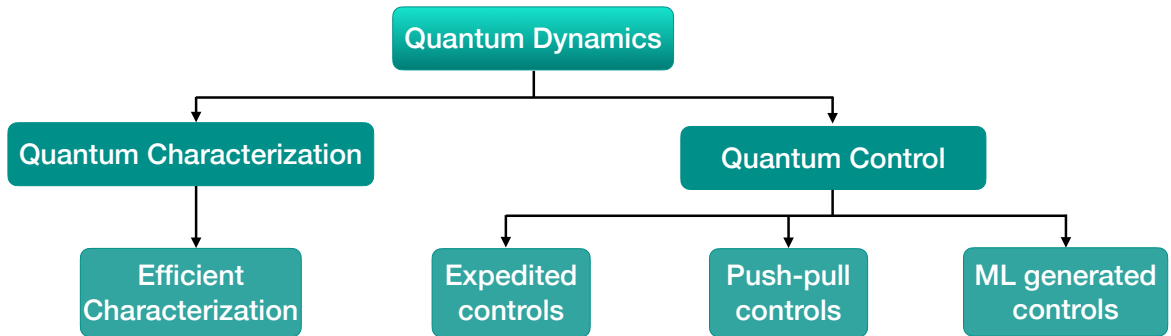


**Figure 1.11:** A brief overview of the thesis.

The thesis delves into four main topics:

- (i) Recommender system-based efficient characterization of quantum dynamics.
- (ii) Utilizing a recommender system to expedite algorithms.
- (iii) Enhancing algorithm convergence by deploying orthogonal operators.
- (iv) Implementing Physics-Informed Neural Network (PINN) for robust controls, as described in the accompanying flowchart 1.11. We now move on to explaining each topic in detail in subsequent chapters.

This comprehensive exploration contributes to advancing the understanding and control of quantum dynamics, providing valuable insights into both characterization and control methodologies.



## CHAPTER 2

---

# Efficient Characterization of Quantum Evolutions via a Recommender System

---

### Abstract

In this chapter, we demonstrate characterization of quantum evolutions via matrix factorization algorithm, a particular type of the recommender system (RS). A system undergoing a quantum evolution can be characterized in several ways. Here we choose (i) quantum correlations quantified by measures such as entropy, negativity, or discord, and (ii) state-fidelity. Using quantum registers with up to 10 qubits, we demonstrate that a RS can efficiently characterize both unitary and non-unitary evolutions. After carrying out a detailed performance-analysis of the RS in two-qubits, we show that it can be used to distinguish a clean database of quantum correlations from a noisy or a fake one. Moreover, we find that the RS brings about a significant computational advantage for building a large database of quantum discord, for which no simple closed-form expression exists. Also, RS can efficiently characterize systems undergoing non-unitary evolutions in terms of quantum discord reduction as well as state-fidelity. Finally, we utilize RS for the construction of discord phase space in a nonlinear quantum system.

### Reported in

**Priya Batra**, Anukriti Singh, and T. S. Mahesh, *Efficient Characterization of Quantum Evolutions via a Recommender System*, [Quantum](#), 5, 598 (2021).

## 2.1 Introduction

Machine learning is increasingly featuring in almost every aspect of our understanding of the world. A popular class of machine learning, namely the Recommender System (RS), is often

used to orient consumers towards certain products according to individual preferences [161–163]. There are many approaches to build an RS, such as the *content based system*, where recommendations are based on users’ past experience [164, 165], *knowledge based system*, where one uses the knowledge of users and items to render the recommendations [166], and the widely used *collaborative filtering*, which exploits the user-item correlation, i.e., the interconnection between users’ preferences among products with the recommendations provided by other users [167, 168]. Collaborative filtering can be implemented by neighborhood methods or by latent-factor modeling. Matrix factorization algorithm (MFA) is a popular tool for implementing latent-factor modeling based RS. It can predict the rating of a specific item by a particular user based on the self-rating of other items as well as others’ ratings of various items [169].

The recent spurt of machine learning applications for quantum information tasks includes its usage in quantum tomography [149, 170], quantum error correction [171], quantum control [172], understanding quantum phase transitions [148, 173], and studying quantum-many-body problems [150, 174]. It has been shown recently that machine learning techniques can work as state classifiers too. Sirui Lu and co-workers have shown the separability criteria of entangled state using convex hull approximation and supervised learning [175]. Ma and Yung showed that it is possible to classify the separable and entangled states using artificial neural networks [176]. The work has been further extended to experimental data [177] and later has been applied to simultaneous learning of multiple nonclassical correlations as well [178]. Valeria Cimini and co-workers proposed an artificial neural network to calculate the negativity of the Wigner function for multi-mode quantum states [179]. The connection between geometric and entropy discord has also been explored using machine learning [180].

### 2.1.1 Objectives

In this work, we employ an RS for characterizing quantum evolutions in terms of change in quantum correlations as well as fidelities. Following this,

- (i) We perform a detailed study of the RS performance on a two-qubit register with respect to prediction accuracy, dependence on the database dimensions, and dependence on the size of latent vectors.
- (ii) By observing the dependence of prediction efficiency on systematically introduced noise in



the input database, we infer that an RS can identify a noisy (or fake) database from a genuine one.

(iii) Using two- and three-qubit registers, we compare the computational efficiency of RS prediction of quantum discord with that of the standard method. We demonstrate that, within certain precision limits, an RS can be considerably faster than the standard method. For example, starting from a sparse database of quantum discord, RS can completely fill it out an order of magnitude faster than the standard methods.

(iv) We then show the scalability of RS in larger systems by predicting quantum correlations and fidelities of unitary evolutions on registers with up to 10 qubits.

(v) We also examine the RS ratings of non-unitary evolutions by predicting discord changes and fidelities of a two-qubit system subjected to independent single-qubit decoherence channels.

(vi) Finally, we demonstrate another important application of RS prediction in studying quantum nonlinear systems. Specifically, we use the RS prediction to efficiently construct the phase space diagram of a quantum kicked top.

These studies help us understand and characterize the behaviour of systems in the deep quantum regime, and thereby aid in building efficient quantum protocols for quantum computing and information processing tasks.

## 2.2 Recommender system via matrix factorization

MFA represents the user-item interaction in a lower dimensional latent space [181]. Consider a set of  $m$  users and a set of  $n$  items. Each user  $i$  is represented using a parameter vector  $\Theta^{(i)} \in \mathbb{R}^f$  and each item  $j$  is represented using a feature vector  $X^{(j)} \in \mathbb{R}^f$  (Fig. 2.1(a)). Here  $\mathbb{R}^f$  is the coordinate space of dimension  $f$  over real numbers. The interaction between a user  $i$  and an item  $j$  is modeled by the scalar product

$$r_{i,j} = \Theta^{(i)} \cdot X^{(j)} = \sum_{l=1}^f \Theta_l^{(i)} X_l^{(j)} \quad (2.1)$$

that is conceived as the predicted rating. Now the task reduces to finding for all users and all items, the latent vectors consistent with known ratings and thereby making the best predictions about the unknown elements.

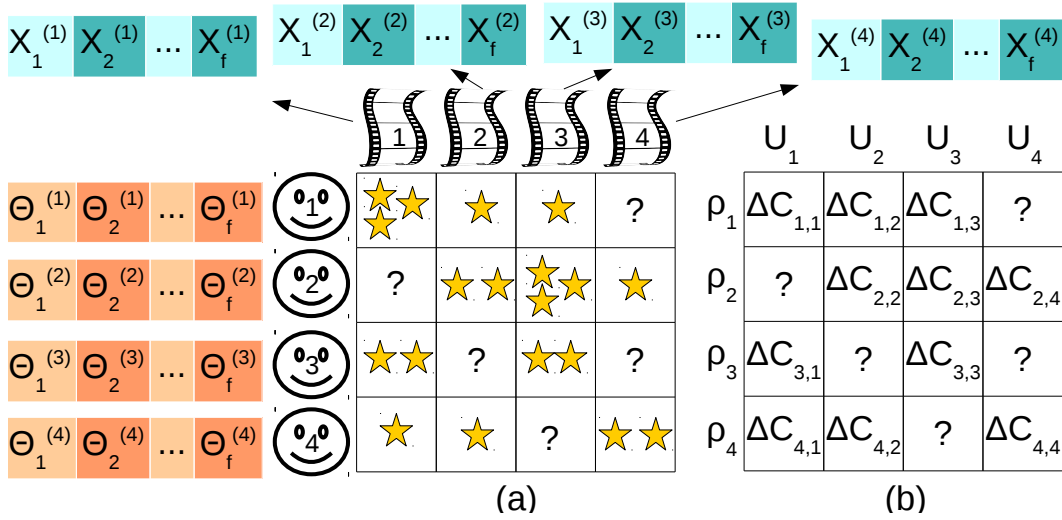


**Figure 2.1:** (a) Movie database. (b) Database of change  $\Delta C_{i,j}$  in quantum correlations of states  $\rho_i$  caused by evolutions  $U_j$ .

We start with random guesses for the latent vectors and evaluate rating elements  $r_{i,j}$ . Let  $\kappa = \{(i, j)\}$  be the set of user-item pairs for which the ratings  $\mathcal{R}_{i,j}$  are known. The mismatch between the evaluated and actual ratings is quantified by

$$J_0 = \sum_{(i,j) \in \kappa} (r_{i,j} - \mathcal{R}_{i,j})^2. \quad (2.2)$$

The next step is to optimize the latent vectors by minimizing the mismatch  $J_0$ . Over-fitting is avoided by including two regularization terms in the objective function

$$J = \frac{J_0}{2} + \frac{\lambda}{2} \sum_{i=1}^m \|\Theta^{(i)}\| + \frac{\lambda}{2} \sum_{j=1}^n \|X^{(j)}\|, \quad (2.3)$$

where  $\lambda$  is the regularization parameter and  $\|\cdot\|$  denotes the norm of the vector. We may now use the first-order gradient descent algorithm for the minimization task. The gradients in the  $k$ th

iteration can be cast as

$$\begin{aligned}
 G_{\Theta^{(i,k)}} &= \frac{\partial J^{(k)}}{\partial \Theta^{(i,k)}} \\
 &= \sum_{j \in \kappa(i, \cdot)} (r_{i,j}^{(k)} - \mathcal{R}_{i,j}) X^{(j,k)} + \lambda \Theta^{(i,k)}, \\
 G_{X^{(j,k)}} &= \frac{\partial J^{(k)}}{\partial X^{(j,k)}} \\
 &= \sum_{i \in \kappa(\cdot, j)} (r_{i,j}^{(k)} - \mathcal{R}_{i,j}) \Theta^{(i,k)} + \lambda X^{(j,k)},
 \end{aligned} \tag{2.4}$$

where  $\kappa(i, \cdot), \kappa(\cdot, j) \subset \kappa$  with the respective indices being fixed. The latent vectors for  $(k + 1)$ th iteration are now updated according to

$$\begin{aligned}
 \Theta^{(i,k+1)} &= \Theta^{(i,k)} - \alpha G_{\Theta^{(i,k)}} \text{ and} \\
 X^{(j,k+1)} &= X^{(j,k)} - \alpha G_{X^{(j,k)}},
 \end{aligned} \tag{2.5}$$

where  $\alpha$  is the suitable step size. After a final number  $K$  of iterations, with a desired value of the objective function, one can calculate the final rating  $r_{i,j}^{(K)} = \Theta^{(i,K)} \cdot X^{(j,K)}$  for all unknown elements  $(i, j) \notin \kappa$  [181, 182].

## 2.3 Adapting the recommender system

It is insightful to consider the example of viewers' ratings of movies. Every viewer rates some of the movies, thereby leaving an imprint of personal tastes or preferences, apart from assessing individual movies (Fig. 2.1(a)). The RS aims to predict ratings for movies not yet seen/rated by the viewer, considering the viewer's tastes as well as the recommendations provided by other viewers. In our RS, quantum states are viewers and quantum evolutions are movies (Fig. 2.1(b)). A state transformed by a quantum evolution undergoes a change in its internal quantum correlation that can be labeled as the state's rating of the evolution. Our objective is to predict unknown ratings in the state-evolution database.

Consider a database  $\mathcal{R}$  formed by  $n_s$  randomly generated quantum states  $\{\rho_1, \rho_2, \dots, \rho_{n_s}\}$  and  $n_u$  randomly generated unitary operators  $\{U_1, U_2, \dots, U_{n_u}\}$ . A random unitary operator is

generated by matrix exponentiation of a random anti-Hermitian generator. Random pure states are generated simply by normalizing a random vector of complex elements. We use Bures method [183, 184] to generate a random mixed state  $\rho = RR^\dagger/\text{Tr}[RR^\dagger]$  with  $R = (\mathbb{1} + U)A$ , where  $\mathbb{1}$  is the identity matrix,  $U$  is a random unitary operator, and  $A$  is a random complex matrix. An element of the database matrix  $\mathcal{R}$ , corresponding to  $i$ th state and  $j$ th unitary operator is the change in a measure  $C$  of quantum correlation,

$$\mathcal{R}_{i,j} = \Delta C_{i,j} = C(U_j \rho_i U_j^\dagger) - C(\rho_i). \quad (2.6)$$

We consider the following three measures of quantum correlation:

(i) *Von Neumann Entropy*  $S(\rho_i^A) = -\text{Tr}[\rho_i^A \log \rho_i^A]$  of a pure state  $\rho_i^{AB} = |\psi_i^{AB}\rangle\langle\psi_i^{AB}|$  [185]. The entropy change  $\Delta S_{i,j} = S(U_j \rho_i^A U_j^\dagger) - S(\rho_i^A)$  is listed in the database as entropy rating.

(ii) *Negativity* of a general quantum state  $\rho_i^{AB}$ , pure or mixed  $N(\rho_i^{AB}) = \frac{\|R_A\| - 1}{2}$ , where  $R_A$  is the partial transpose of  $\rho^{AB}$  with respect to the subsystem  $A$ , and  $\|R_A\| = \text{Tr}\sqrt{R_A^\dagger R_A}$  is the trace norm of  $R_A$ . The change in negativity brought about by a unitary operator  $U_j$  is  $\Delta N_{i,j} = N(U_j \rho_i^{AB} U_j^\dagger) - N(\rho_i^{AB})$ . Since the two-qubit negativity is bounded between 0 and 1/2, it is convenient to compare twice of negativity with other measures.

(iii) *Discord*  $D(\rho_i^{AB}) = I(\rho_i^{AB}) - \max_{\{\Pi^A\}} J(\rho_i^{AB})$ , where  $I(\rho_i^{AB}) = S(\rho_i^A) + S(\rho_i^B) - S(\rho_i^{AB})$  and  $J(\rho_i^{AB}) = S(\rho_i^B) - S(\rho_i^B|\rho_i^A)$  are the classically equivalent measures of mutual information [48, 186]. Discord is estimated numerically by maximizing  $J$  over all possible measurement bases  $\{\Pi^A\}$  in subsystem  $A$ . Despite being a stronger measure of quantum correlation, it has no simple analytical expression unlike entropy and negativity. Yichen Huang has recently shown that the complexity for computing discord is NP complete and the computational resource for computing discord is set to grow exponentially with the dimension of the Hilbert space [187]. Therefore it is interesting to see how well machine learning performs in predicting the change in quantum discord  $\Delta D_{i,j} = D(U_j \rho_i^{AB} U_j^\dagger) - D(\rho_i^{AB})$ . Of course, for an uncorrelated initial state, the prediction is an estimate of the discord content in the transformed state itself.

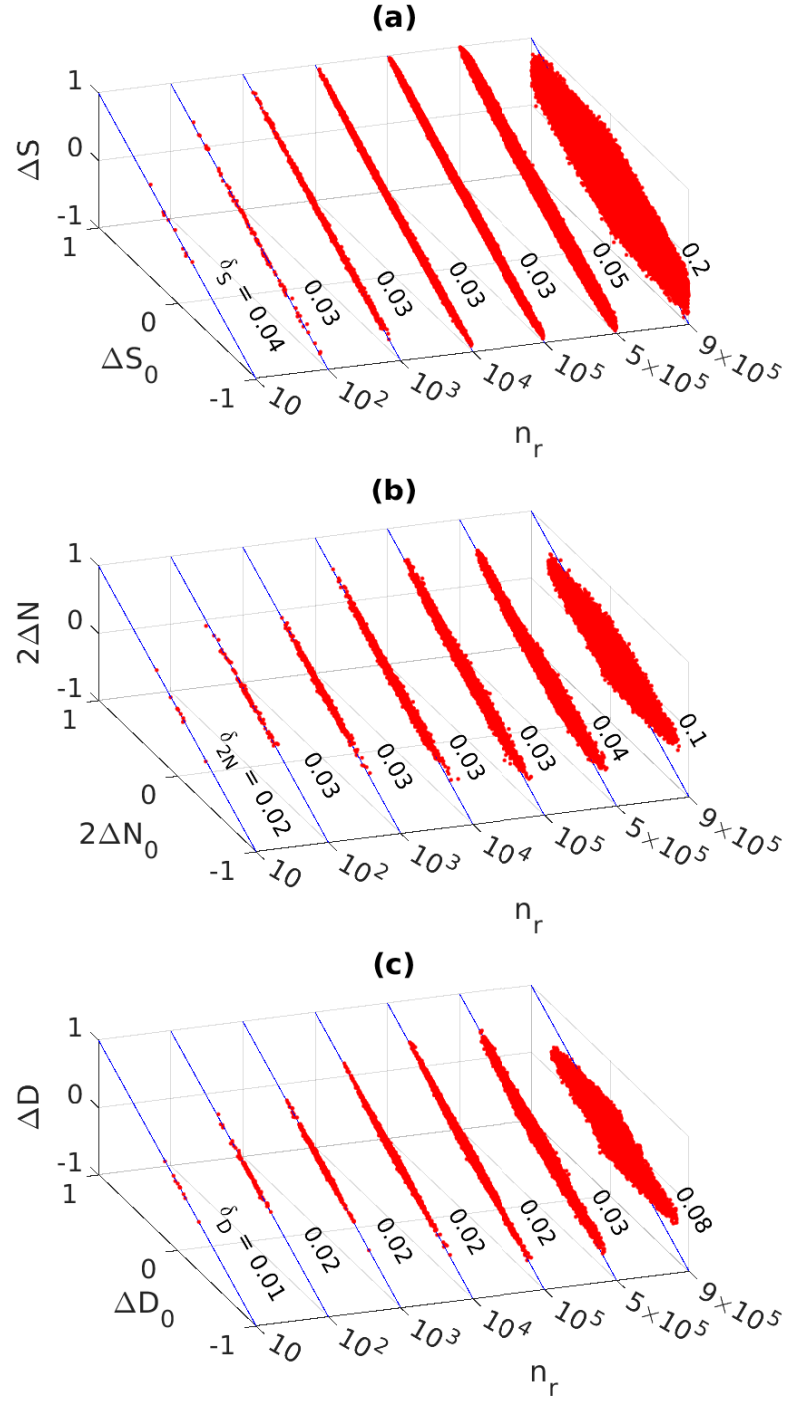


**Figure 2.2:** Red dots represent the RS predictions of changes in two-qubit correlations: entropy change  $\Delta S$  (a), negativity change  $2\Delta N$  (b), and discord change  $\Delta D$  (c), plotted against the actual values ( $\Delta S_0$ ,  $2\Delta N_0$ ,  $\Delta D_0$ ) and the number  $n_r$  of unknown elements in a database of 1000 states and 1000 unitary operators. Blue lines represent the ideal case  $\Delta C_0 = \Delta C$ . The RMSD value  $\delta_C$  is also shown in each case.

## 2.4 Rating unitary evolutions

We first consider a million-element rating database  $\mathcal{R}$  formed by  $n_s = 1,000$  randomly generated two-qubit quantum states and  $n_u = 1,000$  randomly generated two-qubit unitary evolutions. From the complete database, we randomly remove a set  $\bar{\kappa} = \{(i, j)\}$  of  $n_r$  elements, which are to be predicted by the RS. The prediction error is measured by the root-mean-square deviation (RMSD)

$$\delta_C = \left[ \sum_{(i,j) \in \bar{\kappa}} (\Delta C_{0_{i,j}} - \Delta C_{i,j})^2 \right]^{1/2}, \quad (2.7)$$

between the actual correlation changes  $\{\Delta C_{0_{i,j}}\}$  and their predicted values  $\{\Delta C_{i,j}\}$ . Results of the RS predictions for a two-qubit register are displayed in Fig. 2.2 (a-c). Here, the predicted values  $\Delta C$  are plotted versus the actual values  $\Delta C_0$  for various numbers  $n_r$  of unknown ratings. Entropy ratings (Fig. 2.2(a)) are for pure states, while the negativity (Fig. 2.2(b)) and discord ratings (Fig. 2.2(c)) are for mixed states. It is clear that the RS is quite successful in predicting the changes in all the correlation measures. Particularly, the discord predictions are impressive, and even better than that of other correlations. The RMSD values remained below 0.05, except for  $n_r = 9 \times 10^5$  which corresponds to 90% of the million-element database being unknown. A systematic growth of RMSD w.r.t.  $n_r$  is also observed, which is expected since, as the database becomes more and more sparse, the minimum in latent space turns shallower, and accordingly more uncertain will be the predictions.

### 2.4.1 Rating the Werner state

To observe the RS in action with a concrete example, we replace one of the random evolutions with the two-qubit controlled-NOT operation  $U_{\text{CNOT}} = |0\rangle\langle 0| \otimes \mathbb{1}_2 + |1\rangle\langle 1| \otimes \sigma_x$ , where  $\mathbb{1}_2$  is the  $2 \times 2$  identity operation and  $\sigma_x$  is the NOT gate. Additionally, we choose one of the input states to be the separable state,  $\rho_- = (1 - \epsilon)\mathbb{1}_4/4 + \epsilon|-\rangle\langle -| \otimes |1\rangle\langle 1|$ , where  $|-\rangle = (|0\rangle - |1\rangle)/\sqrt{2}$  is the single-qubit superposition state and the scalar quantity  $\epsilon$  is the purity of state. While the state  $\rho_-$  is a pure state for  $\epsilon = 1$  and becomes completely mixed for  $\epsilon = 0$ , it is separable for all values of  $\epsilon$ , and hence has zero negativity and discord. Upon acted by the CNOT operation,  $\rho_-$  transforms into the Werner state  $\rho_W = (1 - \epsilon)\mathbb{1}_4/4 + \epsilon|S_0\rangle\langle S_0|$ , which is the convex sum of the maximally

mixed state and the singlet state  $S_0 = (|01\rangle - |10\rangle)/\sqrt{2}$ . While  $\rho_W$  is quantum correlated and has nonvanishing discord for all values  $\epsilon > 0$ , it is entangled and has nonzero negativity for  $\epsilon > 1/3$  [186]. Here the RS is interesting as the initial state  $\rho_-$  is quantum uncorrelated and therefore the predictions correspond to the amount of discord or negativity in  $\rho_W$  itself. Fig. 2.3 plotting the predicted values  $\Delta N$  and  $\Delta D$  versus the purity factor  $\epsilon$  shows an excellent agreement between actual and predicted values. RMSD also remained less than 0.05 indicating the high quality of predictions.

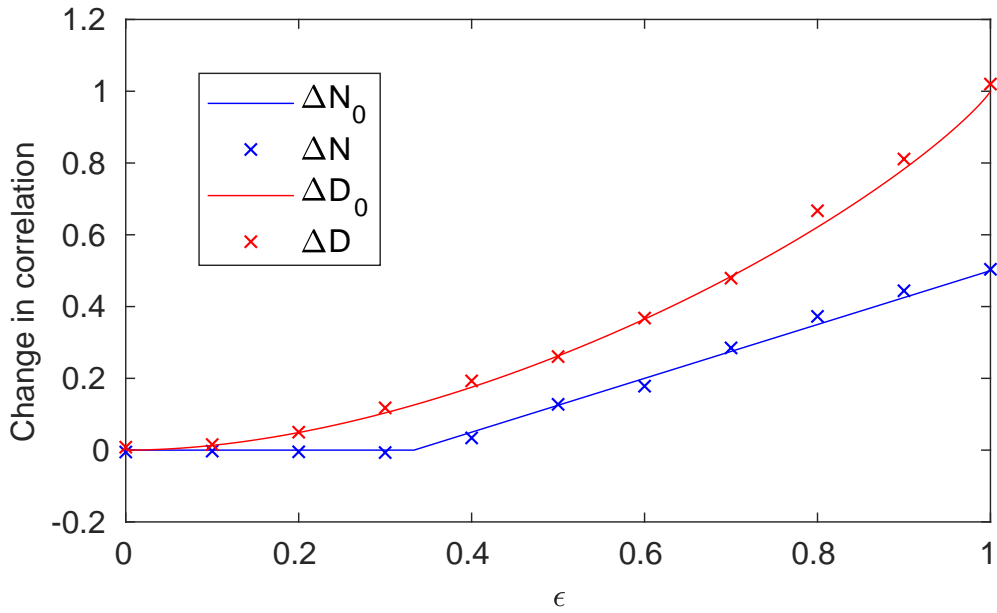


**Figure 2.3:** Symbols indicate the predicted values of  $\Delta N$  and  $\Delta D$  values for the quantum uncorrelated input state  $\rho_-$  transformed into the Werner state  $\rho_W$  by the CNOT operation. Solid lines represent actual values and symbols represent predicted values as indicated by the legend box. The RMSD values are  $\delta_{2N} = 0.026$  and  $\delta_D = 0.038$ .

### 2.4.2 Dependence on the dimensions of database and latent vector

Here we consider the two-qubit case. We can fix the number of unknown ratings  $n_r = 100$ , and vary the dimension of the database. We constructed a set of databases with number of states  $n_s$  varying from 10 to 10,000, and the number of unitaries  $n_u$  varying from 10 to 1000. Fig. 2.4(a-c) display RMSD values of entropy, negativity, and discord respectively. As expected, for a fixed number  $n_r$  of unknown ratings, the RS efficiency in terms of RMSD improves with the size of the database. We observe an interesting diagonal symmetry indicating better efficiency with roughly

equal number of states and evolutions. It is also interesting to note that while the entropy rating is the most sensitive to the database size, the discord rating is least sensitive.

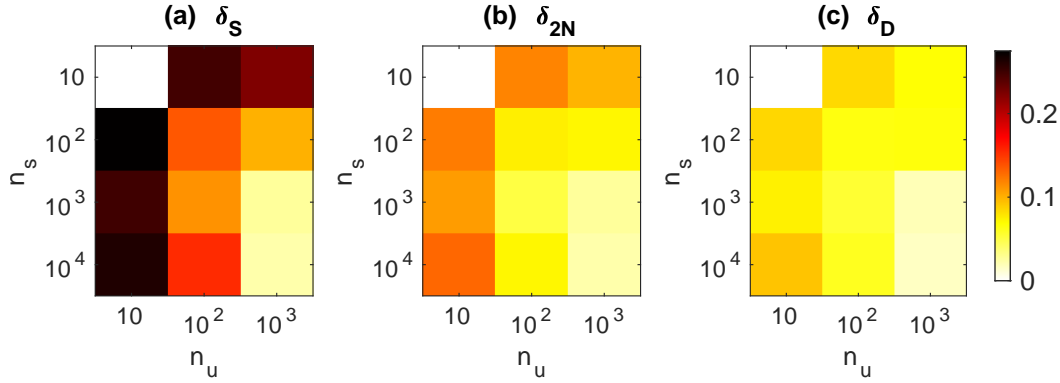


**Figure 2.4:** RMSD values of entropy (a), negativity (b), and discord (c), for various sizes of the database, but with fixed number  $n_r = 100$  of unknown ratings.

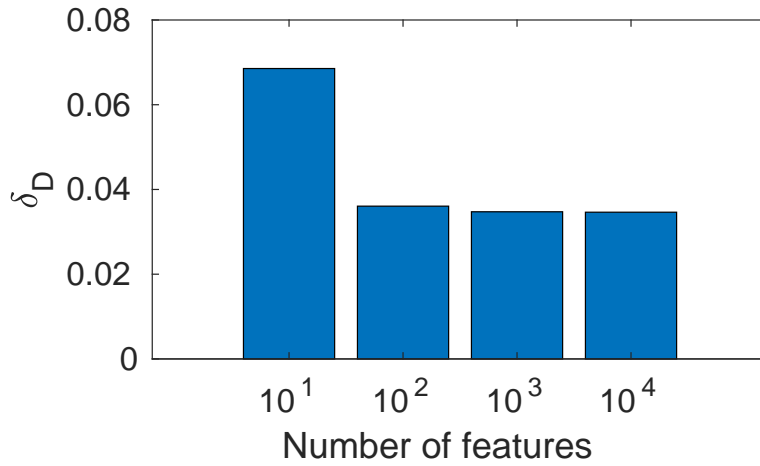


**Figure 2.5:** RMSD values of discord predictions versus number of features ( $f$ ) for 50% sparse  $1000 \times 1000$  database.

Since the latent-vectors capture the mathematical structure of the database and thereby help predicting the unknown ratings, the dimension of the latent space, i.e., number of features  $f$ , becomes very important. In the following example (Fig. 2.5) we consider a  $1000 \times 1000$  two-qubit database of discord ratings with 50% of elements being removed and predicted (i.e.,  $n_r = 500,000$ ). On running the RS for varying number of  $f$ , we find that if the latent vectors are too short, the prediction error becomes too large, since the RS fails to capture the underlying rules of the database. Too large latent vectors also render the RS over-determined and inefficient. One



can find the appropriate number of features with a few trial and error runs. In this particular case,  $f \sim 10^2$  would suffice.

### 2.4.3 Identifying noisy database

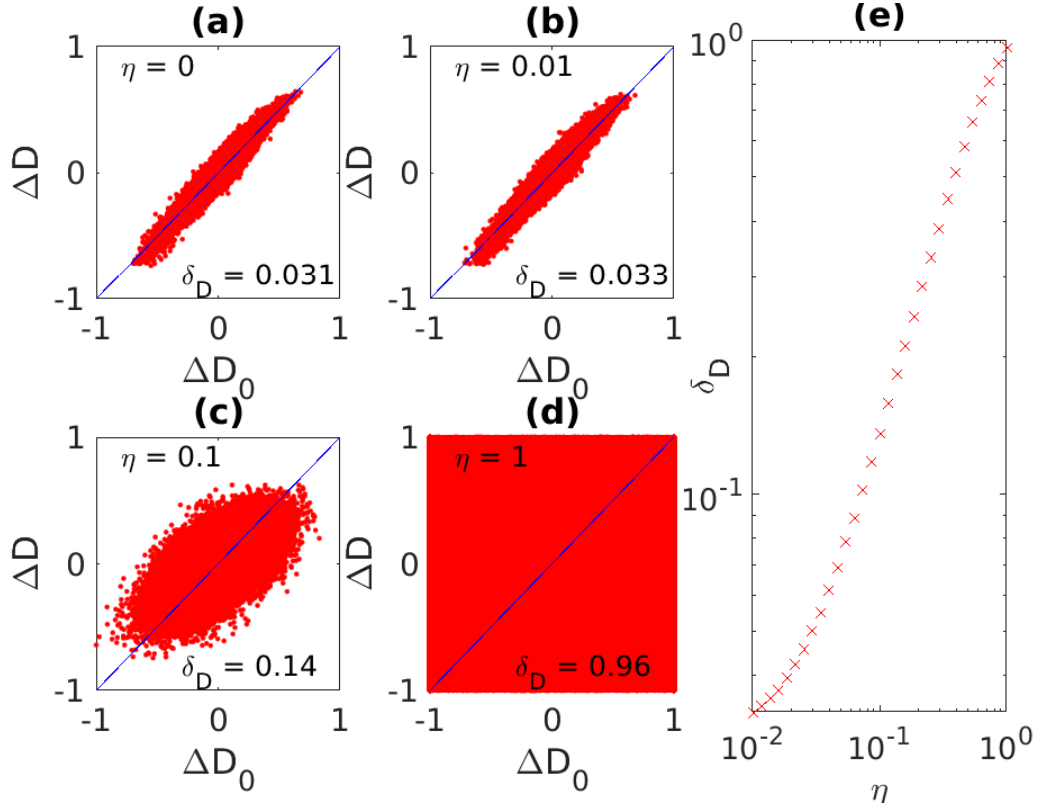


**Figure 2.6:** (a-d) Discord predictions with varying noise parameter  $\eta$ . (e) RMSD  $\delta_D$  versus  $\eta$ . The number of unknowns  $n_r = 500,000$ , which is 50% of the  $1000 \times 1000$  database.

What would be the dependence of prediction efficiency, if the input database itself is noisy, unreliable, or even fake? What if there are no underlying structures in the database so that no latent space exists? Can we use this dependency for asserting if a database, with or without a large number of unknown elements, is genuine or not? In order to probe these questions, we choose discord rating in a two-qubit register. We first construct a  $1000 \times 1000$  noise-free discord database  $\mathcal{R}^{(0)}$ , from which we setup a noisy database  $\mathcal{R}^{(\eta)} = \eta S + (1 - \eta)\mathcal{R}^{(0)}$ , where  $S$  is a random matrix of same dimensions and the noise parameter  $\eta \in [0, 1]$ . Thus, as  $\eta$  discretely varies from 0 to 1, the corresponding database goes from a clean discord database to a random matrix. In each database, corresponding to a fixed value of  $\eta$ , we randomly remove 500,000 entries constituting

50% of elements. We now attempt to predict the missing elements starting from each of these databases. The results shown in Fig. 2.6 indicates that for small noise parameter  $\eta \leq 0.01$ , there is no significant effect on the RMSD value. However, as the noise builds up, the RS finds it increasingly difficult to rate the entries, and RMSD increases by about five times for 10% noise. Finally, as expected, the RS completely fails for the completely random database corresponding to  $\eta = 1$ . Thus, if a control database is provided, the RS can help assess the quality of a target database.

### 2.4.4 Computational Time

Since computing quantum discord is *hard*, it is interesting to compare the computational time  $\tau_{\text{RS}}$  for the RS prediction of quantum discord with the calculation time  $\tau_{\text{std}}$  by the standard approach that involves subtracting maximum possible classical correlation from total correlation [48, 186].

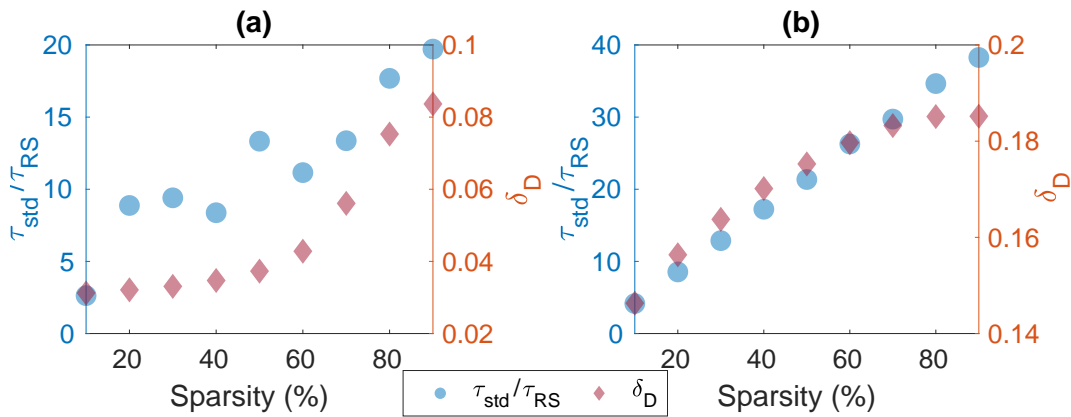


**Figure 2.7:** Computational advantage  $\tau_{\text{std}}/\tau_{\text{RS}}$  (left-vertical axes) and RMSD  $\delta_D$  (right-vertical axes) vs database sparsity (in this case  $n_r/10000$ ) for two- (a) and three-qubit (b) registers.

First we consider a  $1000 \times 1000$  two-qubit database. For a two-qubit system, an optimal set of measurements exists that substantially reduces computational time for estimating the discord [188]. Even in this case, RS brings about a substantial advantage by factors ranging from 3 to 20 for 10% to 90% sparsity of the database, while ensuring RMSD values below 0.1 (Fig 2.7(a)). Unlike the two-qubit case, no optimal measurement-sets are known for larger registers. Therefore we also analyze the RS computational efficiency in a  $1000 \times 1000$  three-qubit database (Fig 2.7(b)). In this case, the computational advantage is up to 40, i.e., almost doubled over the two-qubit case, albeit at the cost of higher RMSD values. Thus RS predictions, within certain

precision limits, can be much faster than the standard calculations.

### 2.4.5 Predicting state fidelity

Like predicting quantum correlations, one can also predict the state-fidelity in the same manner. For a set of pure input states  $\{|\psi_i\rangle\}$  and unitary evolution  $\{U_i\}$ , the database elements  $\mathcal{R}_{i,j} = F_{i,j}(\psi_i, U_j) = |\langle\psi_i|U_j|\psi_i\rangle|^2$  describe the fidelity of output state  $U_j|\psi_i\rangle$  with the input state  $|\psi_i\rangle$ . Similarly, for a set of mixed input states  $\{\rho_i\}$  we may use the Uhlmann trace distance  $\mathcal{R}_{i,j} = F_{i,j}(\rho_i, U_j) = \left| \text{Tr} \sqrt{\rho_i^{1/2} U_j \rho_i U_j^\dagger \rho_i^{1/2}} \right|^2$ . Of course, here instead of the input state, one could have also chosen any other target state. The results of the fidelity predictions using a database of 1000 random states and 1000 unitary evolutions with  $n_r$  unknown elements are shown in Fig. 2.8. Interestingly, the rating is extremely successful for pure states (Fig. 2.8(a)), for which up to 50% of unknown elements ( $n_r = 5 \times 10^5$ ) can be predicted with a low RMSD  $\delta_F \leq 0.003$ . For mixed states the RMSD values are relatively higher, but still  $\delta_F \leq 0.02$  for predicting up to 50% of unknown elements. However, in both cases the predictions fail for 90% of unknown elements.

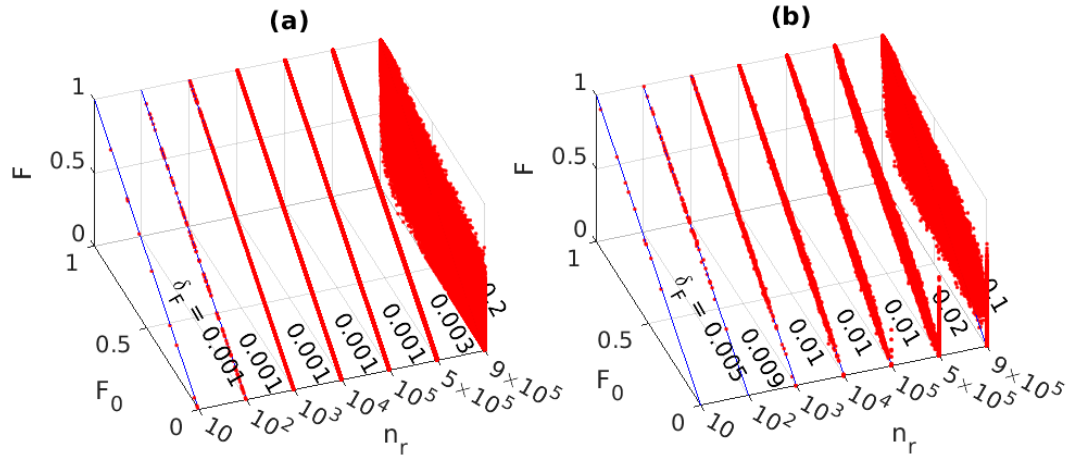


**Figure 2.8:** Predicted fidelity  $F$  versus actual fidelity  $F_0$  and the number  $n_r$  of unknown elements for pure (a) and mixed (b) states. Blue lines represent the ideal case  $F = F_0$ . The RMSD value  $\delta_F$  is shown in each case.

### 2.4.6 Identifying local and nonlocal operators:

Suppose the objective is not to obtain quantitative values for the changes in quantum correlations introduced by unitary operators, but rather to identify local and nonlocal unitary operators. For

this purpose, we generate a database with 1000 randomly generated unitaries, 500 of which are by construction local operators of the form  $U_A \otimes U_B$  that do not change quantum correlations. The remaining  $4 \times 4$  dimensional random unitaries  $U_{AB}$  are mostly nonlocal and introduce changes in quantum correlations. These propagator act on 1000 randomly generated initial states, so that the overall size of the database is  $10^6$ .

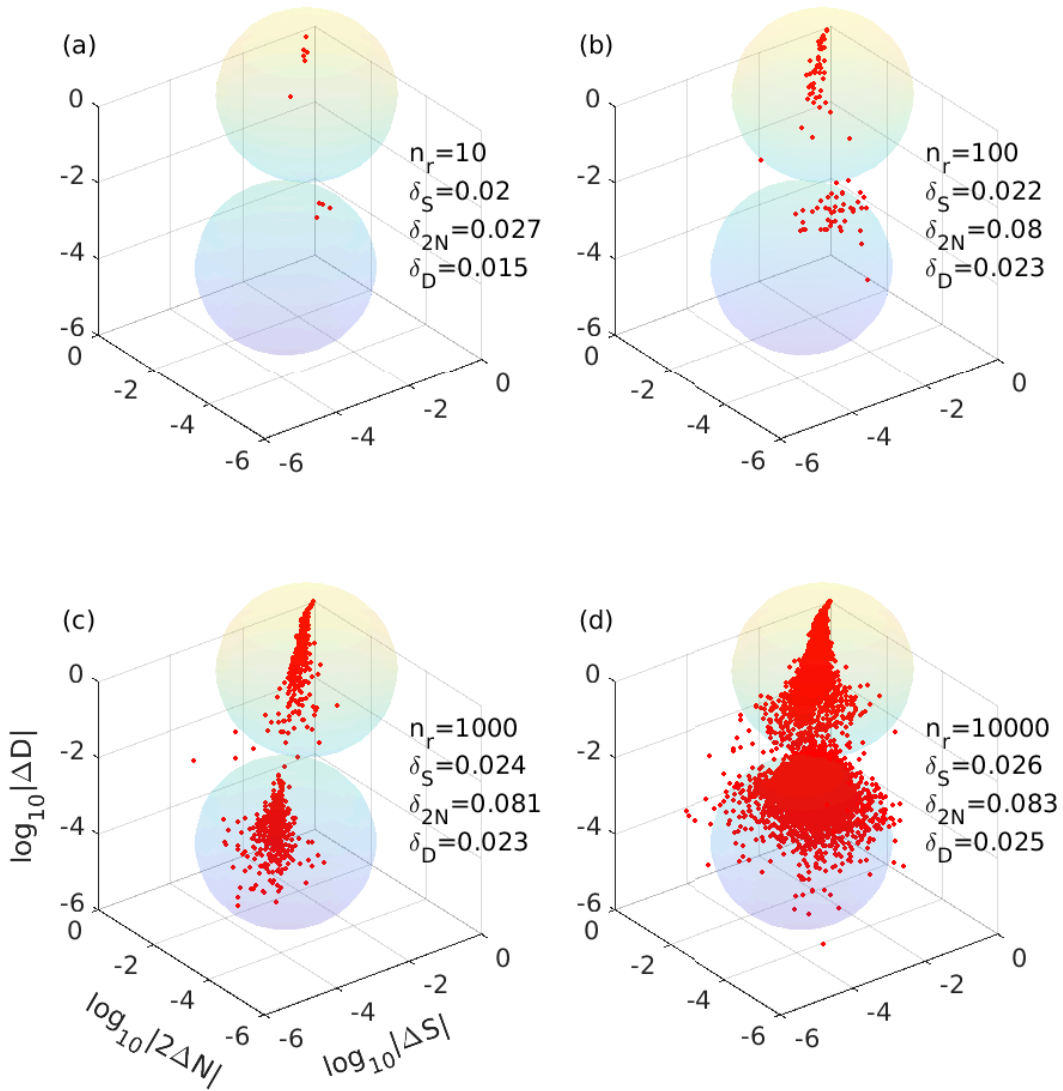


**Figure 2.9:** Binning unitaries into local or nonlocal by predicting the changes in quantum correlations. Subplots correspond to different numbers  $n_r$  of predicted ratings as indicated in each case.

Fig. 2.9 shows the three-dimensional simultaneous plots of predicted entropy, negativity, and discord values for various numbers  $n_r$  of unknown ratings. It is clear that most of the points fall into one of the two bins - negligible correlation changes resulting from local unitaries, or

significant correlation changes brought about by nonlocal unitaries.

### 2.4.7 Scaling to larger registers

We now study the efficiency of the RS in larger quantum registers, with sizes up to 10 qubits. For each register, we constructed a database with 100 random unitary operators and 100 random quantum states. The number of unknown ratings was fixed at  $n_r = 100$ . In larger registers, there are multiple ways of partitioning the system for estimating quantum correlations. For the sake of simplicity, we first partition the whole system of  $n_q$  qubits into two parts: a two-qubit part  $P$  and  $n_q - 2$  qubit part  $Q$ . We estimated quantum correlations in the two-qubit part  $\rho^P = \text{Tr}_Q[\rho^{PQ}]$ , after tracing out  $Q$ . Owing to the small subspace selected, the absolute change of correlation decreases rapidly with the number of qubits. For comparison purposes, we use the rescaled correlation change  $\Delta_C/m_q$ , with  $m_q = \max\{|\Delta C_{0,i,j}|, |\Delta C_{i,j}|\}$  where maximum is taken over all the  $n_r$  rated elements corresponding to the  $n_q$ -qubit register. Fig. 2.10 displays the predicted values of changes in entropy (Fig. 2.10(a)) as well as discord (Fig. 2.10(b)) versus the actual values for various sizes of quantum registers with up to 10 qubits. Here the RMSD values are calculated with respect to the rescaled correlation changes. Despite the smaller size of database, the predictions were largely in agreement with the actual values, and the RMSD values mostly remained below 0.3, thus confirming the feasibility of the RS predictions for various system sizes.

We have also studied the fidelity rating in multi-qubit registers. Fig. 2.10 also displays the results of the fidelity rating of pure (Fig. 2.10(c)) and mixed (Fig. 2.10(d)) states in registers with up to 10 qubits. In each case, we used a database of 100 states and 100 unitaries, while the number of unknown entries was fixed to 100. It is clear that the fidelity rating is largely successful in all these cases.

## 2.5 Rating nonunitary evolutions

Here we consider a noisy two-qubit system with independent single-qubit decoherence channels each of which having an operator-sum representation in terms of Kraus operators  $\{M_k\}$  [189].

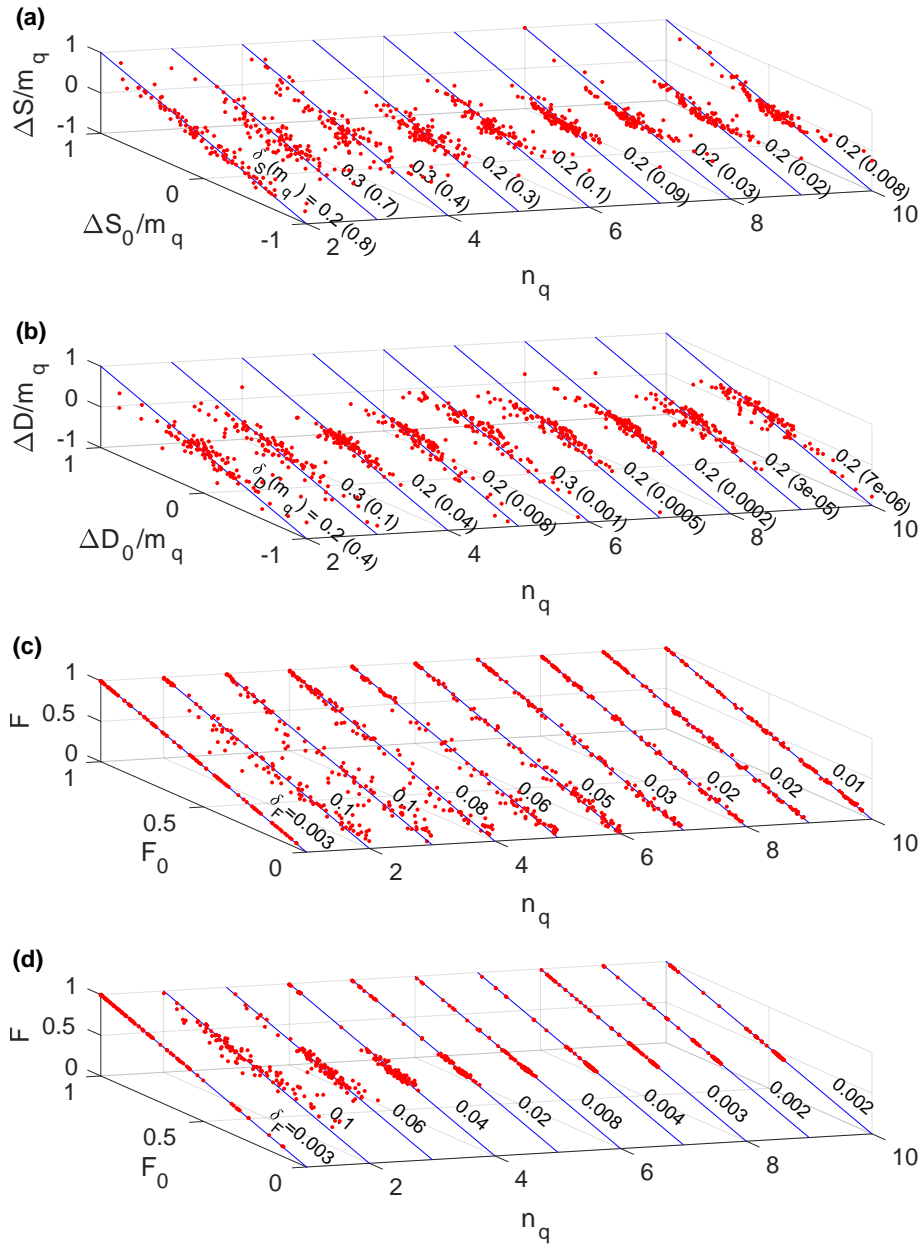


**Figure 2.10:** RS predictions of (a) entropy, (b) quantum discord, (c) fidelity of pure states, and (d) fidelity of mixed states, for registers with  $n_q$  qubits. The RMSD values  $\delta$  are shown in each case and the maximum range  $m_q$  (in parenthesis) are shown in (a) and (b).

An input state  $\rho_i^{AB}$  transforms according to

$$\begin{aligned} \mathcal{E}_j(\rho_i^{AB}) &= \frac{1}{2} \sum_k (M_k^{jA} \otimes \mathbb{1}) \rho_i^{AB} (M_k^{jA} \otimes \mathbb{1}) \\ &\quad + \frac{1}{2} \sum_l (\mathbb{1} \otimes M_l^{jB}) \rho_i^{AB} (\mathbb{1} \otimes M_l^{jB}), \end{aligned} \quad (2.8)$$

wherein the single-qubit channels  $j_A$  and  $j_B$  belong to one of the following channels: bit-flip, phase-flip, bit & phase-flip, depolarization, and amplitude damping as shown below.

(i) Bit-flip:  $M_1^X = \sqrt{x} \mathbb{1}$ ,  $M_2^X = \sqrt{1-x} \sigma_x$ ,

(ii) Phase-flip:  $M_1^Z = \sqrt{z} \mathbb{1}$ ,  $M_2^Z = \sqrt{1-z} \sigma_z$ ,

(iii) Bit & phase-flip:  $M_1^Y = \sqrt{y} \mathbb{1}$ ,  $M_2^Y = \sqrt{1-y} \sigma_y$ ,

(iv) Depolarization:  $M_1^D = \sqrt{1 - \frac{3d}{4}} \mathbb{1}$ ,  $M_2^D = \frac{\sqrt{d}}{2} \sigma_x$ ,  
 $M_3^D = \frac{\sqrt{d}}{2} \sigma_y$ ,  $M_4^D = \frac{\sqrt{d}}{2} \sigma_z$ , and

(v) Amplitude damping:

$$M_1^A = \begin{bmatrix} 1 & 0 \\ 0 & \sqrt{1-a} \end{bmatrix}, M_2^A = \begin{bmatrix} 0 & \sqrt{a} \\ 0 & 0 \end{bmatrix}.$$

Here  $x, y, z, a, d$  are randomly chosen channel probabilities and  $\sigma_x, \sigma_y$ , and  $\sigma_z$  are Pauli operators.

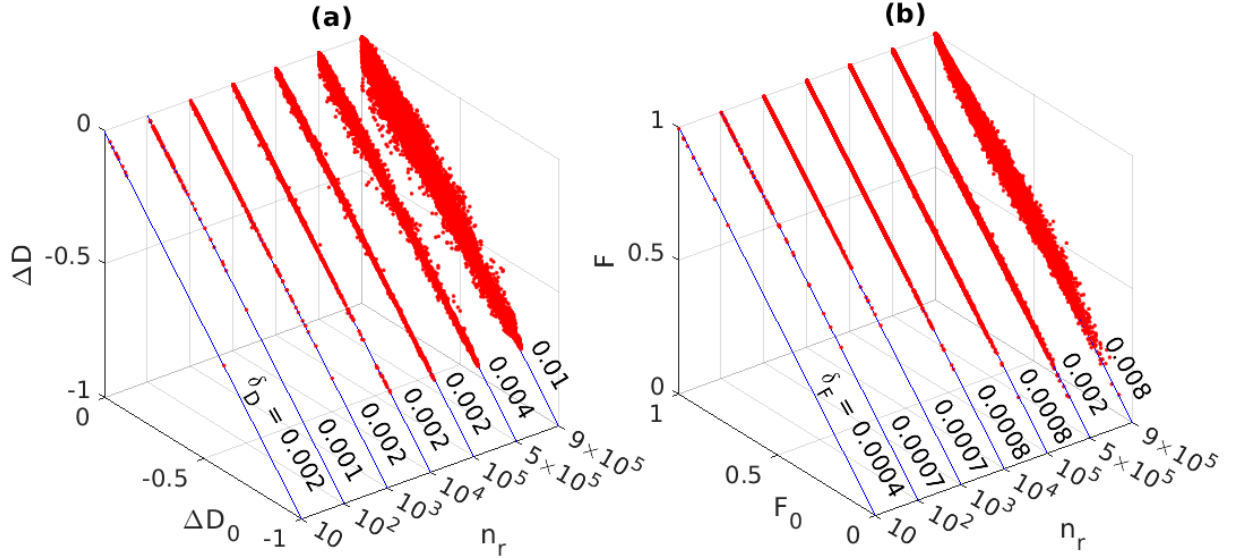


**Figure 2.11:** The RS predictions of nonunitary evolutions. Predicted values (red points) for changes in discord (a) and fidelity (b) versus actual values and the number  $n_r$  of unknown elements. In each case, the size of the database is  $1000 \times 1000$ . Blue lines represent the ideal curves. The RMSD values are shown in each case.

We form a random database of 1000 mixed two-qubit states and 1000 nonunitary evolutions, with a particular pair of channel probabilities, acting independently on the individual qubits. Fig. 2.11 displays the predicted values of change in discord  $\Delta D_{i,j} = D(\mathcal{E}_j(\rho_i)) - D(\rho_i)$  (Fig. 2.11(a))

and of Fidelity  $F_{i,j}(\rho_i, \mathcal{E}_j) = \left| \sqrt{\sqrt{\rho_i} \mathcal{E}_j(\rho_i) \sqrt{\rho_i}} \right|^2$  (Fig. 2.11(b)), plotted versus the actual values for various numbers  $n_r$  of unknown elements. Since the decoherence channels only reduce quantum correlations,  $\Delta D$  is essentially negative. It is evident that the prediction is highly successful, with the RMSD values being 0.01 or lesser even at 90% of unknown elements.

## 2.6 Construction of quantum phase space

As the demonstration of a specific application of RS predicted quantum correlation database, we now describe an efficient construction of discord phase space for studying quantum chaos. Implications of quantum chaos for quantum information processing is well studied [190, 191]. Classical chaos is often studied by observing the trajectory of a dynamical system in a certain phase space [192]. It has been shown that quantum discord phase space can be used to study quantum chaos of a dynamical quantum system [193]. However, the discord calculation is not based on a compact analytical expression, instead requires expensive computation overhead. In the following, we show that RS can efficiently generate discord phase space for quantum dynamical systems, such as a quantum kicked top (QKT) with the Hamiltonian

$$H = \frac{\kappa}{2j\tau} J_z^2 + \frac{\pi}{2} J_x \sum_{n=0}^{\infty} \delta(t - n\tau). \quad (2.9)$$

Here  $\mathbf{J} = [J_x, J_y, J_z]$  is the angular momentum vector of an effective spin- $j$  system. The first term represents the nonlinear evolution for a duration  $\tau$  with chaoticity parameter  $\kappa$ . The second term represents periodic linear kicks. The time evolution is governed by the Floquet propagator

$$U_{QKT} = e^{-i(\pi/2)J_x} e^{-i\kappa J_z^2/(2j)}. \quad (2.10)$$

We model the QKT system using 2 qubits. Starting from an initial state  $|00\rangle$ , we prepare the spin coherent state  $|\theta, \phi\rangle \otimes |\theta, \phi\rangle$ , where

$$|\theta, \phi\rangle = \cos(\theta/2) |0\rangle + e^{i\phi} \sin(\theta/2) |1\rangle \quad (2.11)$$

by first rotating each qubit with an angle  $\theta$  about the y-direction followed by an angle  $\phi$  about the



z-direction in the Bloch sphere.

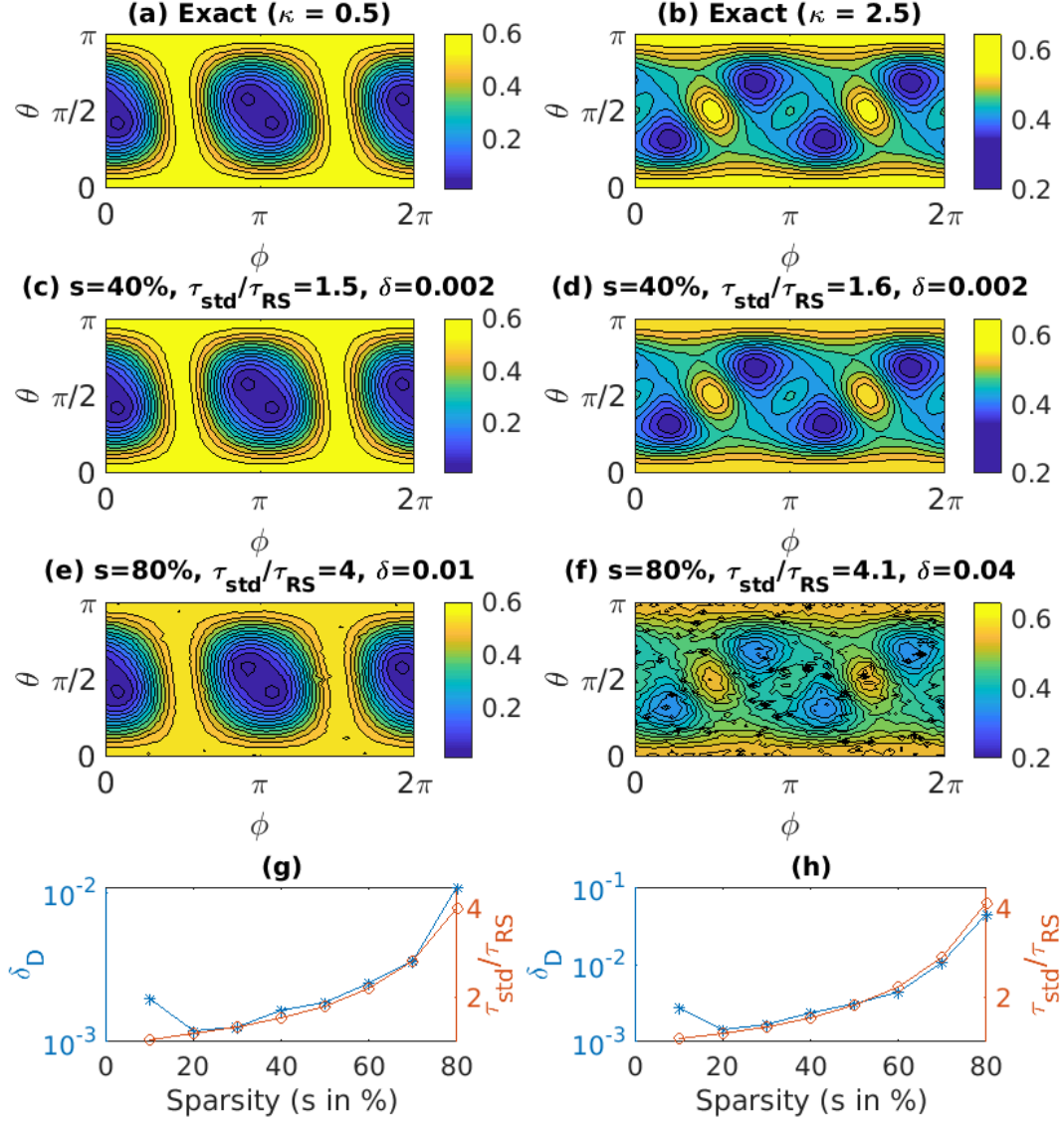


**Figure 2.12:** Discord phase space plots (a-f) for chaoticity parameter  $\kappa = 0.5$  (first column) and for  $\kappa = 2.5$  (second column). The exact phase space plots in (a) and (b) are constructed with standard method, while the other phase space plots are predicted by RS method with sparsity value of either 40% (c,d) or 80% (e,f). The RMSD values ( $\delta_D$ ) quantifying the mismatch between the exact and the RS predicted phase space plots, as well as the corresponding time advantage factors ( $\tau_{\text{std}}/\tau_{\text{RS}}$ ) are also plotted against varying sparsity values (g,h).

Fig. 2.12 shows discord phase space plots of the two-qubit QKT for two chaoticity values viz.,  $\kappa = 0.5$  (first column) and  $\kappa = 2.5$  (second column) obtained by averaging over 100 kicks with a  $51 \times 51$  grid of  $\theta$  and  $\phi$  coordinates. We compare the exact discord phase space diagrams (Fig. 2.12 (a,b)) with those predicted by RS (c-f) using a total feature number  $n_f = 100$ . As expected, at low chaoticity value of  $\kappa = 0.5$ , the QKT mostly undergoes a regular dynamics

and the phase space exhibits large regions of closed trajectories. However, at a higher chaoticity value of  $\kappa = 2.5$ , it undergoes a rather complex dynamics whose phase space exhibits intricate patterns with smaller regular islands surrounded by chaotic ocean. It is evident that for  $\kappa = 0.5$ , RS predicted phase space plots are almost identical with the exact plot even for sparsity value of 80%. It is interesting to see that at higher chaoticity value of  $\kappa = 2.5$ , RS prediction matches well for the sparsity value of 40%, while worsens for 80%. This further reinforces the idea that the chaotic regimes of dynamical systems are hard to predict in general. The sensitivity of QKT to experimental imperfections in such chaotic regimes has been reported earlier by Krithika et al. [194]. Hence, it is natural that RS finds it challenging to recognize the underlying patterns in the database, based on which it can predict the missing entries. In spite of this difficulty, the overall predicted phase space pattern with 80% sparsity is qualitatively similar to the exact one. The RMSD values ( $\delta_D$ ) between the exact and the predicted plots, along with the computational time-advantage ( $\tau_{\text{std}}/\tau_{\text{RS}}$ ) are plotted versus sparsity values in Fig. 2.12 (g,h). While there is a trade off between the prediction error and the time-advantage, it is clear that the RS prediction is quite robust and efficient, and is about four times faster for 80% sparsity. The advantage is likely to be even higher for larger dimensional quantum systems.

## 2.7 Summary and outlook

We have adapted a class of recommender systems, called the matrix factorization algorithm, to characterize quantum evolutions in terms of quantum correlations as well as state-fidelity. First, using two-qubit databases, we have carried out a detailed analysis of the recommender system predicting three types of correlations, namely entropy, negativity, and discord. We found that the recommender system was able to efficiently predict well over 50% of unknown elements in the database. As a particular example, we showed that predictions of negativity and discord of Werner state prepared with different purities matched very well with the expected values. By introducing noise into the database in a systematic way, we observed the prediction efficiency deteriorating with noise. We proposed that this fact, along with a reference database, could be used to distinguish a genuine or clean database from a noisy or a fake database. Predicting quantum discord of a general state, for which a closed-form expression does not exist, is most interesting.

The analysis of computational time shows that the machine prediction, within certain precision limits, can be far more efficient. In million-element databases of two- and three-qubit registers, we observed over an order of magnitude improvement in computational time. To show that the characterization of quantum evolutions via recommender system is scalable with system size, we have demonstrated predicting quantum correlations as well as fidelities of unitary evolutions on larger multiqubit registers with up to ten qubits. We have also demonstrated the capability of the recommender system in characterizing nonunitary evolutions by subjecting it to predict correlation and fidelity ratings of states undergoing certain decoherence channels. Finally, we demonstrate a robust RS prediction of discord phase space diagrams useful to study quantum chaotic systems.

When does the RS fail? We have earlier discussed the noisy database having no underlying pattern and thus fails to converge. RS can fail in many other scenarios. For example, the RS can not predict elements of an empty row or column of a database. We have demonstrated that for a fixed number of unknowns, the prediction error gets worse by shrinking the database along any dimension. Rating a state (or gate) that is far away from all other members of the database may be difficult. We also found that too short latent vectors also fail to capture the mathematical structure beneath the database. For an intricate database, like that of long-range quantum correlations, one needs larger latent vectors and more powerful global optimization methods.

Although here we have only discussed databases of random states and random evolutions, it is straightforward to adapt it to other interesting scenarios such as quantum process tomography [195] and in predicting quantum correlations in a time-evolving many-body system initialized with various possible states. It would also be interesting to predict the behavior of quantum systems under evolutions dictated by more sophisticated master equations. Further improvisations in the precision and speed of machine predictions will go a long way as well. The remarkable efficiency of the recommender system in characterizing quantum evolutions hints at an underlying mathematical structure that may deserve further exploration. We anticipate that such machine learning techniques not only aid the evolution of quantum technologies but also provide deeper insights into mathematical structures in quantum theory itself.



## CHAPTER 3

---

# Recommender System Expedited Quantum Control Optimization

---

### Abstract

Quantum control optimization algorithms are routinely used to synthesize optimal quantum gates or to realize efficient quantum state transfers. The computational resource required for the optimization is an essential consideration in order to scale toward quantum control of larger registers. Here, we propose and demonstrate the use of a machine learning method, specifically the recommender system (RS), to deal with the challenge of enhancing computational efficiency. Given a sparse database of a set of products and their customer ratings, RS is used to efficiently predict unknown ratings. In the quantum control problem, each iteration of a numerical optimization algorithm typically involves evaluating a large number of parameters, such as gradients or fidelities, which can be tabulated as a rating matrix. We establish that RS can rapidly and accurately predict elements of such a sparse rating matrix. Using this approach, we expedite a gradient ascent based quantum control optimization, namely GRAPE, and demonstrate the faster construction of two-qubit CNOT gate in registers with up to 8 qubits. We also describe and implement the enhancement of the computational speed of a hybrid algorithm involving simulated annealing as well as gradient ascent. Moreover, the faster construction of three-qubit Toffoli gates further confirmed the applicability of RS in larger registers.

### Reported in

**Priya Batra**, M. Harshanth Ram, and T.S. Mahesh, *Recommender system expedited quantum control optimization*, [Physics Open](#), page 100127, 2022

### 3.1 Introduction

Quantum control is crucial for the trending quantum technology tasks such as quantum sensing [196], scalable quantum information devices [197], quantum simulations [198], quantum thermodynamics [199], quantum metrology [200], etc. In general, quantum control optimization deals with finding the best implementation of desired quantum dynamics on a given physical hardware [201, 202]. Such optimization algorithms are routinely used for control tasks like unitary synthesis, state transfer [203], quantum parameter estimation [204], etc. There has been a tremendous progress in this area and numerous optimization algorithms have been developed, such as gradient based algorithms [205, 206], variational principle based algorithms [207, 208], chopped basis optimization [209, 210], and metaheuristic algorithms [211, 212]. Lately, machine learning algorithms such as reinforcement learning (RL), have also been used for the tasks like unitary transformation [213], state preparation [214], robust controls [215], as well as to control non-integrable quantum systems [216]. More recently, machine learning protocols have also been used to control quantum thermal machines [217].

A variety of quantum control algorithms have been designed to address different aspects [218, 219]. Superior convergence rate was realized using methods such as variational methods [207, 208], higher-order gradient methods (eg. Quasi-Newton BFGS) [220], using chopped random basis [209, 210], and by push-pull algorithm [221]. Searching for global optimum was made possible by evolutionary algorithms [212, 222]. Robust solutions that overcome imperfections in the control fields can be realized by adiabatic methods [223], combining gradient methods with simulated annealing [224], machine learning [215], etc. Control sequences with physical constraints such as total/maximum power, bandwidth etc., can be achieved by using methods such as incoherent error compensation [225], functional space quantum control [226], auto-GRAPE [227, 228] etc. It is also possible to accommodate environmental effects to improve robustness against decoherence [229–231]. Hybrid methods have also been developed that address multiple aspects simultaneously [224, 232, 233]. An important aspect is the computational efficiency of the algorithm. While there have been several attempts in this direction [222, 234, 235], here we propose a machine learning approach that efficiently evaluates the control sequence, thereby greatly improving the computation speed.

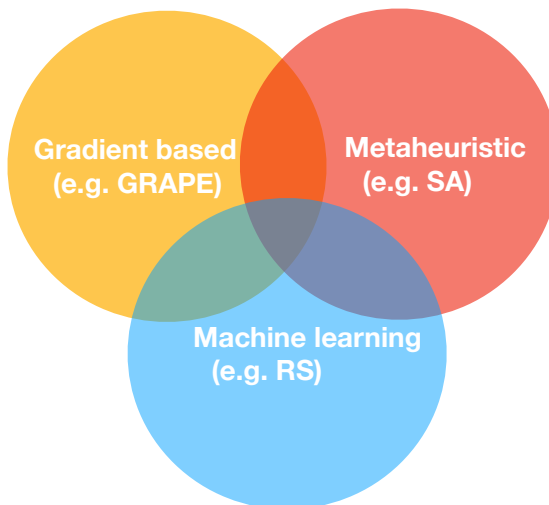


**Figure 3.1:** Expediting gradient method, metaheuristic method, as well as a hybrid of both by using machine learning.

### 3.1.1 Objectives

In the field of machine learning, the recommender system (RS) algorithm is widely used to recommend products to consumers [236, 237]. Here we propose RS assisted speed up of quantum control algorithms. Although the method is quite general and is applicable to a variety of algorithms, we choose to describe it in two cases, namely, a gradient based algorithm and a metaheuristic algorithm, as described below (see Fig. 3.1). Importantly, we demonstrate a significant time advantage of RS expedited algorithms without sacrificing their convergence. In particular, we have performed the following:

- (i) An optimization method with an analytical expression for the gradient is an efficient way to find a local optimum in the parameter space. One such class of optimization algorithms for quantum control applications is based on gradient ascent pulse engineering (GRAPE) [205] and its variants (for example, [220, 221, 226]). The most time-expensive task in GRAPE is the calculation of gradients for every segment of a control sequence in each iteration, which involves exponentiation of matrices. We show that, given a set of exactly calculated gradients, RS can accurately and rapidly predict the remaining ones. Thus, we can significantly improve the time-efficiency of the GRAPE optimization algorithm.
- (ii) Although GRAPE works well for a smooth parameter space, it becomes problematic if there are too many sub-optimal local solutions restricting the algorithm from reaching an optimal so-

lution. On the other hand, metaheuristic algorithms can escape the local optima and therefore perform a robust search in the parameter space. The metaheuristic algorithms such as the Nelder-Mead simplex method [211], evolutionary algorithms [212, 222, 238, 239], simulated annealing (SA) [224], etc. have been successfully adapted for quantum control optimization.

(iii) However, unlike the gradient methods, the metaheuristic algorithms often suffer from slow convergence. To overcome this issue, recently the SAGRAPE algorithm, a hybrid of SA and GRAPE, has been proposed [224]. SA involves a large number of function evaluations in the neighborhood of an iterative solution, which makes it computationally heavy. Here we also demonstrate expediting SA using RS by efficiently predicting the fidelities of the neighborhood points.

## 3.2 Quantum Control Optimization

We consider a quantum system with a constant internal Hamiltonian  $H_0$  and  $m$  control Hamiltonians  $\{H_j\}$ , such that the time-dependent Hamiltonian is given by

$$H(t) = H_0 + \sum_{j=1}^m \omega_j(t) H_j. \quad (3.1)$$

Here  $\omega_j(t)$  is the time-dependent strength of the  $j$ th control Hamiltonian  $H_j$ . For a closed system undergoing Schrödinger evolution for the time duration  $T$ , the corresponding unitary is given by

$$U(T) = D e^{-i \int_0^T H(t) dt}. \quad (3.2)$$

Here  $D$  is the Dyson time ordering operator and we have set  $\hbar = 1$ . Considering the difficulty in evaluating the propagator of a general time-dependent Hamiltonian, we discretize the control function  $\omega_j(t)$  by dividing it into  $N$  segments, each with a constant amplitude  $\omega_{j,k}$  and duration  $\delta = T/N$ . The corresponding unitary for the  $k$ th segment would be

$$U_k = \exp \left[ -i \delta \left( H_0 + \sum_{j=1}^m \omega_{j,k} H_j \right) \right]. \quad (3.3)$$



The total time propagator  $U(T)$  for the entire control sequence can be expressed as the product of segment unitaries

$$U(T) = U_N U_{N-1} \cdots U_2 U_1. \quad (3.4)$$

In this article, we mainly focus on unitary synthesis, although some methods can be adapted for state preparation. Thus, the optimization procedure is aimed at achieving a specific target unitary  $U_t$  by numerically generating the control sequence  $\{\omega_{j,k}\}$ . Optimization function is given by the gate fidelity

$$F = |\text{Tr} [U^\dagger(T)U_t]|^2, \quad (3.5)$$

which is the overlap of target unitary  $U_t$  with the evolved unitary  $U(T)$ . An improved optimization function would maximize the fidelity while minimizing resources. Typically, it amounts to minimizing the power consumption of control fields. Therefore the modified optimization function  $J$  can be cast as follows

$$J = F - \sum_{j,k} \lambda_j \omega_{j,k}^2, \quad (3.6)$$

where  $\lambda_j$  are the scalar penalty parameters. In the following, we discuss two optimization methods, first a gradient method and second a metaheuristic method.

### 3.2.1 Gradient Ascent Pulse Engineering (GRAPE)

The GRAPE algorithm has the following steps:

- Start with a random control sequence  $\{\omega_{j,k}^{(0)}\}$ .
- Forward propagate the initial unitary operator  $U_0 = \mathbb{1}$  till  $k$ th segment, i.e.,  $X_k = U_k U_{k-1} \cdots U_1 U_0$ .
- Backward propagate the target unitary  $U_t$  till  $k$ th segment, i.e.,  $P_k = U_{k+1}^\dagger U_{k+2}^\dagger \cdots U_N^\dagger U_t$ .
- Calculate the gradient for each segment using the first-order (in the norm  $\|\delta H(t)\|$ ) expression [205]

$$g_{j,k} = 2\text{Re} \left( -i\delta \text{Tr} \left[ P_k^\dagger H_j X_k \right] \text{Tr} \left[ X_k^\dagger P_k \right] \right). \quad (3.7)$$

- Update control amplitudes in the direction of gradients, i.e.,  $\omega_{j,k} \rightarrow \omega_{j,k} + \epsilon g_{j,k}$ , where  $\epsilon$  is the step size.

GRAPE is remarkable to have such a simple analytical form for the gradient function.

In a practical scenario, no physical hardware is perfect. For example, a control field is typically associated with a distribution of amplitudes around the nominal value [205]. We need to have a robust quantum control even with such imperfect hardware. To this end, one minimizes the overall cost function  $1 - \bar{J} = 1 - \sum_i p_i J_i$  obtained by summing over the costs  $1 - J_i$  of individual elements in the distribution with respective probabilities  $p_i$ .

### 3.2.2 Simulated Annealing (SA)

In metallurgy, annealing involves heating a material to high temperatures followed by slow cooling to allow the material reach a stable crystalline form by finding its ground state. The same idea is adopted in the numerical procedure namely, simulated annealing (SA) [240, 241]. Given an optimization problem, SA starts with a high-temperature configuration, wherein even non-optimal solutions are selected with a certain probability. As the iterations pass, the temperature parameter is gradually reduced, and optimal solutions are increasingly favored. This stochastic process allows the algorithm to overcome the local minima and reach the global minimum.

The steps for SA are as follows [224]:

- Start with a random control sequence  $\{\omega_{j,k}^{(0)}\}$ . Set the temperature to a high value  $T^0$ .
- In the  $i$ th iteration, determine the control sequence  $\{\omega'_{j,k}\}$  with the best fidelity  $\bar{F}(\{\omega'_{j,k}\})$  among a random set of points in the neighbourhood of the current solution  $\{\omega_{j,k}^{(i)}\}$ .
- If  $\Delta\bar{F}^i = \bar{F}(\{\omega'_{j,k}\}) - \bar{F}(\{\omega_{j,k}^{(i)}\}) \geq Q^i$ , where  $Q^i = -\min \left[ 1, T^i \exp \left( \Delta\bar{F}^i / T^i \right) \right]$  then  $\{\omega_{j,k}^{(i+1)}\} = \{\omega'_{j,k}\}$ ; else,  $\{\omega_{j,k}^{(i+1)}\} = \{\omega_{j,k}^{(i)}\}$ .
- After  $i$ th iteration, set the temperature to a reduced value  $T^{(i+1)} = \gamma T^{(i)}$ , where  $\gamma < 1$  controls the cooling rate.

The above steps are iterated until the desired optimization function is reached or the maximum number of iterations are completed. Note that, for higher temperatures the algorithm may take

a new solution  $\{\omega'_{j,k}\}$  even if its fidelity is lower than the current solution  $\{\omega_{j,k}^{(i)}\}$ . This stage is known as *exploration*. As temperature goes down, the algorithm gradually switches to the *exploitation* mode and it looks for solutions that are either better or only slightly inferior than the current solution. The combination of exploration and exploitation helps SA to escape local optima and travel towards the global optimum.

In our previous work, we had combined SA with GRAPE to form the hybrid SAGRAPE algorithm and demonstrated its superior convergence [224]. In the following, we first describe recommender system, a particular type of machine learning technique, and then explain how it can be used to expedite GRAPE as well as SAGRAPE.

### 3.3 Recommender System (RS)

Collaborative filtering is one of the most popular types of RS that is based on the experience of any particular consumer along with relative preferences among all consumers [242, 243]. Here we use the matrix factorization algorithm for collaborative filtering [169, 244]. It involves setting up a database  $\mathcal{R}$  in the form of a rating matrix, wherein each row represents a particular consumer and each column represents a particular product that is being recommended [237, 245]. The rating matrix can be decomposed in terms of latent vectors of the same dimension  $f$ , known as the number of features. Let the parameter vector  $\Theta^{(i)} \in \mathbb{R}^f$  and the feature vector  $\Phi^{(j)} \in \mathbb{R}^f$  encode latent vectors in real space  $\mathbb{R}^f$  for  $i$ th consumer and  $j$ th product. The predicted rating is then modeled by scalar products

$$r_{i,j} = \Theta^{(i)} \cdot \Phi^{(j)}. \quad (3.8)$$

Depending on the problem at hand, one can specify products, users, as well as ratings, and accordingly set up the rating matrix. One such example, for a hypothetical quantum control problem of executing certain specific tasks with various available control fields, is illustrated in Fig. 3.2. In this example, tasks are users, control fields are products, and the ratings are different levels of feasibility of implementing tasks. The job of RS is to efficiently predict the unknown ratings.

Given a sparse rating matrix  $\mathcal{R}$ , where missing elements correspond to unknown preferences, our goal is to fill those missing elements with the help of the collective information embedded in

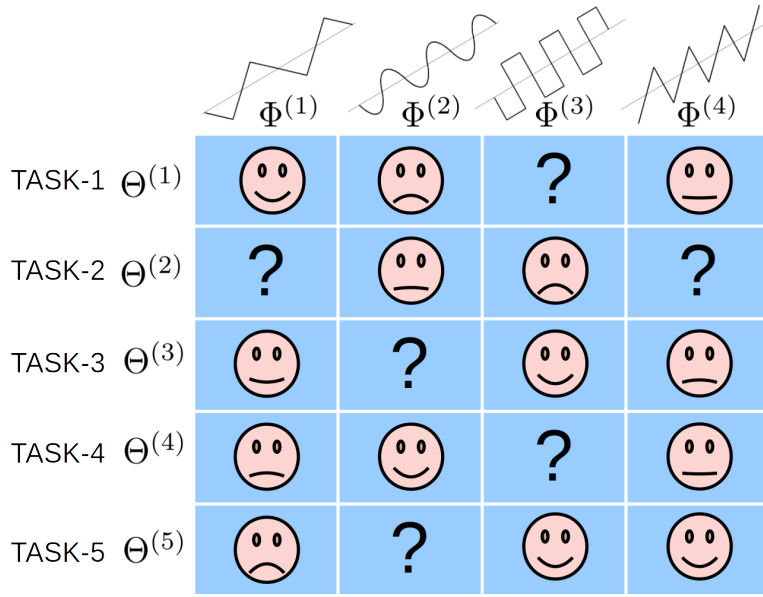


**Figure 3.2:** Illustrating an example application of RS. Here the rating matrix corresponds to different levels of feasibility of various tasks with certain available control fields. The goal of RS is to predict the unknown ratings.

the overall database. Let  $\kappa = (i, j)$  be the elements in the rating matrix for which actual ratings  $\mathcal{R}_{i,j}$  are known. The discrepancy between predicted rating  $r_{i,j}$  and actual rating  $\mathcal{R}_{i,j}$  is quantified by the function  $K_0$  as

$$K_0 = \sum_{(i,j) \in \kappa} (r_{i,j} - \mathcal{R}_{i,j})^2. \quad (3.9)$$

Here, the objective is to minimize the cost function  $K_0$ . Generally two regularization parameters  $(\Lambda_\Theta, \Lambda_\Phi)$  are used to avoid over-fitting, so that the altered cost function can be written as

$$K = \frac{K_0}{2} + \frac{\Lambda_\Theta}{2} \sum_{i=1}^m \|\Theta^{(i)}\| + \frac{\Lambda_\Phi}{2} \sum_{j=1}^n \|\Phi^{(j)}\|. \quad (3.10)$$

The latent vectors  $\Theta^{(i)}$  and  $\Phi^{(j)}$  are then determined by minimizing the cost function using any standard minimization algorithm. In our case, we use the Polack-Ribiere flavour of conjugate gradients to compute search directions and a line-search using quadratic and cubic polynomial approximations for this purpose [182, 246, 247].

### 3.4 RS enhanced GRAPE and SAGRAPE

We shall now explain how we can use RS to speedup GRAPE as well as SAGRAPE. For the sake of clarity, we use the context of quantum control of spin-dynamics via nuclear magnetic resonance (NMR). To study RS enabled speedup, we consider a spin system of  $M = 2 + n$  on-resonant heteronuclear qubits and construct a controlled-NOT (CNOT) gate on the first two qubits, which are coupled by an indirect spin-spin interaction of strength ( $J_{12}$ ). For simplicity, we treat the remaining  $n$  qubits as noninteracting spectator spins, which contribute to the dimension of the overall Hilbert space but not to the complexity of the CNOT gate. This helps us to demonstrate the efficiency of RS expedited algorithms for varying size of qubit register with the same gate complexity. The internal NMR Hamiltonian for the system in the multiply-rotating frame is given by

$$H_0 = 2\pi J_{12} I_z^1 I_z^2, \quad (3.11)$$

where  $I_z^i$  represents the  $z$ -component of the  $i$ th spin operator. For the  $k$ th segment of the  $n + 2$  channel control sequence, the total Hamiltonian

$$H_k = H_0 + \sum_{j=1}^{2+n} \omega_{x,j,k} I_x^j + \omega_{y,j,k} I_y^j. \quad (3.12)$$

Here  $\omega_{x,j,k}$  and  $\omega_{y,j,k}$  are the  $x$  and  $y$  components of radio frequency (RF) field on the  $j$ th nuclear species in  $k$ th segment of the control sequence. In practice however, there exists a spatial RF inhomogeneity (RFI) of amplitudes over the volume of the sample. One usually models RFI with an  $L$ -point distribution and associates a scaling factor  $\{\xi_{j,l}\}$  with respective probabilities  $\{p_{j,l}\}$ . Thus, the Hamiltonian for the  $k$ th control segment with the  $l$ th RFI element is

$$H_k^{(l)} = H_0 + \sum_{j=1}^{2+n} \xi_{j,l} \omega_{x,j,k} I_x^j + \xi_{j,l} \omega_{y,j,k} I_y^j. \quad (3.13)$$

As explained in the last part of Sec. 3.2.1, the overall cost function  $1 - \bar{J} = 1 - \sum_l p_l J_l$  is obtained by the weighted sum of cost functions of all the individual elements in the RFI distribution. In the following, we describe how we can incorporate RS to expedite GRAPE.

RFI	$l = 1 \dots$			
Qubits	$j=1 \dots$		$j=2+n$	
phases				
segments (k)	x	y	x	y
1	$g_{x,1,1,1}$	$g_{y,1,1,1}$	?	$g_{y,2+n,1,1}$
2	$g_{x,1,2,1}$	?	$g_{x,2+n,2,1}$	?
3	$g_{x,1,3,1}$	$g_{y,1,3,1}$	?	$g_{y,2+n,3,1}$
4	?	$g_{y,1,4,1}$	$g_{x,2+n,4,1}$	?
$\vdots$	$\vdots$	$\vdots$	$\vdots$	$\vdots$

**Table 3.1:** The rating matrix for RSGRAPE. Here rows correspond to various segments ( $k = 1, 2, \dots, N$ ) and columns correspond to the  $x(y)$  RF amplitudes on all the heteronuclear qubits ( $j = 1, 2, \dots, 2+n$ ) with various RFI distribution elements ( $l = 1, 2, \dots, L$ ). The elements  $g_{x(y),j,k,l}$  are the gradients, and the goal of RS is to predict the unknown elements (indicated by ‘?’).

### 3.4.1 RS expedited GRAPE (RSGRAPE)

Let us first consider the GRAPE algorithm for the NMR context described above. As explained in Sec. 3.2.1, the  $x(y)$  gradients for the  $j$ th channel in  $k$ th segment with  $l$ th RFI element are expressed by the explicit form of Eq. 3.7, i.e.,

$$g_{x(y),j,k,l} = 2\text{Re} \left( -i\delta \text{Tr} \left[ P_{k,l}^\dagger I_{x(y)}^j X_{k,l} \right] \text{Tr} \left[ X_{k,l}^\dagger P_{k,l} \right] \right). \quad (3.14)$$

Here  $X_{k,l}$  and  $P_{k,l}$  are respectively the forward and backward propagators for the  $k$  segment with  $l$ th RFI element. In the traditional GRAPE algorithm, one evaluates all the gradients and then calculates the update values for the control amplitudes as described in Sec. 3.2.1. This is the heart of the algorithm and involves evaluating a large number of propagators via matrix exponentiation. Accordingly, this is the bottleneck for numerical efficiency, especially for the larger number of qubits. Here comes the application of machine learning. Instead of evaluating all the gradients, we only need to evaluate a fraction of the gradients, form a rating matrix, and then let RS predict the rest of the gradients. In the language of RS, we treat each segment as a consumer and each RF amplitude (corresponding to indices  $x(y), j, l$ ) as a product. The corresponding rating matrix is in the form of the TABLE 3.1.

We first study the dependence of RSGRAPE on the sparsity of the rating matrix. To this end,

we generate a two-qubit CNOT gate while varying the sparsity of the rating matrix from 0% to 90%. In each case, we monitor, at the end of 500 iterations, the final infidelity and the time advantage

$$\Gamma(\text{RSGRAPE}) = \tau(\text{RSGRAPE})/\tau(\text{GRAPE}), \quad (3.15)$$

the ratio of computational times of RSGRAPE and GRAPE.

We now demonstrate RSGRAPE for generating an optimal control sequence implementing a CNOT gate on the first two qubits of the  $2 + n$  qubit system. In our analysis we have varied  $2 + n$  from 2 to 8 and in each case generated an optimal control sequence with  $N = 200$  segments. For RS prediction we used latent vectors of dimension 10. RFI is modeled by  $L = 5$  point distribution with  $\xi_{j,l} \in \{0.8, 0.9, 1.0, 1.1, 1.2\}$  and uniform probability  $p_{j,l} = 0.2$ . Firstly, we vary the sparsity ( $s$ ) from 10% to 90% and compare the gradients for the standard GRAPE ( $g_a$ ) vs gradients predicted by RS ( $g_p$ ) as shown by red dots in Fig. 3.3 (a). For reference, also shown are the ideal expected curves  $g_a = g_p$  (in blue lines in Fig. 3.3 (a)). It's clear that RS is able to predict the gradients quite efficiently, especially for sparsity values below 70%. As expected, for larger sparsity values, the RS predictions gradually become inaccurate, and therefore convergence of the algorithm is affected.

Now, we iterate (for  $i = 1, \dots, 500$ ) GRAPE as well as RSGRAPE algorithms. In Fig. 3.3 (b), we plot the final infidelity  $1 - \bar{F}$  (circles) as well as time advantage  $\Gamma(\text{RSGRAPE})$  (stars) vs sparsity ( $s$ ) for two (solid curves) and four (dashed curves) qubit systems. Here for reliable analysis, all the data points are obtained by averaging 10 independent trials each starting from a random initial guess. We find that the final infidelity remains low ( $< 0.005$ ) till about 70% sparsity and increases afterward. Also, we achieve time advantages up to a factor of two or more, for both two and four qubits systems.

We now set the sparsity of the rating matrix to 50%, meaning only half the number of gradients randomly selected out of the total  $2N(2 + n)L$  elements need to be evaluated using Eq. 3.14. The rest of the gradients in each iteration are predicted by the RS algorithm. Again, for reliable analysis, we average the results of 15 independent trials of RSGRAPE algorithm each starting from a random initial guess. For comparison, we also carry out the standard GRAPE algorithm in each case and monitor the time advantage  $\Gamma(\text{RSGRAPE})$ . Fig. 3.3 (c) shows the infidelity

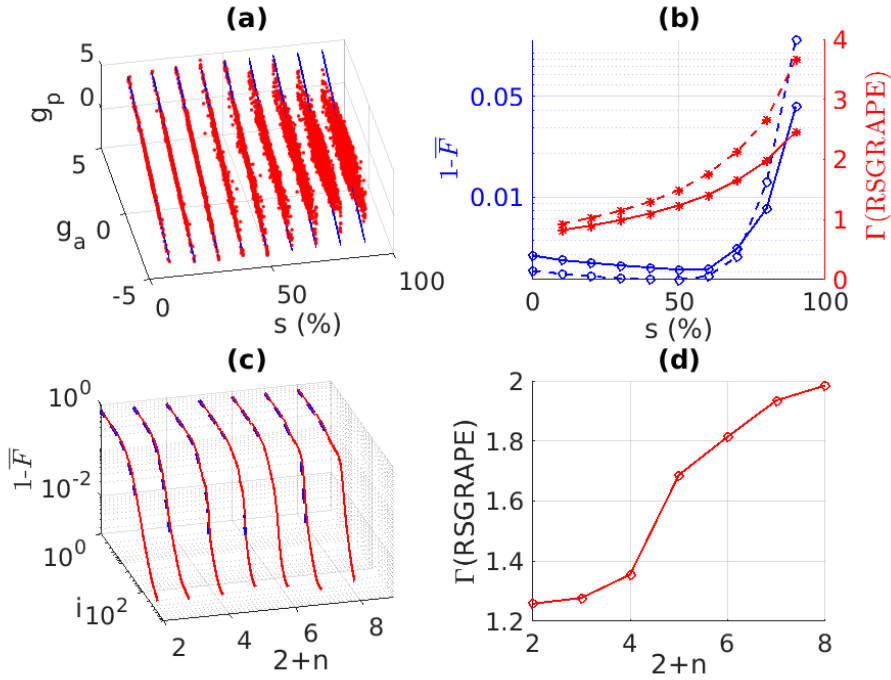


**Figure 3.3:** (a) Exact  $g_a$  and predicted  $g_p$  gradients vs sparsity ( $s$  in %). (b) Infidelity  $1 - \bar{F}$  (circles) and time advantage  $\Gamma(\text{RSGRAPE})$  (stars) vs sparsity ( $s$  in %) of a CNOT gate generated using RSGRAPE in two (solid line) and four (dashed line) qubit systems. (c) Infidelity  $1 - \bar{F}$  vs number  $i$  of iterations varying from 1 to 500 and for size  $2 + n$  of the qubit register varying from 2 to 8. Here solid-red and dashed-blue lines correspond to RSGRAPE and GRAPE algorithms. (d)  $\Gamma(\text{RSGRAPE})$  vs size  $2 + n$  of the qubit register. Here (c) and (d) are obtained with a sparsity value of 50 %.

$(1 - \bar{F})$  versus iteration number  $i$  for various sizes  $2 + n$  of the qubit register. It is clear that the convergence of RSGRAPE is not compromised compared to the standard GRAPE algorithm, despite only 50% of the gradients being exactly evaluated. In all the cases, the infidelity was well below 0.01.

Fig. 3.3 (d) shows the time-advantage for various sizes of the qubit register with 50% sparsity of the rating matrix. For small qubit registers (up to 4 qubits), the advantage is above 20%, while for larger registers (for 8 qubits), we find almost 100% time advantage. This is because the RS overhead is dependent on (i) the dimension of the rating matrix, which increases only linearly with the size of the qubit register, and (ii) the dimensions of latent vectors. Therefore, as the complexity of GRAPE algorithm increases exponentially with the size of the qubit register, the RS overhead becomes increasingly insignificant, and the time-advantage improves. However, for 50 % sparsity,  $\Gamma(\text{RSGRAPE})$  remains bounded by a factor of 2.

We now discuss the importance of efficient prediction of gradients. To this end, we randomly



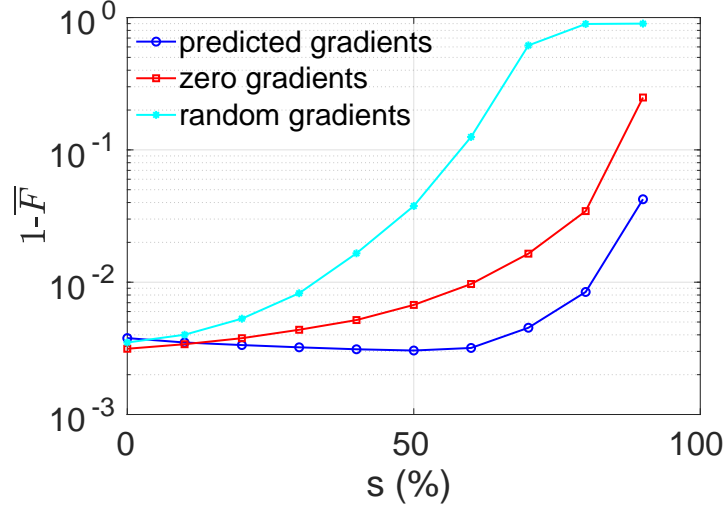


**Figure 3.4:** Averaged final infidelity ( $1 - \bar{F}$ ) vs sparsity for three different schemes of handling the sparse elements.

select  $s\%$  of the sparse elements in the rating matrix in each iteration and apply one of the following three schemes: (i) RS predicted gradients, (ii) zero-gradients, i.e., segments unchanged from the previous iteration, and (iii) random gradients. We now compare the final infidelity ( $i = 500$ ) for a two-qubit CNOT gate obtained with these methods. The results averaged over 10 independent trials are shown in Fig. 3.4. As expected, replacing the sparse elements with random gradients completely fails the optimization. Keeping zero-gradients, or retaining the segments from the previous iteration for a small sparsity is tolerable. However, RS predicted gradients are most efficient and lead to the least final infidelity values even up to 80% sparsity.

To further demonstrate RS prediction in a multiqubit register, we generated a 1000 segment ( $\delta = 20 \mu\text{s}$ ) Toffoli gate on a three qubit register with  $J_{12} = 1000 \text{ Hz}$ ,  $J_{23} = 1000 \text{ Hz}$ , and  $J_{13} = 100 \text{ Hz}$ . Fig. 3.5 displays the infidelity of GRAPE (dashed line) and RSGRAPE (solid line) with 50% sparsity averaged over five independent trials. In this case, we obtained an average time advantage  $\Gamma(\text{RSGRAPE}) = 1.42$ .

To emphasize the scalability with larger registers, we now consider the case of a 6 qubit system having the similar Hamiltonian structure as shown previously. The task is to create a two-qubit CNOT gate between the first two qubits. Fig. 3.6 (a) represents the infidelity vs iteration for GRAPE (blue) and RSGRAPE (red) obtained with 50% sparsity. Here, the thick lines indicate

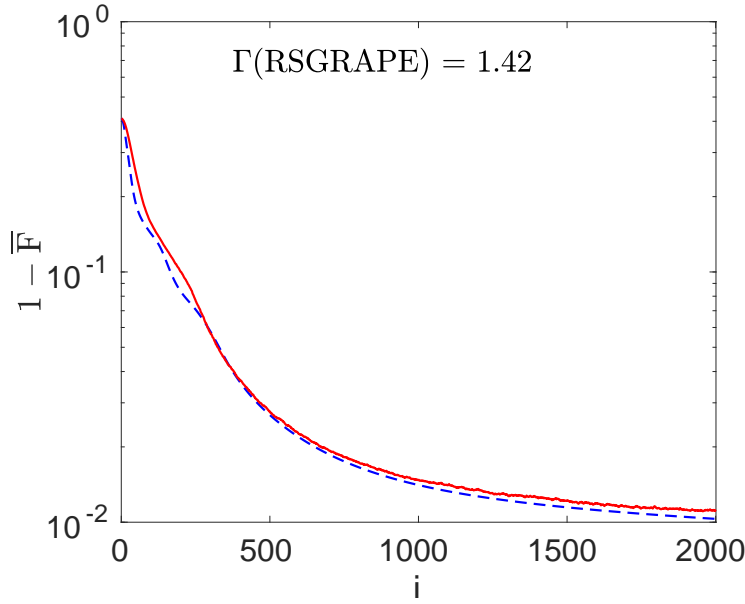


**Figure 3.5:** Average infidelity vs iteration number for the 3-qubit Toffoli gate obtained by GRAPE (dashed line) and RSGRAPE (solid line) with a sparsity of  $s = 50\%$ .

the average of 20 independent trials, each shown by a thin line. Fig. 3.6 (b) plots infidelity vs the CPU time for each of the 20 trials (thin line) and their average (thick line). It's clear from Fig. 3.6 (b) that RSGRAPE (red) takes considerably lesser time than GRAPE (blue) to reach the similar infidelity. Fig. 3.6 (c) and (d) respectively show the  $x$  and  $y$  components for the GRAPE (blue) and RSGRAPE (red) pulse shapes from one of the trial runs. It is easy to note that even with 50 % sparsity, the GRAPE and RSGRAPE pulses are remarkably similar, further indicating that the speedup, by almost a factor of two, is not gained at the cost of quality.

### 3.4.2 RS expedited SAGRAPE (RSSAGRAPE)

We now explain the RS expedited hybrid SAGRAPE algorithm. As explained in Sec. 3.2.2, an important step in SA in every iteration is to scan the neighborhood points of the current solution. To obtain a set of neighborhood points, we add random deviation functions to the current control sequence (of each heteronuclear qubit). Since one needs to scan a large number of neighbourhood points, this step forms a bottleneck in the standard SAGRAPE algorithm. This is where RS can bring about a significant speedup.

The entire control sequence of current iteration can be represented in the matrix form  $\Omega^{(i)} \equiv \{\omega_{x(y),j,k}^{(i)}\}$  of dimension  $N \times 2(2 + n)$ . In our method, we first select a set of  $Q$  spline vectors

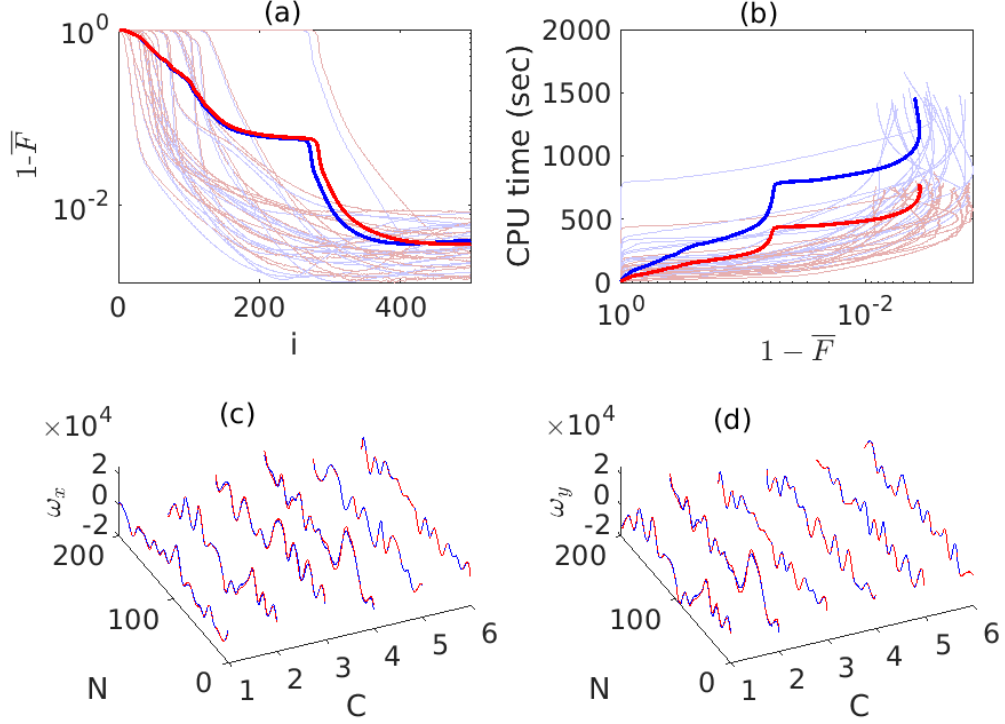


**Figure 3.6:** Comparison of GRAPE (blue) and RSGRAPE (red) for a 6 qubit system. (a) Iteration ( $i$ ) vs infidelity ( $1 - \bar{F}$ ) average over 20 independent trials (thick lines). (b) Infidelity ( $1 - \bar{F}$ ) vs CPU time (thick line). (c)  $x$  component of pulse shape for each channel  $C$ . (d)  $y$  component of pulse shape for each channel  $C$  corresponding to one of the trials.

$\{s_q\}$ , each of dimension  $N \times 1$ . We also choose a set of  $M$  random scaling vectors  $\{c_m\}$ , each of size  $1 \times 2(2 + n)$ . We now setup the neighborhood points by adding the deviation function  $w^{(i)} s_q \cdot c_m$ , i.e.,

$$\Omega_{q,m} = \Omega^{(i)} + w^{(i)} c_m \cdot s_q, \quad (3.16)$$

where  $w^{(i)}$  is a scalar weight parameter which can be gradually reduced with iteration number to shrink the neighbourhood region. Now, we determine the average fidelity  $\bar{F}_{q,m}$  and form the rating matrix (see TABLE. 3.2). In the RS expedited algorithm, we don't need to evaluate all the elements of the rating matrix, but only a set of randomly selected elements. Rest of the elements are efficiently predicted by RS. The sequence  $\Omega_{q,m}$  corresponding to the maximum fidelity  $\bar{F}_{q,m}$  is then passed to the SA algorithm for comparing with the threshold function as explained in Sec. 3.2.2.

Based on the procedure explained above, we now employ RSSAGRAPE to generate a CNOT

scaling ( $c_m$ ) \\\ spline ( $s_q$ )	$c_1$	$c_2$	$c_3$	$c_4 \dots$
$s_1$	$\overline{F}_{1,1}$	$\overline{F}_{1,2}$	?	$\overline{F}_{1,4}$
$s_2$	$\overline{F}_{2,1}$	?	$\overline{F}_{2,3}$	?
$s_3$	$\overline{F}_{3,1}$	$\overline{F}_{3,2}$	?	$\overline{F}_{3,4}$
$s_4$	?	$\overline{F}_{4,2}$	$\overline{F}_{4,3}$	?
$\vdots$	$\vdots$	$\vdots$	$\vdots$	$\vdots$

**Table 3.2:** The rating matrix for the RSSAGRAPE algorithm. Here rows correspond to various spline functions  $s_q$  and columns correspond to the scaling factors  $c_m$ . Each element of rating matrix is the fidelity  $\overline{F}_{q,m}$  of the neighbourhood point  $(q, m)$  obtained from the current solution by adding the deviation function  $w^{(i)}_{s_q} \cdot c_m$ .

gate on a two-qubit system, using five iterations of GRAPE after every iteration of SA. We used  $N = 200$  segment control sequence and scanned 100 neighbourhood points (using  $Q = 10$  spline functions and  $M = 10$  scaling vectors) in each SA iteration. We again set the dimension of the latent vectors to 10. The red dots in Fig. 3.7(a) correspond to the exact fidelities ( $F_a$ ) plotted against the predicted fidelities ( $F_p$ ) for a set of random neighborhood points at various values of sparsity  $s$ . The blue lines corresponding to expected distribution  $F_p = F_a$  are also shown for reference. Evidently, we see a good correlation of the predicted fidelities with the exact values, thus confirming the effectiveness of RS, especially for lower sparsity values.

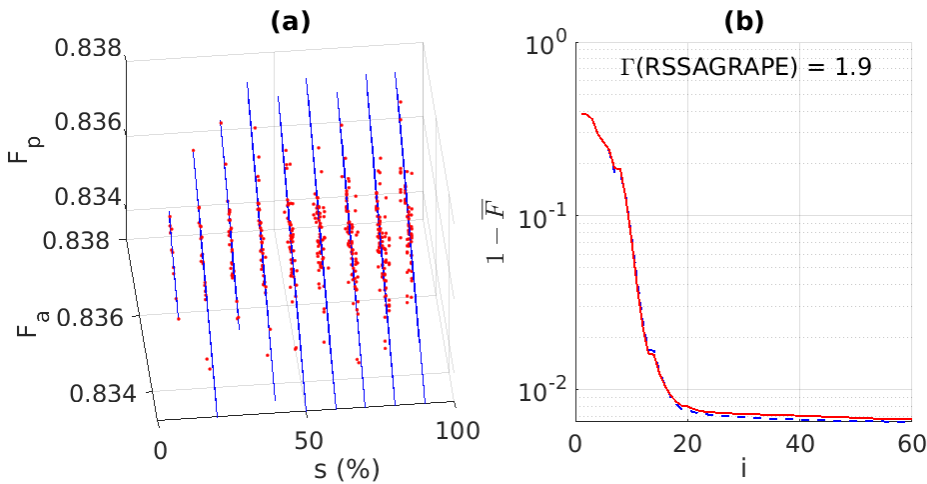


**Figure 3.7:** (a) Exact ( $F_a$ ) and predicted ( $F_p$ ) fidelities of random neighbourhood points versus sparsity ( $s$  in %) in a particular SA iteration. (b) Infidelity  $1 - \overline{F}$  vs number of iterations  $i$  for a 2 qubit system with SAGRAPE (dashed blue line) or RSSAGRAPE (solid red line). In (b) RS was carried out with sparsity  $s = 50$  %.

We now set the sparsity of the rating matrix to 50%, meaning only half the neighborhood points are evaluated exactly, while the remaining ones are predicted by RS. Fig. 3.7(b) displays the infidelity  $1 - \overline{F}$  (averaged over 10 independent trials each starting with a random initial guess) plotted versus iteration number  $i$  for SAGRAPE (dashed blue line) as well as RSSAGRAPE (solid red line). It is clear from the average infidelity trajectory that the convergence is not sacrificed by the partial prediction of the rating matrix by RS. Furthermore, when compared with the SAGRAPE algorithm, we found a time advantage

$$\Gamma(\text{RSSAGRAPE}) = \frac{\tau(\text{SAGRAPE})}{\tau(\text{RSSAGRAPE})} = 1.9, \quad (3.17)$$

meaning the RS enhancement has almost doubled the speed of the SAGRAPE algorithm.

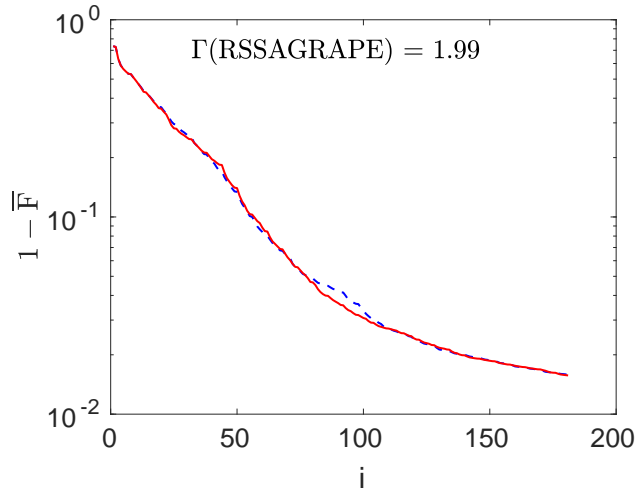


**Figure 3.8:** Average infidelity vs iteration number for the 3-qubit Toffoli gate obtained by SAGRAPE (dashed line) and RSSAGRAPE (solid line) with a sparsity of  $s = 50\%$ .

Again, we study the performance of RS prediction by generating a Toffoli gate on a three-qubit register (same couplings and other parameters as in the case of RSGRAPE). The infidelity averaged over 10 independent trials are plotted vs iteration number in Fig. 3.8. It is evident that the convergence of RSSAGRAPE (with 50% sparsity) is as good as SAGRAPE, but yields an average time-advantage of  $\Gamma(\text{RSSAGRAPE}) = 1.99$ .

### 3.5 Summary and outlook

Machine learning techniques are increasingly being utilized in almost every field of science. Here we use the recommender system (RS) a type of machine learning technique to enhance the efficiency of quantum control algorithms. Although, in principle RS can be adopted for any optimization routine, we demonstrate it in two specific cases: a gradient method (GRAPE) and a meta-heuristic method (simulated annealing (SA)). Because of the analytical form for gradients, GRAPE is a powerful tool, but evaluating gradients for all the constant-Hamiltonian segments is a computationally intensive task. Here we address this issue by employing RS to efficiently predict a significant fraction of gradients and thereby to remarkably speed up the GRAPE algorithm. We demonstrated the RSGRAPE algorithm for up to eight qubits.

The superiority of the final infidelity of RSGRAPE compared to no prediction (zero-gradients) as well as with random gradients confirmed the importance of RS prediction.

Going further, we incorporated RS even in SA, for rapid evaluation of a large set of random neighborhood points. Finally, by expediting both SA and GRAPE simultaneously, we demonstrated almost doubling the speed of SAGRAPE algorithm.

Also, to demonstrate the feasibility of RS prediction in larger registers, we generated three-qubit Toffoli gates using RSGRAPE as well as RSSAGRAPE, both of which yielded significant time advantages.

The entirely different approaches of using RS in GRAPE and SA exemplifies the flexibility and freedom of incorporating RS in quantum control problems. Note that the particular approaches we have used are not unique. One can think of different ways of encoding consumers and products to set up a rating matrix for implementing RS. The generality of RS approach should allow its application in conjunction with other gradient methods such as BFGS [220], function-space control [226], etc. RS can also be used to enhance other meta-heuristic algorithms as well as global search methods such as genetic algorithm [222].

There are a few points to keep in mind while adopting RS. It may fail when the elements of the matrix are convoluted, i.e., when none of the elements can be calculated independently and parallelly. RS may be inefficient or inaccurate if there exists no underlying structure in the rating database, for example, one with high sparsity. When there are multiple options, the rating matrix

needs to be carefully chosen to maximize the RS efficiency. Since RS needs at least a fraction of database to predict the rest, it can only be used in conjunction with another method, which also determines the overall efficiency.

Nonetheless, we believe, the present work encourages further applications of machine learning protocols in quantum information tasks.





## CHAPTER 4

---

### Push-Pull Optimization of Quantum Controls

---

#### Abstract

Optimization of quantum controls to achieve a target process is centered around an objective function comparing the realized process with the target. We propose an objective function that incorporates not only the target operator but also a set of its orthogonal operators, whose combined influences lead to an efficient exploration of the parameter space, faster convergence, and extraction of superior solutions. The *push-pull* optimization, as we call it, can be adopted in various quantum control scenarios. We describe adopting it to a gradient based and a variational-principle based approaches. Numerical analysis of quantum registers with up to seven qubits reveal significant benefits of the push-pull optimization. Finally, we describe applying the push-pull optimization to prepare a long-lived singlet-order in a two-qubit system using NMR techniques.

#### Reported in

**Priya Batra**, V. R. Krithika, and T. S. Mahesh, *Push-Pull Optimization of Quantum Controls*, [Phys. Rev. Research 2, 013314 \(2020\)](#).

## 4.1 Introduction

Optimal control theory finds applications in diverse fields such as finance, science, engineering, etc. [248, 249]. Quantum optimal control has also gained significant attention over the last several years [250, 251] and is routinely used in robust steering of quantum dynamics as in chemical kinetics [252, 253], spectroscopy [254–256], quantum computing [257, 258], and many more[203]. Here we focus on optimization of quantum controls to either transfer from one state to another, henceforth called state control, or to realize a target unitary evolution, hence-

forth called gate control. Relevant numerical techniques fall into several categories including: stochastic-search methods such as strongly modulating pulses [211]; gradient based approaches such as gradient ascent pulse engineering (GRAPE) [205, 259] and gradient optimization of analytical control (GOAT) [260]; variational-principle based Krotov optimization [208, 261, 262]; truncated basis approach such as chopped random basis optimization (CRAB) [263, 264]; genetic algorithm enabled bang-bang controls [265, 266]; and machine learning based approaches [267, 268]. These control schemes have been implemented on various quantum architectures such as NMR [211, 256, 265, 269], NV centers [197], ion trap [270], superconducting qubits [271], magnetic resonance imaging [272], cold atoms [258] etc.

### 4.1.1 Objectives

This work introduces a newly developed method for quantum control. In particular,

(i) An objective function evaluating the overlap of the realized process with the target process is at the core of an optimization algorithm and therefore should be chosen carefully [273, 274].

Here we propose a hybrid objective function that not only depends on the target operator, but also on a set of orthogonal operators. One may think of control parameters being *pulled* by the target operator as well as *pushed* by the orthogonal operators. Accordingly, we refer to this method as *Push-Pull Optimization of Quantum Controls* (PPOQC).

(ii) We describe adopting PPOQC for GRAPE and Krotov algorithms and demonstrate its superior convergence over the standard *pull-only* methods.

(iii) We also experimentally demonstrate the efficacy of PPOQC in a NMR quantum testbed by preparing long-lived singlet-order.

## 4.2 The optimization problem

Consider a quantum system with an internal or fixed Hamiltonian  $H_0$  and a set of  $M$  control operators  $\{A_k\}$  leading to the full time-dependent Hamiltonian  $H(t) = H_0 + \sum_{k=1}^M u_k(t)A_k$ , where control amplitudes  $u_k(t)$  are amenable to optimization. The propagator for a control sequence of duration  $T$  is  $D \exp\left(-i \int_0^T H(t')dt'\right)$ , where  $D$  is the Dyson time-ordering operator. The standard approach to simplify the propagator is via piecewise-constant control amplitudes with

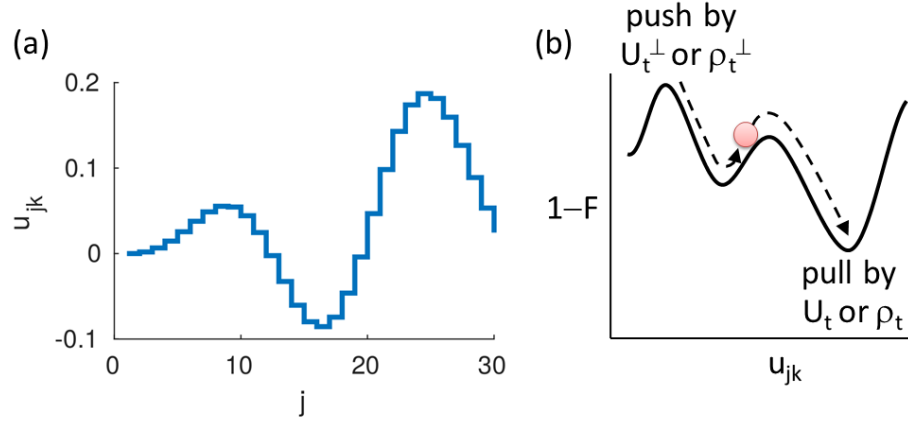


**Figure 4.1:** (a) Piecewise-constant control parameter  $u_{jk}$  versus the segment number  $j$ . (b) Infidelity  $1 - F$  versus  $u_{jk}$ .

$N$  segments each of duration  $\tau$  (see Fig. 4.1(a)). In this case, the overall propagator is of the form  $U_{1:N} = U_N U_{N-1} \cdots U_2 U_1$ , where  $U_j = \exp(-iH_j\tau)$  is the propagator for the  $j$ th segment and  $H_j = H_0 + \sum_{k=1}^M u_{jk} A_k$ . Our task is to optimize the control sequence  $\{u_{jk}\}$  depending on the following two kinds of optimizations:

- (i) *Gate control* (GC): Here the goal is to achieve an overall propagator (gate)  $U_t$  that is independent of the initial state. This is realized by maximizing the gate-fidelity  $F(U_{1:N}, U_t) = |\langle U_t | U_{1:N} \rangle|^2 = \left| \text{Tr}\{U_t^\dagger U_{1:N}\} \right|^2$ .
- (ii) *State control* (SC): Here the goal is to drive a given initial state  $\rho_0$  to a desired target state  $\rho_t$ . This can be achieved by maximizing the state-fidelity  $F(\rho_{1:N}, \rho_t) = \langle \rho_t | \rho_{1:N} \rangle = \text{Tr}\{\rho_t \rho_{1:N}\}$ , where  $\rho_{1:N} = U_{1:N} \rho_0 U_{1:N}^\dagger$ .

In practice, hardware limitations impose bounds on the control parameters  $\{u_{jk}\}$  and therefore it is desirable to minimize the overall control resource  $r_k = \sum_j u_{jk}^2$ . To this end, we use the performance function  $J = F - \sum_{k=1}^M \lambda_k r_k$ , where  $\lambda_k$  are penalty constants.

*PPOQC*: Be it gate control or state control, for a  $d$ -dimensional target operator, we can efficiently setup  $d - 1$  orthogonal operators via Gram-Schmidt orthogonalization procedure [275]. The target operator *pulls* the control-sequence towards itself, whereas the orthogonal operators

push it away from them (see Fig. 4.1(b)). We define the *push* fidelities as

$$\begin{aligned} \text{GC: } F_o(U_{1:N}, \{V_l\}) &= \frac{1}{L} \sum_{l=1}^L F(U_{1:N}, V_l) \quad \text{and} \\ \text{SC: } F_o(\rho_{1:N}, \{R_l\}) &= \frac{1}{L} \sum_{l=1}^L F(\rho_{1:N}, R_l), \end{aligned} \quad (4.1)$$

where  $\{V_l\}$  and  $\{R_l\}$  are  $L \leq d-1$  orthogonal operators such that  $F(U_t, V_l) = 0$  and  $F(\rho_t, R_l) = 0$ . Of course,  $d$  increases exponentially with the system size, but as we shall see later, a small subset of  $L$  orthogonal operators can bring about a substantial advantage. Also, note that for a given target operator, the set of orthogonal operators is not unique and can be generated randomly and efficiently in every iteration. We define the *push-pull* performance function

$$J_{PP} = F - \alpha F_o - \sum_{k=1}^M \lambda_k r_k. \quad (4.2)$$

The *push* weight  $\alpha$  can be a constant or adaptively adjusted. In the following, we describe incorporating PPOQC into two popular optimal quantum control methods.

### 4.2.1 GRAPE optimization

Being a gradient based approach, it involves an efficient calculation of the maximum-ascent direction [205]. While it is sensitive to the initial guess and looks for a local optimum, it is nevertheless simple, powerful, and popular. The algorithm iteratively updates control parameters  $\{u_{jk}\}$  in the direction of gradient  $g_{jk}^{(i)} = \partial J^{(i)} / \partial u_{jk}^{(i)}$ :

$$\begin{aligned} \text{GC: } g_{jk}^{(i)}(U_t) &= 2\tau \text{Im}\{\langle P_j | A_k U_{1:j} \rangle \langle U_{1:j} | P_j \rangle\} \\ \text{SC: } g_{jk}^{(i)}(\rho_t) &= -i\tau \langle \tilde{\rho}_j | [A_k, \rho_{1:j}] \rangle, \end{aligned} \quad (4.3)$$

where  $i$  denotes iteration number,  $P_j = U_{j+1:N}^\dagger U_t$  and  $\tilde{\rho}_j = U_{j+1:N}^\dagger \rho_t U_{j+1:N}$  [205]. Collective updates  $u_{jk}^{(i+1)} = u_{jk}^{(i)} + \epsilon g_{jk}^{(i)}$  after iteration  $i$  on all the segments with a suitable step size  $\epsilon$ , proceeds with monotonic convergence.

*Push-pull GRAPE (PP-GRAPE)*: Using Eq. 4.2 we recast the gradients as

$$\begin{aligned} \text{GC: } G_{jk}^{(i)}(U_t, \{V_l\}) &= g_{jk}^{(i)}(U_t) - \frac{\alpha}{L} \sum_{l=1}^L g_{jk}^{(i)}(V_l) \quad \text{and} \\ \text{SC: } G_{jk}^{(i)}(\rho_t, \{R_l\}) &= g_{jk}^{(i)}(\rho_t) - \frac{\alpha}{L} \sum_{l=1}^L g_{jk}^{(i)}(R_l), \end{aligned} \quad (4.4)$$

and the update rule as  $u_{jk}^{(i+1)} = u_{jk}^{(i)} + \epsilon G_{jk}^{(i)}$ . The revised gradients form the basis of PP-GRAPE.

## 4.2.2 Krotov optimization

Based on variational-principle, this method aims for the global optimum [276]. Here the performance function is maximized with the help of an appropriate Lagrange multiplier  $B_j$ . One sets up a Lagrangian of the form [256],

$$\mathcal{L} = F - \sum_{k=1}^M \lambda_k r_k - \sum_{j=1}^N \text{Re} \left\langle B_j \left| \frac{d}{dt} + iH_j \right| U_{0:j} \right\rangle, \quad (4.5)$$

where the first two terms are same as the performance function  $J$ , and looks for a stationary point satisfying  $\frac{\partial \mathcal{L}}{\partial F} = 0$ ,  $\frac{\partial \mathcal{L}}{\partial u_{jk}} = 0$ , and,  $\frac{\partial \mathcal{L}}{\partial B_j} = 0$ . The second differential equation leads to  $u_{jk} = \frac{1}{\lambda_k} \text{Im} \langle B_j | A_k U_{0:j} \rangle$ , and the last differential equation constrains evolution according to the Schrödinger equation  $\dot{B}(t) = -iH(t)B(t)$ .

At every iteration  $i$ , the Krotov algorithm evaluates the control sequence  $\{u_{jk}^{(i)}\}$  as well as its co-sequence  $\{\tilde{u}_{jk}^{(i)}\}$ . Starting with a random guess  $\{u_{jk}^{(0)}\} = \{\tilde{u}_{jk}^{(0)}\}$ , forward propagation of the sequence  $\{u_{jk}^{(0)}\}$  gives  $U_{1:j}$  and backward propagation of the co-sequence  $\{\tilde{u}_{jk}^{(0)}\}$  from the boundary  $B_N = \partial F / \partial U_{1:N}$  leads to  $B_j$ . Specifically,

$$\begin{aligned} \text{GC: } B_N &= \langle U_t | U_{0:N} \rangle U_t \\ \text{SC: } B_N &= \rho_t U_{0:N} \rho_0 + \kappa U_{0:N}. \end{aligned} \quad (4.6)$$

Here  $U_{0:N} = U_0 U_{1:N}$ ,  $U_0 = \mathbb{1}$ , and  $\kappa$  is a positive constant that ensures the positivity of fidelity.

Back propagating the co-sequence, we obtain

$$B_j = \tilde{U}_{j+1}^\dagger \cdots \tilde{U}_{N-1}^\dagger \tilde{U}_N^\dagger B_N, \quad (4.7)$$

where  $\tilde{U}_j = \exp(-i\tilde{H}\tau)$  and  $\tilde{H}_j = H_0 + \sum_{k=1}^M \tilde{u}_{jk} A_k$ . Now the sequence  $\{u_{jk}^{(i)}\}$  is updated according to

$$u_{jk}^{(i)} = (1 - \delta)\tilde{u}_{jk}^{(i-1)} + \frac{\delta}{\lambda_k} \text{Im}\langle B_j^{(i-1)} | A_k U_{0:j-1}^{(i)} \rangle \quad (4.8)$$

and propagator  $U_{0:j}^{(i)}$  is evaluated. Iterating the last two steps delivers propagators  $U_{0:1}^{(i)}, U_{0:2}^{(i)}, \dots, U_{0:N}^{(i)}$ . The terminal Lagrange multiplier  $B_N^{(i)}$  is evaluated using the Eq. 4.6. To setup the co-sequence  $\{\tilde{u}_{jk}^{(i)}\}$  we first evaluate the terminal control  $\tilde{u}_{Nk}$  using

$$\tilde{u}_{jk}^{(i)} = (1 - \eta)u_{jk}^{(i)} + \frac{\eta}{\lambda_k} \text{Im}\langle B_j^{(i)} | A_k U_{0:j}^{(i)} \rangle \quad (4.9)$$

with  $j = N$ . The Lagrange multiplier  $B_{N-1}^{(i)} = \tilde{U}_N^\dagger B_N^{(i)}$  is now evaluated by back-propagating with the updated amplitude  $\tilde{u}_{Nk}^{(i)}$ . Iterating the last two steps updates the whole co-sequence  $\{\tilde{u}_{jk}^{(i)}\}$ . The algorithm is continued until the desired fidelity is reached.

*Push-pull Krotov (PP-Krotov):* Here we use  $L$  additional co-sequences  $\{\tilde{v}_{jkl}^{(i)}\}$  corresponding to orthogonal operators  $\{V_l\}$  or  $\{R_l\}$ . Terminal Lagrange multipliers  $\{C_{Nl}\}$  are obtained using similar equations as in Eq. 4.6: GC:  $C_{Nl} = \langle V_l | U_{0:N} \rangle V_l$  and SC:  $C_{Nl} = R_l U_{0:N} \rho_0 + \kappa U_{0:N}$ . Revised update rule is

$$\begin{aligned} u_{jk}^{(i)} &= (1 - \delta)\tilde{u}_{jk}^{(i-1)} + \frac{\delta}{\lambda_k} \text{Im}\langle B_j^{(i-1)} | A_k U_{0:j-1}^{(i)} \rangle \\ &+ \frac{\alpha\delta}{L} \sum_{l=1}^L \left[ \tilde{v}_{jkl} - \frac{1}{\lambda_k} \langle C_{jl}^{(i-1)} | A_k U_{0:j-1}^{(i)} \rangle \right], \end{aligned} \quad (4.10)$$

where  $\tilde{v}_{jkl}^{(i)} = \frac{\alpha\eta}{L} \left[ u_{jk}^{(i)} - \frac{1}{\lambda_k} \sum_{l=1}^L \text{Im}\langle C_{jl}^{(i)} | A_k U_{0:j}^{(i)} \rangle \right]$  and  $\alpha$  is the push weight as in Eq. 4.2.

### 4.3 Numerical analysis

Results of PPOQC analysis in a model two-qubit Ising-coupled system are summarized in Fig. 4.2. For GC, we use CNOT gate as the target, while for SC, the task is a transfer from  $|00\rangle$  state

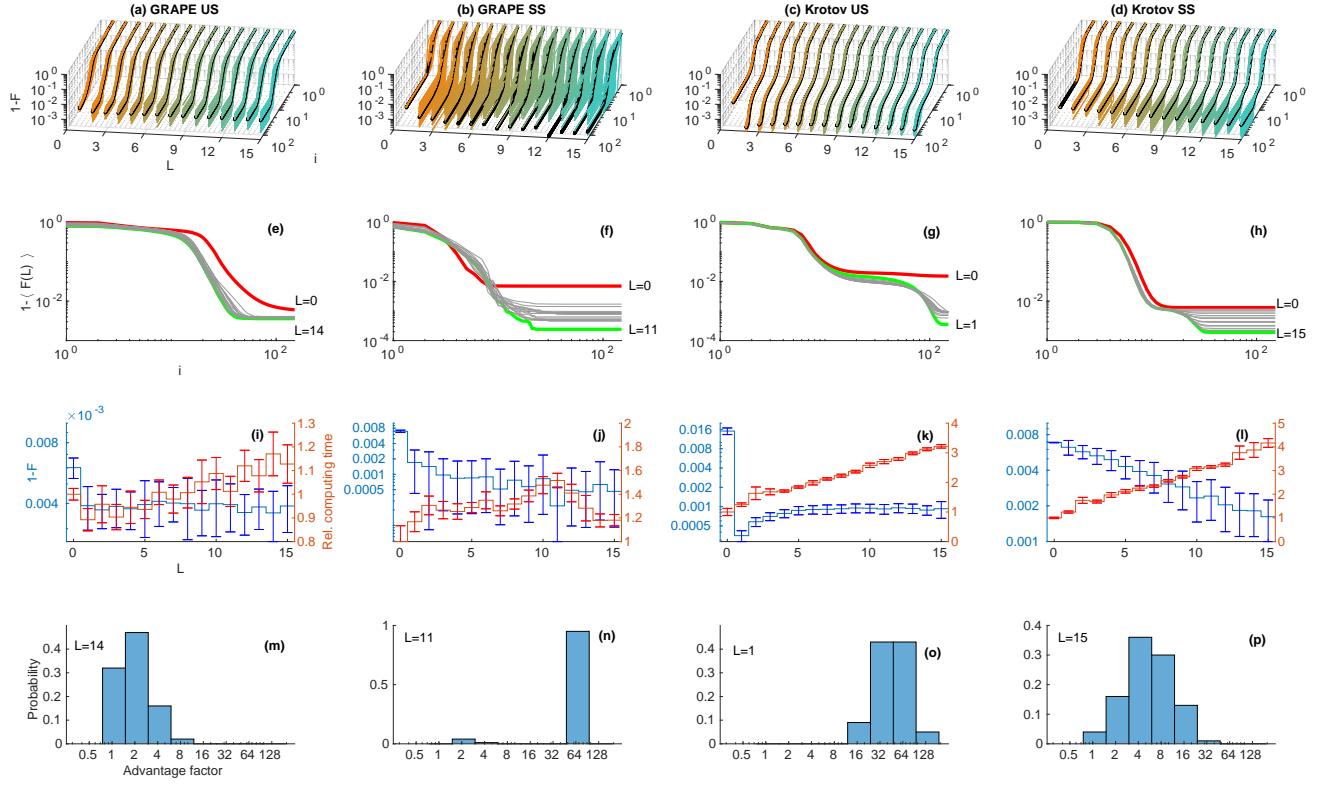


**Figure 4.2:** Performance analysis on a two-qubit system for GRAPE US (1st column), GRAPE SS (2nd column), Krotov US (3rd column), and Krotov SS (4th column). (a-d) Infidelity  $1 - F$  of two-qubit controls versus iteration number ( $i$ ) and number ( $L$ ) of orthogonal operators for GRAPE and Krotov as indicated. Black lines represent mean infidelities. (e-h) Mean infidelity versus  $i$ . Curves for  $L = 0$  (red) and for  $L$  leading to the maximum final fidelity (green) are highlighted. (i-l) Mean final infidelity (left axis) and relative computing time (right axis) versus  $L$ . Error bars represent one standard deviation. (m-p) Probability versus advantage factor.

to singlet state  $|S_0\rangle = (|01\rangle - |10\rangle)/\sqrt{2}$ . In each case, we use a fixed set of one hundred random guess-sequences. PP-GRAPE and PP-Krotov algorithms were run for various sizes of orthogonal sets ( $L \in [1, 15]$  with push weight  $\alpha = 0.2$ ) and compared with the pull-only ( $L = 0$ ) results (Fig. 4.2(a-d)). PPOQC outperformed the pull-only algorithms in terms of the mean final fidelity in all the cases (Fig. 4.2 (e-h)). More importantly, while the pull-only fidelities tend to saturate by settling into local minima, the push-pull trials appeared to explore larger parameter space and thereby extracted solutions with better fidelities. While the computational time for PP-GRAPE is weakly dependent on  $L$ , we find a slow but linear increase in the case of PP-Krotov (Fig. 4.2 (i-l)). To quantify the advantage of PPOQC over the standard algorithms, we define the advantage factor  $(1 - F(L = 0))/(1 - F(L_{\text{best}}))$ , where  $L_{\text{best}}$  corresponds to the one with maximum mean of

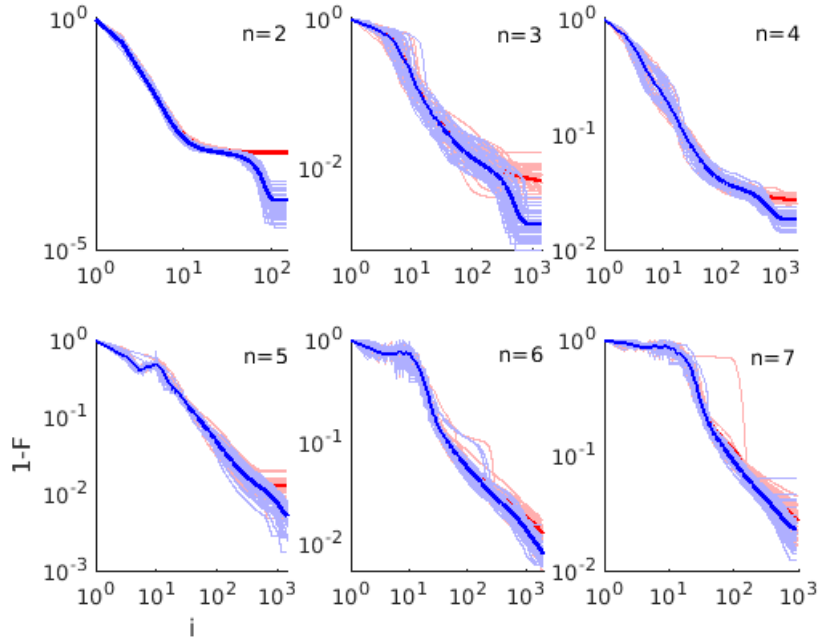


**Figure 4.3:** Infidelities for 40 random guesses (thin lines) and their mean (thick lines) versus iteration number  $i$  with KrotoV (red) and with PP-KrotoV (blue;  $L = 1$ ;  $\alpha = 0.2$ ) for QFT on qubit-registers of varying sizes ( $n$  as indicated).

final-fidelity (Fig. 4.2 (m-p)). In all the cases PPOQC ( $L \geq 1$ ) resulted in superior convergences than the standard *pull-only* ( $L = 0$ ) algorithms. In particular, PP-Grape SC and PP-KrotoV GC reached advantage factors up to 64, while PP-KrotoV SC reached up to 16. Only in PP-Grape GC, the advantage factor was modest 2.

To analyze the performance of PPOQC in larger systems, we implement Quantum Fourier Transform (QFT), which is central to several important quantum algorithms [256]. We implement the entire  $n$ -qubit QFT circuit, consisting of  $n$  local and  $O(n^2)$  conditional gates, into a single PP-KrotoV GC sequence. The results, with registers up to seven qubits, shown in Fig. 4.3 assure that PPOQC advantage persists even in larger systems.

The push-pull technique can also be combined with other convergence improvement techniques such as conjugate-gradient [277], which is illustrated by the best performance of conjugate PP-GRAPe in Fig. 4.4 (a). Moreover, in the pull-only algorithms, the step-size  $\epsilon$  may be optimized to ensure the best convergence. Similarly, in PPOQC, one can simultaneously optimize both the step-size  $\epsilon$  and the push-weight  $\alpha$  to realize the best convergence rate. This is illustrated in Fig. 4.4 (b). Notice that we now obtain an order of magnitude improvement in the infidelity compared to the pull-only algorithm.



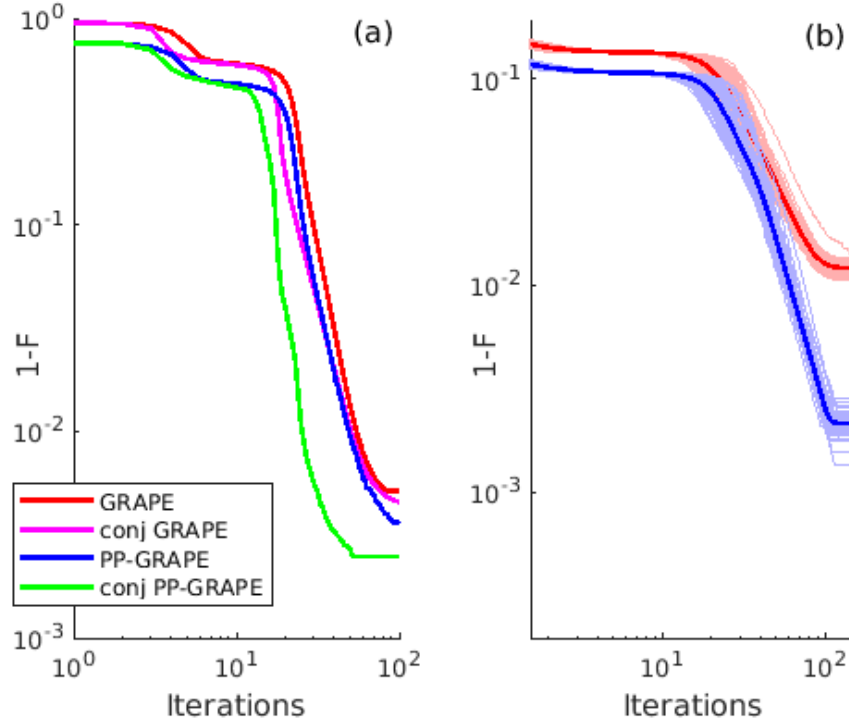


**Figure 4.4:** Mean infidelities (thick lines) of GRAPE sequences implementing a two-qubit CNOT gate. (a) Performance with/without conjugate gradients. (b) Pull-only ( $L = 0$ ) with adoptive step-size  $\epsilon$  (red) and Push-Pull ( $L = 15$ ) with simultaneously adopted step-size as well as push-weight  $\alpha$  (blue).

### 4.3.1 Rapid parameter search in push-pull approach

To gain insight into the superiority of push-pull over pull-only approach, we observed how the gradients evolve over time. Fig. 4.5 displays the evolution of gradients versus control amplitudes over several iterations. The simulations are carried out for a two-qubit CNOT gate with both pull-only and push-pull GRAPE algorithms. Push-pull algorithm ultimately converged to a better fidelity (0.993) than the pull-only algorithm (0.981). Notice that the push-pull gradients show more rapid changes than the pull-only algorithm, indicating a more robust parameter search in action. This behavior appears to be the crucial factor for the faster convergence of the push-pull approach.

### 4.3.2 Push-weight

Fig.4.6 displays infidelities of PP-GRAPE as well as PP-Krotov algorithms versus the push-weight  $\alpha$ . We notice that, on the positive side, the infidelity is generally superior to the pull-

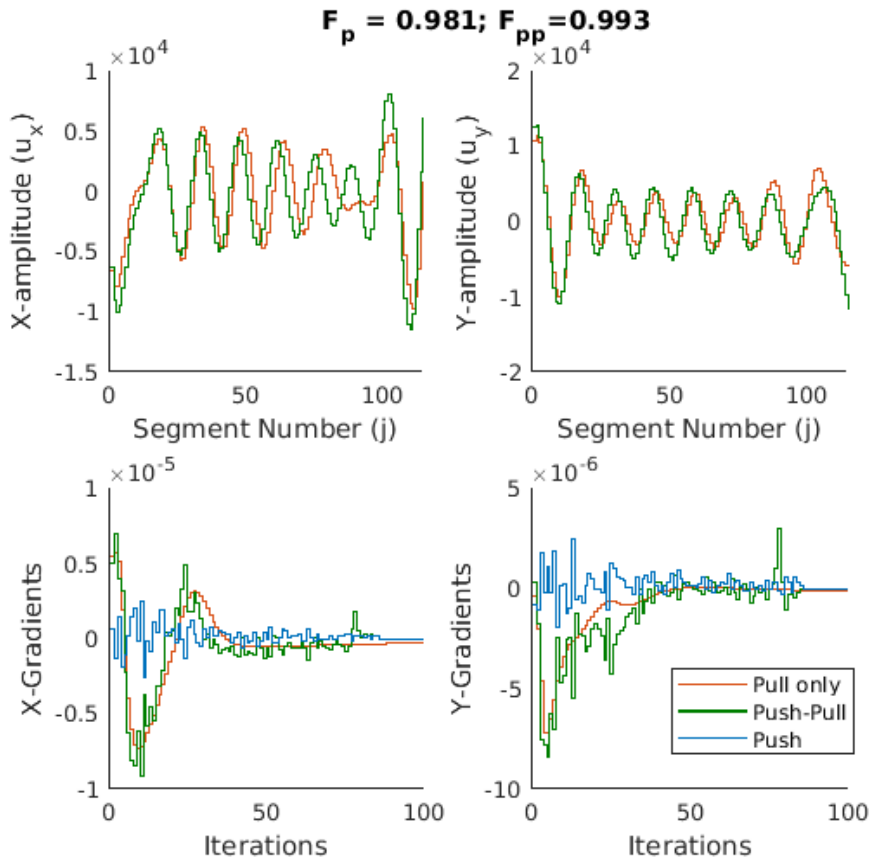


**Figure 4.5:** Top row: X and Y amplitudes for a two-qubit CNOT gate with pull-only GRAPE (red) and push-pull PP-GRAPE (green;  $L = 5$ ) algorithms. Bottom row: Evolution of X and Y gradients versus iteration number for one particular segment (segment number 78). Notice how the mean push gradients (blue) from the orthogonal operators modulate the effective push-pull gradients (green).

only algorithm ( $\alpha = 0$ ). In each case, there exists an optimal push-weight roughly in the range  $\alpha \in [0.1, 0.3]$  at which the PPOQC works best. It is interesting to see that some negative regions also display superior performances.

## 4.4 NMR experiments

We now study the efficacy of PPOQC via an important application in NMR spectroscopy, i.e., preparation of a long-lived state (LLS). Carravetta *et al.* had demonstrated that the singlet-order of a homonuclear spin-pair outlives the usual life-times imposed by spin-lattice relaxation time constant ( $T_1$ ) [278, 279]. Prompted by numerous applications in spectroscopy and imaging, several efficient ways of preparing LLS have been explored [280]. In the following, we utilize

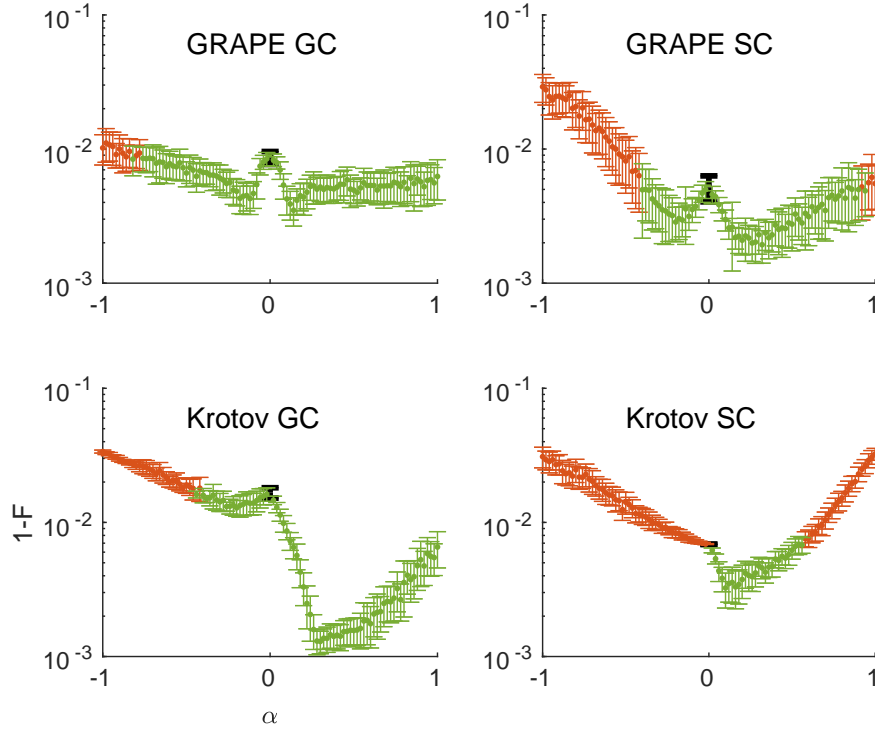


**Figure 4.6:** Infidelity versus the push-weight  $\alpha$  for  $L = 6$ . Error bars indicate one standard deviation. The black point at  $\alpha = 0$  corresponds to the standard pull-only algorithms. The green and red regions respectively indicate superior and inferior performances of PPOQC w.r.t. pull-only algorithm.

PP-Krotov SC optimization for this purpose.

We prepare LLS on two protons of 2,3,6-trichlorophenol (TCP; see Fig. 4.7 (a)). Sample consists of 7 mg of TCP dissolved in 0.6 ml of deuterated dimethyl sulfoxide. The experiments are carried out on a Bruker 500 MHz NMR spectrometer at an ambient temperature of 300 K. Standard NMR spectrum of TCP shown in Fig. 4.7 (a) indicates resonance offset frequencies  $\pm\Delta\nu/2$  to be  $\pm 63.8$  Hz and the scalar coupling constant  $J = 8.8$  Hz. The internal Hamiltonian of the system, in a frame rotating about the direction of the Zeeman field at an average Larmor frequency is  $H_0 = -\pi\Delta\nu I_z^A + \pi\Delta\nu I_z^B + 2\pi J I_z^A I_z^B$ , where  $I_z^A$  and  $I_z^B$  are the  $z$ -components of the spin angular momentum operators  $\mathbf{I}^A$  and  $\mathbf{I}^B$  respectively.

The thermal equilibrium state at high-field and high-temperature approximation is of the form  $\rho_0 = I_z^A + I_z^B$  (up to an identity term representing the background population). The goal is to design an RF sequence  $\{u_x(t), u_y(t)\}$  introducing a time-dependent Hamiltonian

$$H(t) = H_0 + u_x(t)(I_x^A + I_x^B) + u_y(t)(I_y^A + I_y^B)$$

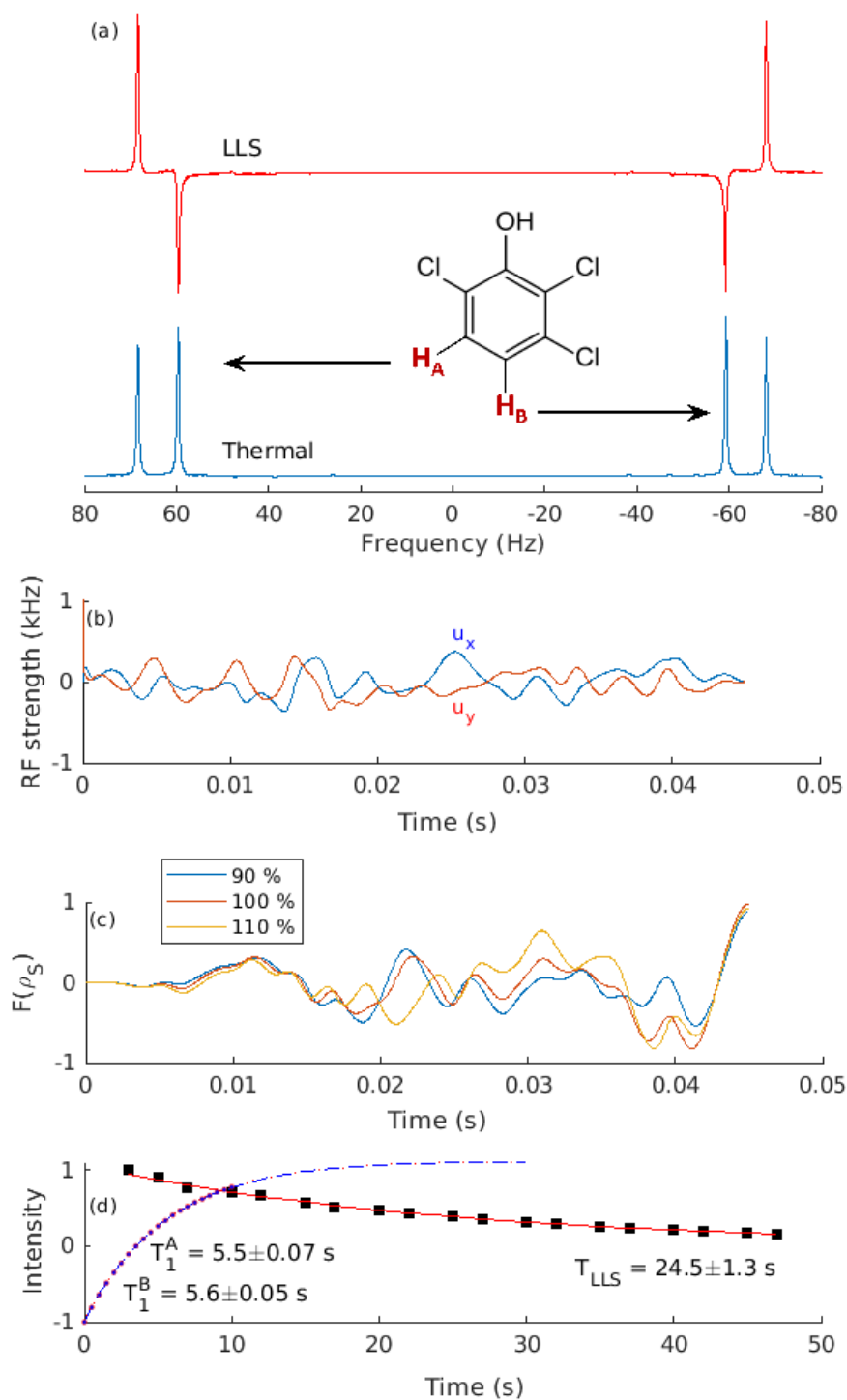


**Figure 4.7:** (a) Thermal and LLS spectra of TCP (molecule in inset). (b) PP-Krotov SC sequence ( $L = 5$ ) preparing LLS directly from the thermal state. (c) LLS fidelity evolution during the sequence in (b) at different RF inhomogeneity levels. (d)  $T_1$  values measured by the inversion recovery experiment and the  $T_{LLS}$  measured by storage under spin-lock.

that efficiently transfers  $\rho_0$  into zero-quantum singlet-triplet order  $\rho_S = -\mathbf{I}^A \cdot \mathbf{I}^B$ . Under an RF spin-lock the triplet order decays rapidly while the singlet order  $\rho_{LLS}$  remains long-lived. The PP-Krotov SC pulse-sequence shown in Fig. 4.7 (b) consists of 1000 segments in a total duration of 45 ms, which is 30% shorter than the standard sequence that requires  $\frac{1}{2J} + \frac{3}{4\Delta\nu} = 63$  ms [279]. The fidelity profile shown in Fig. 4.7 (c) indicates the robustness of the sequence against 10% RF inhomogeneity distribution with an average final fidelity above 95%. The LLS spectrum shown in Fig. 4.7(a) is the characteristic of the singlet state  $\rho_S$ . Fig. 4.7 (d) shows the experimental results of LLS storage under 1 kHz WALTZ-16 spin-lock. It confirms the long life-time  $T_{LLS}$  of about 24.5 s or about 4.5 times  $T_1^A$  and  $T_1^B$  measured by inversion recovery experiments. A comparison with the standard method (as in ref. [279]) revealed 27% higher singlet order, further indicating the superiority of the PP-Krotov SC sequence.

## 4.5 Summary and outlook

At the heart of optimization algorithms lies a performance function that evaluates a process in relation to a target. Using a hybrid objective function that simultaneously takes into account a given target operator as well as a set of orthogonal operators we devised the *push-pull* optimization of quantum controls. Combined influences of these operators not only results in a faster convergence of the optimization algorithm, but also effects a better exploration of the parameter space and thereby generates better solutions. Although the orthogonal set grows exponentially with the system size, it is not necessary to include an exhaustive set. Even a small set of orthogonal operators, generated randomly during the iterations, can bring about a significant improvement in convergence.

While the push-pull approach can be implemented in a wide variety of quantum control routines, we described adopting it into a gradient based as well as a variational-principle based optimizations. We observed considerable improvements in the convergence rates, without overburdening computational costs. The numerical analysis with up to seven qubits confirmed that push-pull method retained superiority even in larger systems. Combining push-pull method with conjugate gradients also resulted in a better performance. Numerical analysis revealed a further improvement with adoptive step-sizes and adoptive push-weights.

Finally, using NMR methods, we experimentally verified the robustness of a push-pull Krotov control sequence preparing a long-lived singlet order. Further work in this direction includes optimizing the functional forms of orthogonal gradients and generalization to open quantum controls.

## CHAPTER 5

---

# Physics-Informed Neural Network for Robust Quantum Control

---

### Abstract

Machine learning is becoming increasingly integral across various domains. In this context, we present a novel approach utilizing a Physics Informed Neural Network for constructing quantum gates. We focus on creating a two-qubit CNOT gate and a protocol for state-to-state transfer, specifically designing a pulse to prepare a long-lived singlet state. These sequences are implemented on a nuclear magnetic resonance platform to assess the algorithm's effectiveness. We also show the robustness of singlet-state preparation under noise. On the other hand, the significance of geometric quantum computation lies in its inherent robustness against certain types of parameter noise. Therefore, it becomes imperative to devise innovative algorithms for generating geometric quantum gates applicable to diverse quantum platforms. Our study highlights the robust nature of the one-qubit phase gate compared to the conventional hard pulse approach. This comparison sheds light on the algorithm's resilience, a critical aspect of developing practical quantum computing solutions.

### Reported in

**Priya Batra**, and T. S. Mahesh, manuscript under preparation.

## 5.1 Introduction

Quantum control has become one of the central topics in the upcoming quantum technology. It deals with the problem of efficient transfer of one state to another and unitary synthesis. Finding hardware-specific controls is another essential task. It has a long history of successful devel-

opment of various numerical optimization algorithms [89, 90, 106, 122, 256]. One of the most necessary criteria of these optimization algorithms relies on the initial discretization of the control sequence. It is a valuable approximation; however, there are problems of under and over-discretization. On the other side, noise is another crucial factor affecting these control pulses' performance in practical quantum systems. The geometric phase offers a distinct paradigm by inherently becoming robust against certain types of noises. Panchratnam first proposed the idea of a geometric phase using polarised light [281]. It was first mathematically formalized by Berry in the adiabatic setting [282] and was later extended to the non-adiabatic limit by Aharonov and Anandan [283]. Wilczek and Zee extended it to the non-commuting (non-abelian) geometric phase in the adiabatic limit [284]. It was again performed to a non-abelian phase using a similar approach as shown in [283] useful for universal quantum computation [285]. In the adiabatic limit, it reduces to Wilczek and Zee holonomy [284]. Sjoqvist et al. [286, 287] have reviewed all the possible settings of geometric phase, which include adiabatic or non-adiabatic, Abelian, or non-Abelian in the context of geometric quantum computation. It has been experimentally realized in a variety of platforms such as NMR [288–291], superconducting qubits [290, 292, 293], Rydberg atoms [294, 295], NV center [296], etc. Recently, Li et al. [297, 298] presented the inverse engineering of Hamiltonian, which beforehand includes the two necessary conditions of cyclic evolution and parallel transport for geometric gates. One can directly generate the desired evolution by following the path of time-dependent Hamiltonian parameters.

The use of machine learning protocols for different quantum problems has been a point of attention recently [299, 300]. A physics-informed neural network (PINN) is a type of ML algorithm that takes information about physical procedures in the form of differential equations. After successfully implementing a neural network for solving Navier Stokes's equation [301, 302], PINN started to gain attention for solving various other types of differential equations [303, 304]. It is said to be a universal function approximator [305]. Recently, it has been proposed to solve Schrödinger's equation [132] as well as the open quantum system Lindbladian equation [133]. An essential strength of the PINN algorithm is that it utilizes smooth basis functions to convert network parameters into the control function. Therefore, it generates smooth controls with low bandwidth that are easier to implement in experimental hardware [132]. PINN also avoids the need for any pre-discretization prevalent in other quantum control algorithms.



### 5.1.1 Objectives

In this work, we dive into the problem of piece-wise constant approximation, applicability of PINN in practical quantum setup and noise in quantum systems. In the following sections, we discuss

- (i) We utilize PINN to design a state-to-state transfer to prepare a two-qubit long-lived singlet (LLS) state and a two-qubit CNOT gate. We also check the noise robustness for the LLS state by solving the open quantum system Lindbladian equation.
- (ii) We then execute these control pulses on NMR hardware to check the efficacy of PINN.
- (iii) The effect of discretization on time-dependent continuous control pulses in simulation and experiments has also been explored in both unitary evolution and state-to-state transfer cases.
- (iv) We engineer a one-qubit geometric phase gate having built-in robustness against control errors.

## 5.2 Physics-informed neural networks (PINNs)

Consider the total Hamiltonian  $H(t)$  consisting of two components, a constant part  $H_0$  and a time-dependent part such that

$$H(t) = H_0 + \sum_{k=0}^M u_k(t) H_k, \quad (5.1)$$

where  $u_k(t)$  are the time-dependent control amplitudes and  $H_k$  are corresponding control operators. The task of a general quantum control problem is to find the  $u_k(t)$  to achieve a target unitary  $U_t$  or a target state  $\rho_t$  efficiently. For this purpose, we utilize a deep learning-based method called a physics-informed neural network (PINN).

We employ a feed-forward network, as shown in figure 5.1, with the time  $t$  as input and control amplitudes  $u_k(t)$  as output of the network. The output of the first layer is written as

$$L_1 = \Gamma(W_1 \cdot t + B_1), \quad (5.2)$$

where  $W_1$  and  $B_1$  are the weight and bias matrices for the first layer, and  $\Gamma$  is the activation

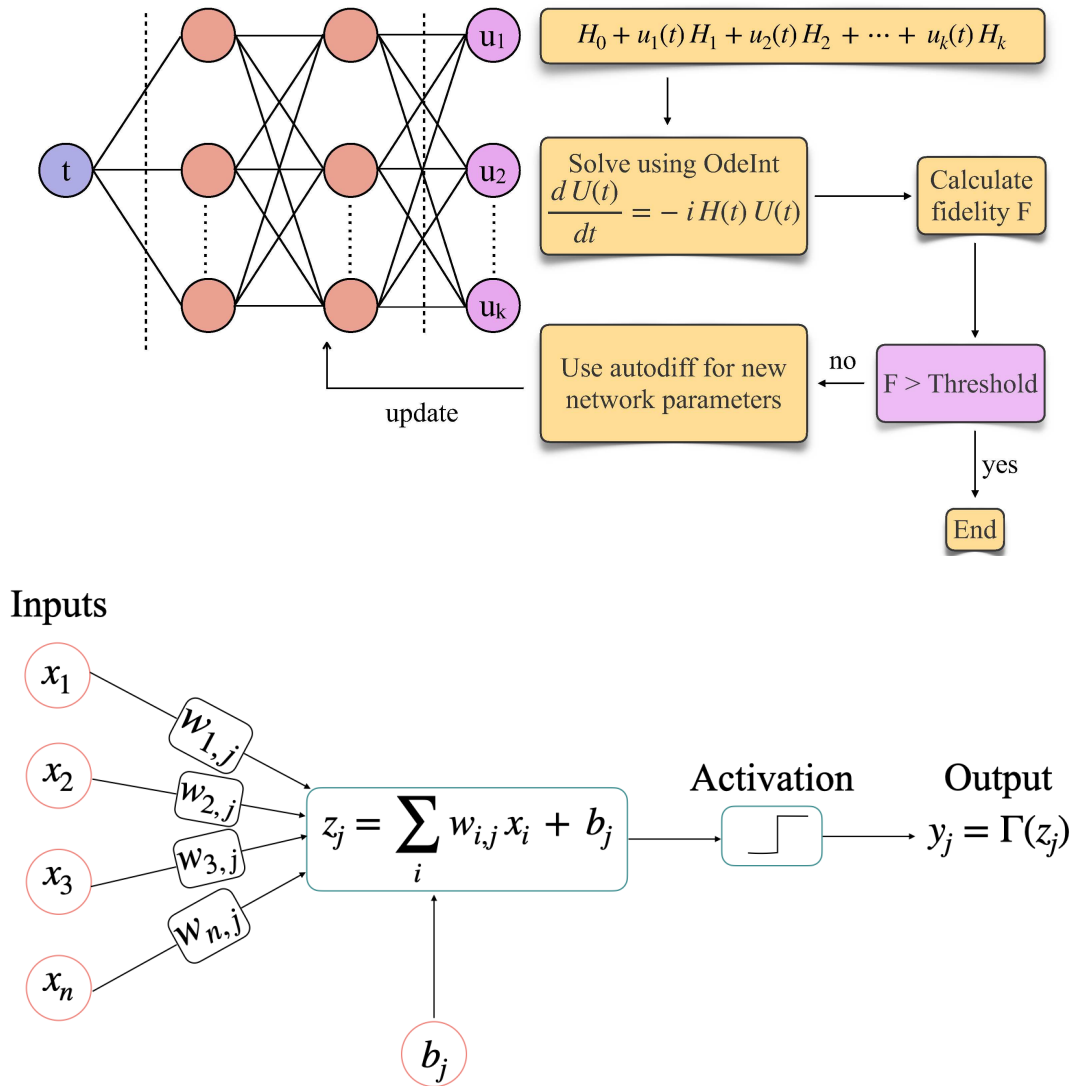


**Figure 5.1:** (top) Neural network; (bottom) Mathematical processing of a neural network where  $x_i$  are inputs,  $w_{i,j}$  are the weights,  $b_j$  are bias, and  $y_j$  are output.

function. In our work, we use the hyperbolic tangent function as the activation. The neural network output can be cast as the consecutive operations of different layers,

$$u_k(t) = L_K \circ L_{K-1} \circ \dots \circ L_1. \tag{5.3}$$

Here  $K$  represents the number of layers in the network. The output of the network is used in the eq. 5.1 to reconstruct Hamiltonian  $H(t)$ . It is important to notice that our control parameters are a

function of time and network parameters. One needs to find the optimized network parameters to get the desired controls for target unitary  $U_t$  or state  $\rho_t$ . To this end, we inject Hamiltonian  $H(t)$  into Schrödinger's equation and solve it.

We use JAX's ordinary differential equation solver to solve the Schrödinger equation [306]. We simulate the neural network with Jax's Haiku library [307]. We start with the random value of network parameters and calculate the fidelity or optimization function

$$\begin{aligned}
 F &= \left| \text{Tr} \left( U_t^\dagger U(T) \right) \right|^2 \\
 &\text{or} \\
 &= \text{Tr}(\rho(T)\rho_t),
 \end{aligned} \tag{5.4}$$

where  $U(T)$  and  $\rho(T)$  are the simulated unitary and state respectively. The goal here is to maximize the optimization function by updating the parameters of the network. After calculating the fidelity, we take the derivative of the fidelity function with respect to network parameters. We use the auto differentiation (autodiff) algorithm in the Optax module [308] until we maximize the fidelity function. Automatic differentiation is different from symbolic differentiation. Unlike GRAPE and other quantum control algorithms, we do not take derivatives directly with respect to controls. We parameterize the controls as network parameters and then use autodiff. It is based on converting the program into a sequence of primitive operations. Autodiff is efficient (linear in the cost of computing the value) and numerically stable.

### 5.3 State to state transfer

We aim to drive an initial state  $\rho_i$  to a target state  $\rho_t$  using external time-dependent parameters  $u_k(t)$ . The quality of the process can be quantified using the fidelity function between target state  $\rho_t$  and simulated state  $\rho(T)$  after total time  $T$  given as

$$F = \text{Tr}(\rho(T)\rho_t). \tag{5.5}$$

We use NMR as our test bed to simulate state-to-state transfer.

### 5.3.1 Preparation of long-lived singlet state in NMR

We prepare a special state called the singlet state, which is long-lived compared to the inherent relaxation time. The singlet state is written as

$$|S_0\rangle = \frac{|01\rangle - |10\rangle}{\sqrt{2}}. \quad (5.6)$$

We use a 2-qubit sample 2,3,6-trichlorophenol (TCP) (shown in the inset of fig. (a) 5.2) in a liquid state in a 500 MHz NMR spectrometer. To prepare the singlet state, we utilize the two protons of TCP. The internal Hamiltonian for TCP is given by

$$H_0 = 2\pi J I_{1z} I_{2z} - 2\pi\nu_1 I_{1z} - 2\pi\nu_2 I_{2z}, \quad (5.7)$$

where coupling between two qubits is  $J = 8.75$  Hz and chemical shift difference is  $\Delta\nu = \nu_2 - \nu_1 = 127.5$  Hz with  $I_z$  representing the  $z$ -component of spin operator. The external RF field has the following Hamiltonian

$$H_{RF}(t) = \omega_x(t)(I_{1x} + I_{2x}) + \omega_y(t)(I_{1y} + I_{2y}), \quad (5.8)$$

with  $\omega_x(t)$  and  $\omega_y(t)$  being the  $x$  and  $y$ -control amplitudes.

The pulse sequence is then applied to the NMR spectrometer. Since the LLS state has no magnetization, the pulse sequence is followed by a  $\pi/2$ -pulse to bring the magnetization to  $x$ -axis. The antiphase LLS spectra are shown 5.2 (a). To prepare the singlet state, we start with thermal equilibrium  $\rho_i = I_{1z} + I_{2z}$ . We employ the PINN to find the control amplitudes so that  $\rho_i$  reaches  $\rho_t = |S_0\rangle\langle S_0|$ . Figure 5.2 (b) shows the simulated pulse sequence. To measure the lifetime of LLS, we keep the singlet state under the WALTZ-16 spin lock for a duration of  $T = 0 - 44$  sec. Due to the symmetry of LLS, it decays very slowly under spin lock and follows an exponential behavior. Fig 5.2 (c) shows the magnetization vs time.

#### Effect of discretization

In most numerical quantum control optimization algorithms (such as GRAPE or Krotov), one starts with a pre-discretized pulse shape, which undergoes iterative optimization. The pulse thus

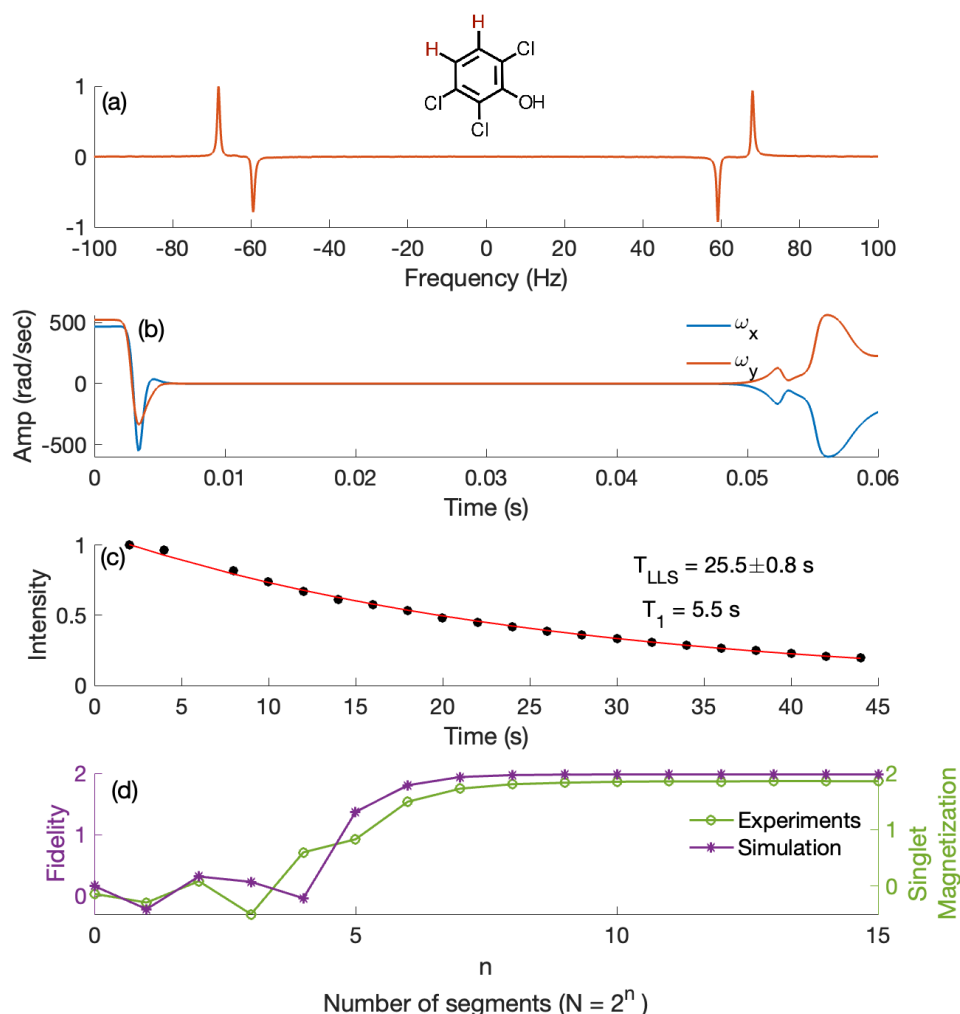


**Figure 5.2:** (a) LLS spectrum (b) Pulse sequence,  $x$  and  $y$  control amplitudes for  $^1\text{H}$  as a function of time (c) Decay of singlet magnetization under WALTZ 16 spin-lock. The  $T_1$  values of the two protons are 5.5 s and 5.6 s. Thus, LLS outlives the single-spin non-equilibrium magnetization by a factor of around 5. (d) Effect of discretization on continuous time pulse in simulation as well as experiments.

generated does not necessarily harness the full capability of the experimental hardware. Under-digitization often compromises the fidelity of the pulse. On the other hand, over-digitization is not only computationally expensive but also might prohibit the pulse from being realized in a given hardware of a specific memory.

One of the critical features of PINN is that it encodes the entire shape of the control amplitudes in terms of the network parameters. This allows one to extract a vectorized pulse shape with optimal discretization for any given hardware. Thus, PINN avoids the need for any prior

discretization of pulse shape. The neural network may also provide a compact way to store the pulse shape that can be extracted as a discretized vector of arbitrary precision when required.

In figure 5.2 (d), we also study the effect of under and over-discretization of pulse shapes in simulations and experimental hardware. The result for discretization vs fidelity in the simulated case is plotted with a purple line, while discretization vs total singlet magnetization in experiments is plotted with a green line.

### 5.3.2 Effect of noise on singlet state preparation

To have a robust singlet state, we need to counter the effect of noise. We solve the Lindbladian equation for this, considering the noise to build the control sequence. We prepare the singlet state with robustness against control noise. The Lindbladian equation can be given as

$$\frac{d\rho_S}{dt} = -\frac{i}{\hbar} [H_S(t), \rho_S] + \sum_n \gamma_n \left( V_n \rho_S V_n^\dagger - \frac{1}{2} \{ \rho_S, V_n^\dagger V_n \} \right). \quad (5.9)$$

Control noise plays a significant role in NMR or in almost all architectures. For this purpose,

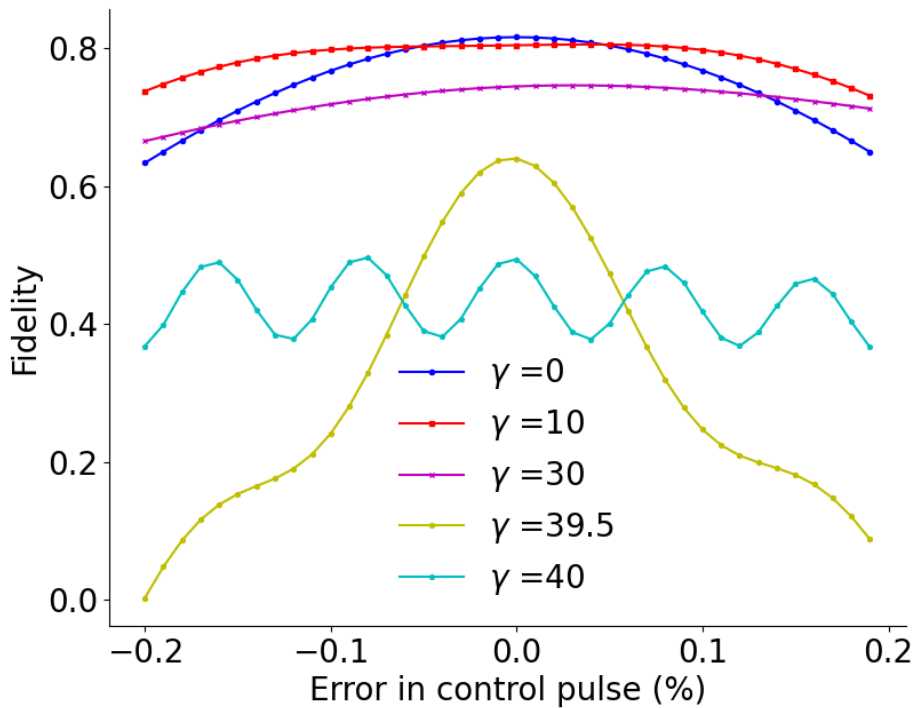


**Figure 5.3:** Fidelity vs control noise (in percentage) for different gamma values for LLS state preparation.

we take  $V_1 = I_{1x} + I_{2x}$  and  $V_2 = I_{1y} + I_{2y}$  and  $\gamma_1 = \gamma_2 = \gamma$  which we vary to see the nature of robustness. We use the parameters of the 2-chloroacrylonitrile (CAN) with  $J = 17.22$  Hz and  $\delta v = v_2 - v_1 = 45.13$  Hz to simulate the robustness response.

Figure 5.3 plots the fidelity of singlet state vs control error in percentage for different gamma values. Here, the blue line represents robustness without any external noise being considered while achieving the pulse sequence. However, as we increase the value of gamma, it is evident from the red line that robustness increases quite a bit. As we further increase the value of gamma, the noise part starts dominating during optimization, and the overall fidelity and robustness decrease. It is interesting to see that at around  $\gamma = 40$ , there is a sudden change in the robustness behavior.

### 5.3.3 Unitary synthesis

Logic gates are important ingredients for quantum computation. Single-qubit gates and a two-qubit CNOT gate comprise a universal set of gates. Here, we employ PINN to prepare a 2-qubit CNOT gate and implement it on the NMR set-up. We use a 2-qubit system, diethyl fluoromalonate (DEFM) (shown in inset 5.4), in a liquid state in a 500MHz spectrometer. DEFM has a  $^1\text{H}$  and  $^{19}\text{F}$  nuclei which work as two distinct qubits. The internal Hamiltonian for the system is

$$H_0 = 2\pi J I_{1z} I_{2z}, \quad (5.10)$$

where  $J = 48.2\text{Hz}$  is scalar coupling and  $I_z$  is the  $z$ -component of spin operator. The external RF Hamiltonian is of the following form

$$H_{RF}(t) = \omega_{1x}(t)I_{1x} + \omega_{2x}(t)I_{2x} + \omega_{1y}(t)I_{1y} + \omega_{2y}(t)I_{2y}, \quad (5.11)$$

with  $\omega_{1(2),x(y)}$  being the  $x(y)$  control amplitudes for qubit 1(2). In our case  $^{19}\text{F}$  is the control qubit while the  $^1\text{H}$  is the target qubit. The pulse sequence and NMR spectrum for both qubits are shown in fig 5.4.

We also show the effect of discretization while synthesizing the unitary. We prepare the CNOT gate in DEFM as described below. We then plot fidelity vs the number of segments in simulation and experiments. We perform diagonal tomography in experiments to calculate the

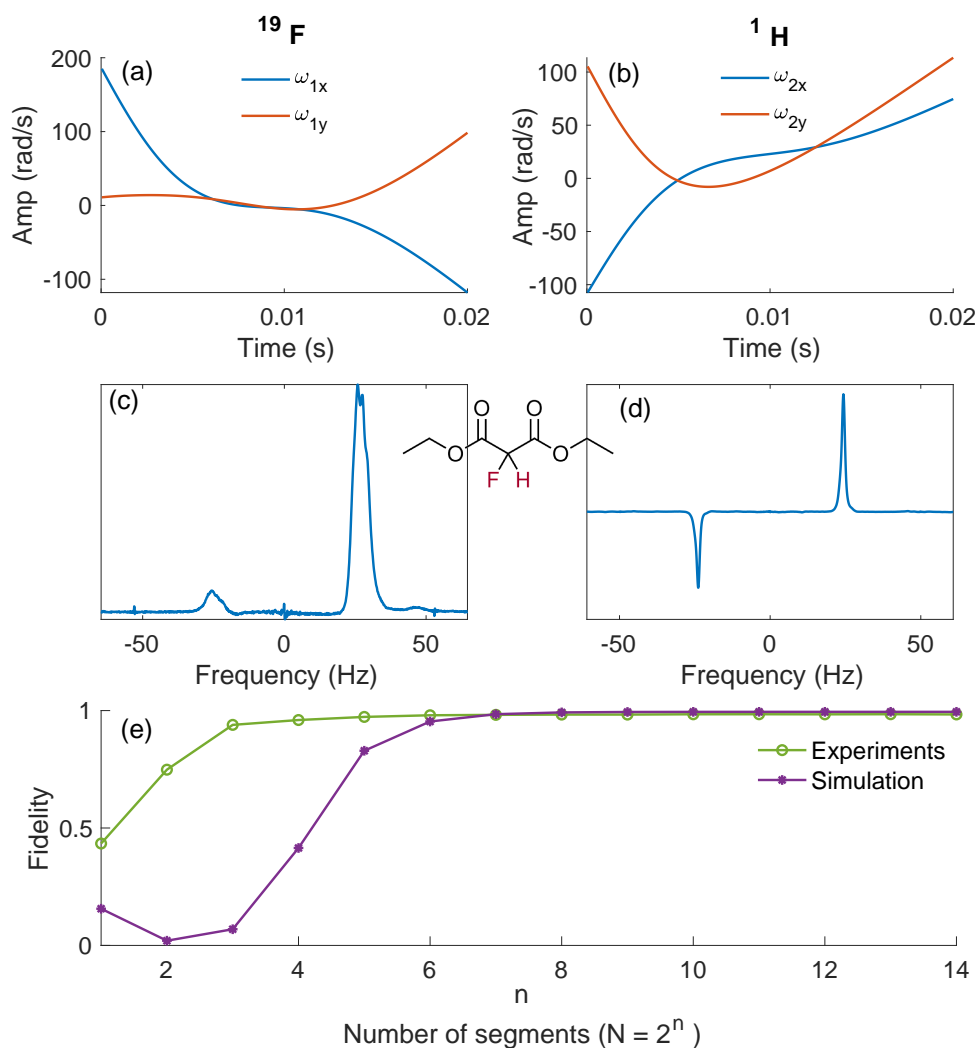


**Figure 5.4:** (a) x and y amplitude and NMR spectra (c) for  $^{19}\text{F}$ , (b) x and y amplitude and NMR spectra (d) for  $^1\text{H}$ , (e) Effect of discretization in terms of fidelity of final state in the experiment (green) and simulation (purple).

fidelity of the CNOT gate. For that, we do not need to perform multiple experiments. Instead, we need to perform one experiment. The signal obtained after one experiment for  $^{19}\text{F}$  and  $^1\text{H}$  is used along with the magnetization matrix to achieve the state after applying CNOT. The corresponding transitions are shown in figure 5.4 (e).



## 5.4 Geometric quantum gates

The geometric phase has the exquisite properties of being inherently robust for parameter fluctuations [297, 298]. Considering an  $N$ -dimensional quantum system with Hamiltonian  $H(t)$  and its time-dependent quantum states  $\{|\phi_k(t)\rangle\}_{k=1}^N$ . For a quantum system evolving cyclically with period  $\tau$ , the time-dependent state is

$$|\phi(\tau)\rangle = \exp[i\alpha(\tau)] |\phi(0)\rangle, \quad (5.12)$$

where total phase  $\alpha(\tau) = \beta(\tau) + \gamma(\tau)$  is the sum of dynamical phase  $\beta(\tau) = -\int_0^\tau \langle \phi(t) | H(t) | \phi(t) \rangle dt$  and non-adiabatic geometric phase  $\gamma(\tau)$ .

For a system having only a geometric phase, we design an inverse problem of finding  $H(t)$  such that,

$$|\phi(\tau)\rangle = \exp[i\gamma(\tau)] |\phi(0)\rangle \quad (5.13)$$

and

$$\langle \phi(t) | H(t) | \phi(t) \rangle = 0. \quad (5.14)$$

The equation 5.13 and 5.14 are also known as cyclic evolution and parallel transport conditions, respectively. To find the Hamiltonian satisfying above conditions, we start with finding an auxiliary set of basis vector  $\{|v_k(t)\rangle\}_{k=1}^N$  such that  $|v_k(t)\rangle = \exp[-i\gamma_k(t)] |\phi_k(t)\rangle$  and  $|v_k(\tau)\rangle = |v_k(0)\rangle = |\phi(0)\rangle$ .

Since  $\phi_k(t)$  is the quantum state and thus satisfies Schrödinger equation

$$i|\dot{\phi}_k(t)\rangle = H(t) |\phi_k(t)\rangle. \quad (5.15)$$

By choosing auxiliary basis, we want  $|\phi_k(t)\rangle = \exp[i\gamma_k(t)] |v_k(t)\rangle$  which modifies the Hamilto-

nian in equation 5.15,

$$\begin{aligned}
 H(t) &= i \sum_{k=1}^N |\dot{\phi}_k(t)\rangle \langle \phi_k(t)| \\
 &= i \sum_{l \neq k}^N \langle v_l(t) | \dot{v}_k(t) \rangle |v_l(t)\rangle \langle v_k(t)|.
 \end{aligned}
 \tag{5.16}$$

The above equation 5.16 satisfies the cyclic evolution and parallel transport condition. Thus, by choosing the auxiliary basis appropriately, we can inverse engineer the Hamiltonian under which we only achieve states with geometric phases, thus having inherent robustness in parameter space.

### One-qubit case

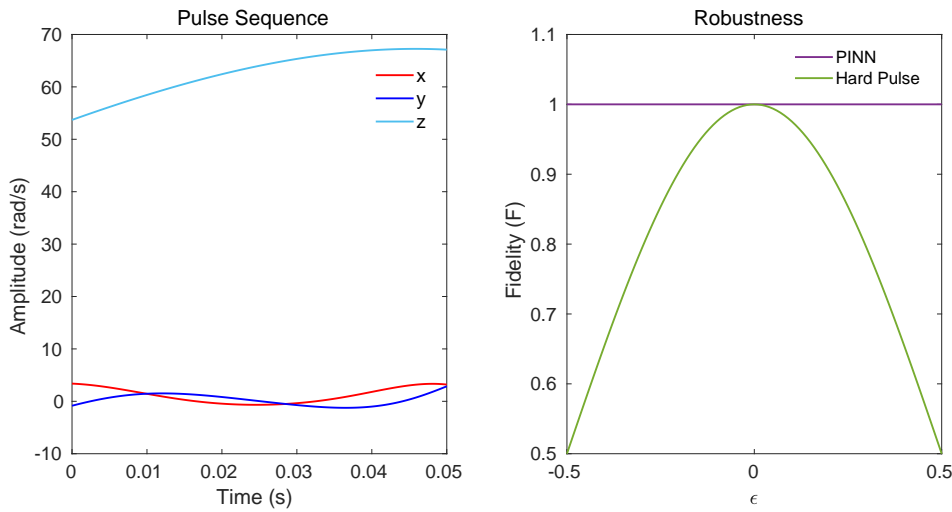


**Figure 5.5:** (a) Pulse sequence for x, y, and z components of Hamiltonian (b) Robustness of x and y control errors in PINN generated sequence as well as hard pulse sequence.

To prepare a universal set of one-qubit gate, we choose the auxiliary basis  $|v_1(t)\rangle$  and  $|v_2(t)\rangle$  in terms of computational basis  $|0\rangle$  and  $|1\rangle$ , such that,

$$|v_1(t)\rangle = \cos\left(\frac{\vartheta(t)}{2}\right) |0\rangle + e^{i\varphi(t)} \sin\left(\frac{\vartheta(t)}{2}\right) |1\rangle
 \tag{5.17}$$

$$|v_2(t)\rangle = e^{i\varphi(t)} \sin\left(\frac{\vartheta(t)}{2}\right) |0\rangle - \cos\left(\frac{\vartheta(t)}{2}\right) |1\rangle,
 \tag{5.18}$$

where  $\vartheta(t)$  and  $\varphi(t)$  are the time-dependent parameters in the 2-dimensional Hilbert space. By inserting the above basis vectors in equation 5.16, we obtain the Hamiltonian  $H(t)$  given as

$$\begin{aligned}
H(t) = & -\frac{1}{2}[\dot{\vartheta}(t) \sin \varphi(t) + \dot{\varphi}(t) \sin \vartheta(t) \cos \vartheta(t) \cos \varphi(t)] \sigma_x \\
& + \frac{1}{2}[\dot{\vartheta}(t) \cos \varphi(t) - \dot{\varphi}(t) \sin \vartheta(t) \cos \vartheta(t) \sin \varphi(t)] \sigma_y \\
& + \frac{1}{2}\dot{\varphi}(t) \sin^2 \vartheta(t) \sigma_z,
\end{aligned} \tag{5.19}$$

where  $\{\sigma_k\}_{k=x,y,z}$  are the Pauli operators.

By employing PINN here, we insert time  $t$  as the neural network input and get the time-dependent parameters  $\vartheta(t)$  and  $\varphi(t)$  as neural network output. We take the neural network of size (1,40,40,2) and construct a one-qubit PH gate. We then compare the robustness against control errors  $x$  and  $y$  for the PINN pulse sequence compared to the hard pulse.

## 5.5 Summary and outlook

At the core of optimization algorithms is the essential requirement of piece-wise constant approximation. Employing a physics-informed neural network (PINN), which offers smooth controls and eliminates the need for discretization, we formulate the control sequence for a two-qubit CNOT gate and the preparation of a Long-Lived Singlet (LLS) state. Exploiting the inherent advantage of geometric phases, we also utilize PINN to create a one-qubit phase gate, showcasing improved robustness compared to dynamical phase approaches. While PINN proves adaptable across various quantum systems, we specifically illustrate its application in Nuclear Magnetic Resonance (NMR) for implementing unitary operations and generating LLS states.

Future endeavours in this domain involve extending geometric gates to holonomic gates and integrating noise with geometric conditions to enhance robustness. This research trajectory aims to advance the versatility and effectiveness of quantum control protocols based on PINN.

## Appendix

Below, we provide the sample code for preparing the LLS state starting from thermal equilibrium in the TCP molecule. Code has three major parts: first importing necessary modules, second defining the Hamiltonian parameters for TCP, third building a neural network, and then employing its optimization.

```

In [ ]: ##### Import necessary package
import numpy as np
import jax
import jax.numpy as jnp
from jax import grad, value_and_grad, jacfwd, jacrev, vmap, jit
from jax.experimental import ode
from jax.example_libraries import optimizers, stax
import jax.nn as nn
import time
import haiku as hk
import optax
from scipy import linalg
import matplotlib.pyplot as plt
from jax.config import config
config.update('jax_enable_x64', True)
import jax.lax.linalg as lax_linalg
import random
from jax.numpy import trace as TR, kron as KRON, array as ar, \
sqrt as SQRT, sin as sin
from datetime import datetime, date

## Load the Hamiltonian parameters
#Pauli matrices
sx = 0.5*ar([[0,1],[1,0]])
sy = 0.5*ar([[0,-1j],[1j,0]])
sz = 0.5*ar([[1,0],[0,-1]])
I = jnp.identity(2)

rhoi = KRON(sz, I) + KRON(I, sz)
rhof = -2*(KRON(sx,sx) + KRON(sy,sy))

n = 2
J = 8.75
T = 0.02
dim = 2**n
Ns = 500
t1 = jnp.linspace(0.0001, T, Ns)
dt = T/(Ns)
v1 = -63.75
v2 = 63.75

#Neural network
def FeedForward(t):
    mlp = hk.Sequential([hk.Flatten(), jnp.tanh,
                        hk.Linear(40), jnp.tanh,
                        hk.Linear(40), jnp.tanh,
                        hk.Linear(4),])

    return mlp(t)

learning_rate = 8e-3
model = hk.transform(FeedForward)

```

```

optimizer = optax.adam(learning_rate)
rng = jax.random.PRNGKey(42)

@jit
def neural_net(weights,t):
    Hin = jnp.array([t])
    H = Hin
    pt = model.apply(weights, rng, H)
    H0 = 2*jnp.pi*j*(KRON(sz, sz)) - 2*jnp.pi*v1*KRON(sz, I) \
    - 2*jnp.pi*v2*KRON(I, sz)
    Ht = 2*jnp.pi*(pt[0]*sin(pt[1])*(KRON(sx, I) + KRON(I, sx))
    + pt[2]*sin(pt[3])*(KRON(sy, I) + KRON(I, sy)))
    return [H0,Ht,pt]

@jit
def rhs(rhot,t, weights):
    [H0,Hf1,_] = neural_net(weights,t)
    Ht = Hf1
    rh = -1j*((H0+Ht)@rhot - rhot@(H0+Ht))
    return rh

@jit
def fidelity(rhof, weights):
    rhot = ode.odeint(rhs, rhoi+1j*0, jnp.array([0.0, T]), weights)
    fid = jnp.real(TR(rhot[-1]@rhof)/SQRT(TR(rhot[-1]@rhot[-1]) \
    *TR(rhof@rhof)))
    return fid

@jit
def loss(weights):
    fid = fidelity(rhof,weights)
    J = 1 - fid
    return J

##Optimization
params = model.init(rng, jnp.array([T]))
opt_state = optimizer.init(params)
epochs = 5000
IF = []

for steps in range(1, epochs+1):
    grads = grad(loss)(params)
    updates, opt_state = optimizer.update(grads, opt_state)
    params = optax.apply_updates(params, updates)
    ls = 1 - fidelity(rhof,params)
    IF.append(ls)
    if steps%10 == 0:
        print("IF : {:.4f}".format(ls))

```



# Thesis Summary

---

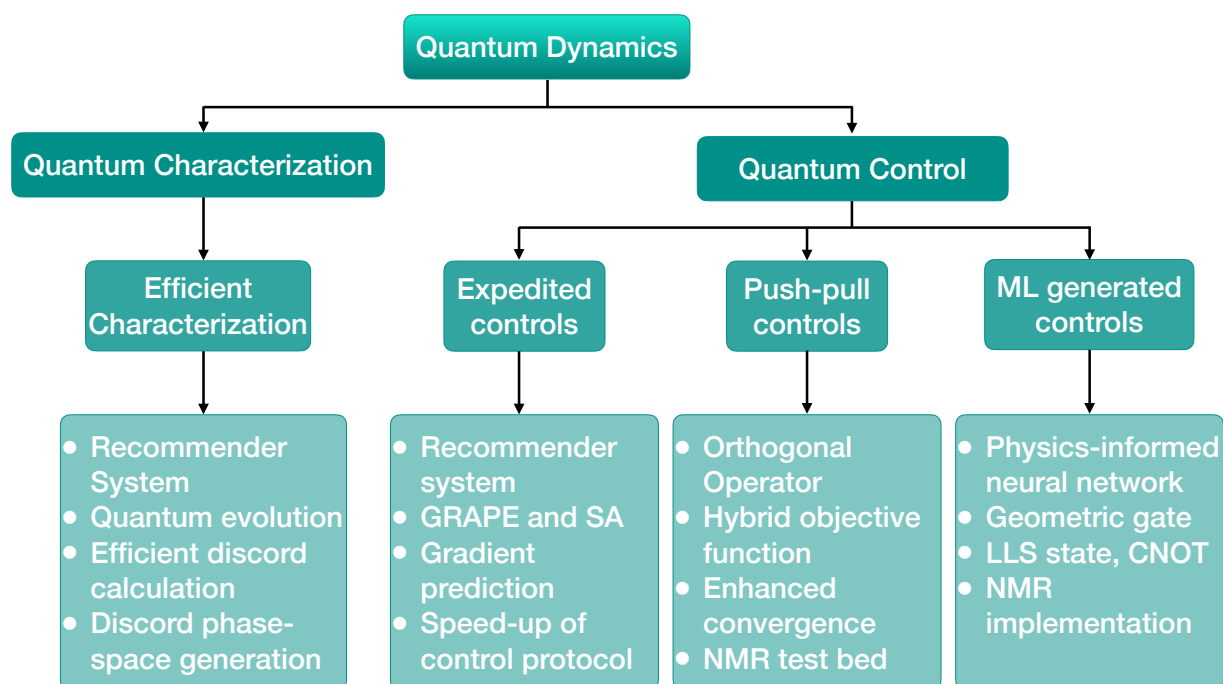


**Figure T1:** Summary of the thesis, and concepts covered in the chapters therein.

In this thesis, we have explored new computational methodologies including machine learning for quantum characterization and control using NMR architecture. Quantum characterization was done for quantum dynamics using quantum correlations such as entanglement and discord, as well as state fidelity. For this, a machine learning based technique called recommender system was utilized and prediction of phase-space plot was done for a non-linear quantum kicked top model. Quantum control algorithms were shown to expedite using the recommender system based method and have better convergence using push-pull method which employed orthogonal operators. Another control algorithm based on physics informed neural network resulted in robust control against control errors. These control algorithms were implemented on NMR test bed to check their efficacy. This thesis highlights some relevant studies of quantum dynamics and applications of these algorithms for usage in quantum computing as well as other upcoming quantum technologies.





---

## Bibliography

---

- [1] Isaac Newton, 1642-1727. *Newton's Principia : The Mathematical Principles of Natural Philosophy*. First American edition, carefully revised and corrected / with a life of the author, by N. W. Chittenden. New-York : Daniel Adee, 1846., 1846. Translation of *Philosophiae naturalis principia*.;Also available in PDF and TIFF formats from the NOAA Central Library.  
Translation of *Philosophiae naturalis principia*.;Also available in PDF and TIFF formats from the NOAA Central Library.
- [2] A. Einstein. Zur Elektrodynamik bewegter Körper. *Ann. Phys.*, 322(10):891–921, 1905. ISSN 1521-3889. doi: 10.1002/andp.19053221004.
- [3] Max Planck. Ueber das Gesetz der Energieverteilung im Normalspectrum. *Ann. Phys.*, 309(3):553–563, 1901. ISSN 1521-3889. doi: 10.1002/andp.19013090310.
- [4] Albert Einstein. Über die von der molekularkinetischen Theorie der Wärme geforderte Bewegung von in ruhenden Flüssigkeiten suspendierten Teilchen. *Ann. Phys.*, vol. 4, t. 17, 1905.
- [5] N. Bohr. I. On the constitution of atoms and molecules. *Lond. Edinb. Dublin Philos. Mag. J. Sci.*, 26(151):1–25, July 1913. ISSN 1941-5982. doi: 10.1080/14786441308634955.
- [6] W. Gerlach and O. Stern. Der experimentelle Nachweis des magnetischen Moments des Silberatoms. *Z Phys.*, 8(1):110–111, December 1922. ISSN 0044-3328. doi: 10.1007/BF01329580.
- [7] Walther Gerlach and Otto Stern. Der experimentelle Nachweis der Richtungsquantelung im Magnetfeld. *Z Phys.*, 9(1):349–352, December 1922. ISSN 0044-3328. doi: 10.1007/BF01326983.

- [8] Walther Gerlach and Otto Stern. Das magnetische Moment des Silberatoms. *Z Phys.*, 9(1): 353–355, December 1922. ISSN 0044-3328. doi: 10.1007/BF01326984.
- [9] Louis De Broglie. Waves and Quanta. *Nature*, 112(2815):540–540, October 1923. ISSN 1476-4687. doi: 10.1038/112540a0.
- [10] M. Born, W. Heisenberg, and P. Jordan. Zur Quantenmechanik. II. *Z Phys.*, 35(8):557–615, August 1926. ISSN 0044-3328. doi: 10.1007/BF01379806.
- [11] E. Schrödinger. An Undulatory Theory of the Mechanics of Atoms and Molecules. *Phys. Rev.*, 28(6):1049–1070, December 1926. doi: 10.1103/PhysRev.28.1049.
- [12] Vlatko Vedral and Martin B. Plenio. Basics of quantum computation. *Prog. Quantum Electron.*, 22(1):1–39, January 1998. ISSN 0079-6727. doi: 10.1016/S0079-6727(98)00004-4.
- [13] J. S. Bell. On the Einstein Podolsky Rosen paradox. *Phys. Phys. Fiz.*, 1(3):195–200, November 1964. doi: 10.1103/PhysicsPhysiqueFizika.1.195.
- [14] David Deutsch and Roger Penrose. Quantum theory, the Church–Turing principle and the universal quantum computer. *Proc. R. Soc. Lond. Math. Phys. Sci.*, 400(1818):97–117, January 1997. doi: 10.1098/rspa.1985.0070.
- [15] P.W. Shor. Algorithms for quantum computation: Discrete logarithms and factoring. In *Proc. 35th Annu. Symp. Found. Comput. Sci.*, pages 124–134, November 1994. doi: 10.1109/SFCS.1994.365700.
- [16] Lov K. Grover. A fast quantum mechanical algorithm for database search. In *Proc. Twenty-Eighth Annu. ACM Symp. Theory Comput.*, STOC '96, pages 212–219, New York, NY, USA, July 1996. Association for Computing Machinery. ISBN 978-0-89791-785-8. doi: 10.1145/237814.237866.
- [17] C. E. Shannon. A mathematical theory of communication. *Bell Syst. Tech. J.*, 27(3):379–423, July 1948. ISSN 0005-8580. doi: 10.1002/j.1538-7305.1948.tb01338.x.

- [18] J. Bardeen and W. H. Brattain. The Transistor, A Semi-Conductor Triode. *Phys. Rev.*, 74 (2):230–231, July 1948. doi: 10.1103/PhysRev.74.230.
- [19] Richard P. Feynman. Simulating physics with computers. *Int J Theor Phys*, 21(6):467–488, June 1982. ISSN 1572-9575. doi: 10.1007/BF02650179.
- [20] Adrian Cho. Google claims quantum computing milestone. *Science*, 365(6460):1364–1364, September 2019. doi: 10.1126/science.365.6460.1364.
- [21] Michael Brooks. Beyond quantum supremacy: The hunt for useful quantum computers. *Nature*, 574(7776):19–22, October 2019. ISSN 00280836.
- [22] Elizabeth Gibney. Quantum computer race intensifies as alternative technology gains steam. *Nature*, 587(7834):342–343, November 2020. doi: 10.1038/d41586-020-03237-w. Bandiera\_abtest: a Cg\_type: News Subject\_term: Technology, Computer science, Quantum information.
- [23] Jonathan A. Jones. Quantum computing with NMR. *Prog. Nucl. Magn. Reson. Spectrosc.*, 59(2):91–120, August 2011. ISSN 0079-6565. doi: 10.1016/j.pnmrs.2010.11.001.
- [24] J. R. Weber, W. F. Koehl, J. B. Varley, A. Janotti, B. B. Buckley, C. G. Van de Walle, and D. D. Awschalom. Quantum computing with defects. *Proc. Natl. Acad. Sci.*, 107(19): 8513–8518, May 2010. doi: 10.1073/pnas.1003052107.
- [25] Peter Michler, editor. *Quantum Dots for Quantum Information Technologies*. Nano-Optics and Nanophotonics. Springer International Publishing, Cham, 2017. ISBN 978-3-319-56377-0 978-3-319-56378-7. doi: 10.1007/978-3-319-56378-7.
- [26] H Haffner, C Roos, and R Blatt. Quantum computing with trapped ions. *Phys. Rep.*, 469 (4):155–203, December 2008. ISSN 03701573. doi: 10.1016/j.physrep.2008.09.003.
- [27] M. H. Devoret and R. J. Schoelkopf. Superconducting Circuits for Quantum Information: An Outlook. *Science*, 339(6124):1169–1174, March 2013. doi: 10.1126/science.1231930.
- [28] C. Monroe. Quantum information processing with atoms and photons. *Nature*, 416(6877): 238–246, March 2002. ISSN 1476-4687. doi: 10.1038/416238a.

- [29] M. Saffman, T. G. Walker, and K. Mølmer. Quantum information with Rydberg atoms. *Rev. Mod. Phys.*, 82(3):2313–2363, August 2010. ISSN 0034-6861, 1539-0756. doi: 10.1103/RevModPhys.82.2313.
- [30] Heinz-Peter Breuer and Francesco Petruccione. *The Theory of Open Quantum Systems*. Oxford University Press, 2002. ISBN 978-0-19-852063-4.
- [31] Angel Rivas and Susana F. Huelga. *Open Quantum Systems: An Introduction*. Springer-Briefs in Physics. Springer, Berlin, Heidelberg, 2012. ISBN 978-3-642-23353-1 978-3-642-23354-8. doi: 10.1007/978-3-642-23354-8.
- [32] Daniel Manzano. A short introduction to the Lindblad master equation. *AIP Adv.*, 10(2): 025106, February 2020. ISSN 2158-3226. doi: 10.1063/1.5115323.
- [33] Vladimir B. Braginsky and Farid Ya Khalili. *Quantum Measurement*. Cambridge University Press, May 1995. ISBN 978-0-521-48413-8.
- [34] Kavan Modi, Aharon Brodutch, Hugo Cable, Tomasz Paterek, and Vlatko Vedral. The classical-quantum boundary for correlations: Discord and related measures. *Rev. Mod. Phys.*, 84(4):1655–1707, November 2012. doi: 10.1103/RevModPhys.84.1655.
- [35] Gerardo Adesso, Thomas R. Bromley, and Marco Cianciaruso. Measures and applications of quantum correlations. *J. Phys. A: Math. Theor.*, 49(47):473001, November 2016. ISSN 1751-8121. doi: 10.1088/1751-8113/49/47/473001.
- [36] Felipe Fernandes Fanchini, Diogo De Oliveira Soares Pinto, and Gerardo Adesso, editors. *Lectures on General Quantum Correlations and Their Applications*. Quantum Science and Technology. Springer International Publishing, Cham, 2017. ISBN 978-3-319-53410-7 978-3-319-53412-1. doi: 10.1007/978-3-319-53412-1.
- [37] A. Einstein, B. Podolsky, and N. Rosen. Can Quantum-Mechanical Description of Physical Reality Be Considered Complete? *Phys. Rev.*, 47(10):777–780, May 1935. doi: 10.1103/PhysRev.47.777.

- [38] John F. Clauser, Michael A. Horne, Abner Shimony, and Richard A. Holt. Proposed Experiment to Test Local Hidden-Variable Theories. *Phys. Rev. Lett.*, 23(15):880–884, October 1969. doi: 10.1103/PhysRevLett.23.880.
- [39] B. S. Tsirel'son. Quantum analogues of the Bell inequalities. The case of two spatially separated domains. *J Math Sci*, 36(4):557–570, February 1987. ISSN 1573-8795. doi: 10.1007/BF01663472.
- [40] Stuart J. Freedman and John F. Clauser. Experimental Test of Local Hidden-Variable Theories. *Phys. Rev. Lett.*, 28(14):938–941, April 1972. doi: 10.1103/PhysRevLett.28.938.
- [41] Alain Aspect, Jean Dalibard, and Gérard Roger. Experimental Test of Bell's Inequalities Using Time-Varying Analyzers. *Phys. Rev. Lett.*, 49(25):1804–1807, December 1982. doi: 10.1103/PhysRevLett.49.1804.
- [42] Dik Bouwmeester, Jian-Wei Pan, Klaus Mattle, Manfred Eibl, Harald Weinfurter, and Anton Zeilinger. Experimental quantum teleportation. *Nature*, 390(6660):575–579, December 1997. ISSN 1476-4687. doi: 10.1038/37539.
- [43] Ludwig Burger, Niklas Pollard, and Jonathan Allen. Sleuths of 'spooky' quantum science win Nobel physics prize. *Reuters*, October 2022.
- [44] Michael Schirber. Nobel Prize: Quantum Entanglement Unveiled. *Physics*, 15:153, October 2022. doi: 10.1103/PhysRevLett.49.1804.
- [45] Asher Peres. Separability Criterion for Density Matrices. *Phys. Rev. Lett.*, 77(8):1413–1415, August 1996. ISSN 0031-9007, 1079-7114. doi: 10.1103/PhysRevLett.77.1413.
- [46] Charles H. Bennett, David P. DiVincenzo, John A. Smolin, and William K. Wootters. Mixed-state entanglement and quantum error correction. *Phys. Rev. A*, 54(5):3824–3851, November 1996. doi: 10.1103/PhysRevA.54.3824.
- [47] Ryszard Horodecki, Paweł Horodecki, Michał Horodecki, and Karol Horodecki. Quantum entanglement. *Rev. Mod. Phys.*, 81(2):865–942, June 2009. doi: 10.1103/RevModPhys.81.865.

- [48] Harold Ollivier and Wojciech H. Zurek. Quantum Discord: A Measure of the Quantumness of Correlations. *Phys. Rev. Lett.*, 88(1):017901, December 2001. ISSN 0031-9007, 1079-7114. doi: 10.1103/PhysRevLett.88.017901.
- [49] Kavan Modi. A Pedagogical Overview of Quantum Discord. *Open Syst. Inf. Dyn.*, 21(01n02):1440006, June 2014. ISSN 1230-1612. doi: 10.1142/S123016121440006X.
- [50] Alexander Streltsov. Quantum Correlations Beyond Entanglement. In Alexander Streltsov, editor, *Quantum Correlations Beyond Entanglement: And Their Role in Quantum Information Theory*, SpringerBriefs in Physics, pages 17–22. Springer International Publishing, Cham, 2015. ISBN 978-3-319-09656-8. doi: 10.1007/978-3-319-09656-8\_4.
- [51] Yichen Huang. Computing quantum discord is NP-complete. *New J. Phys.*, 16(3):033027, March 2014. ISSN 1367-2630. doi: 10.1088/1367-2630/16/3/033027.
- [52] Yeong-Cherng Liang, Yu-Hao Yeh, Paulo E. M. F. Mendonça, Run Yan Teh, Margaret D. Reid, and Peter D. Drummond. Quantum fidelity measures for mixed states. *Rep. Prog. Phys.*, 82(7):076001, June 2019. ISSN 0034-4885. doi: 10.1088/1361-6633/ab1ca4.
- [53] Benjamin Schumacher. Quantum coding. *Phys. Rev. A*, 51(4):2738–2747, April 1995. doi: 10.1103/PhysRevA.51.2738.
- [54] A. Uhlmann. The “Transition probability” in the state space of a  $C^*$ -Algebra. *Rep. Math. Phys.*, 9(2):273–279, April 1976. ISSN 0034-4877. doi: 10.1016/0034-4877(76)90060-4.
- [55] Richard Jozsa. Fidelity for Mixed Quantum States. *J. Mod. Opt.*, December 1994. doi: 10.1080/09500349414552171.
- [56] T. D. Ladd, F. Jelezko, R. Laflamme, Y. Nakamura, C. Monroe, and J. L. O’Brien. Quantum computers. *Nature*, 464(7285):45–53, March 2010. ISSN 1476-4687. doi: 10.1038/nature08812.
- [57] Laszlo Gyongyosi and Sandor Imre. A Survey on quantum computing technology. *Comput. Sci. Rev.*, 31:51–71, February 2019. ISSN 1574-0137. doi: 10.1016/j.cosrev.2018.11.002.

- [58] Ivan Oliveira, Roberto Sarthour Jr, Tito Bonagamba, Eduardo Azevedo, and Jair C. C. Freitas. *NMR Quantum Information Processing*. Elsevier, April 2011. ISBN 978-0-08-049752-5.
- [59] P. Krantz, M. Kjaergaard, F. Yan, T. P. Orlando, S. Gustavsson, and W. D. Oliver. A quantum engineer's guide to superconducting qubits. *Appl. Phys. Rev.*, 6(2):021318, June 2019. ISSN 1931-9401. doi: 10.1063/1.5089550.
- [60] Pieter Kok, W. J. Munro, Kae Nemoto, T. C. Ralph, Jonathan P. Dowling, and G. J. Milburn. Linear optical quantum computing with photonic qubits. *Rev. Mod. Phys.*, 79(1):135–174, January 2007. doi: 10.1103/RevModPhys.79.135.
- [61] Fulvio Flamini, Nicolò Spagnolo, and Fabio Sciarrino. Photonic quantum information processing: A review. *Rep. Prog. Phys.*, 82(1):016001, November 2018. ISSN 0034-4885. doi: 10.1088/1361-6633/aad5b2.
- [62] Sergei Slussarenko and Geoff J. Pryde. Photonic quantum information processing: A concise review. *Appl. Phys. Rev.*, 6(4):041303, October 2019. ISSN 1931-9401. doi: 10.1063/1.5115814.
- [63] Jörg Wrachtrup and Fedor Jelezko. Processing quantum information in diamond. *J. Phys.: Condens. Matter*, 18(21):S807, May 2006. ISSN 0953-8984. doi: 10.1088/0953-8984/18/21/S08.
- [64] Sébastien Pezzagna and Jan Meijer. Quantum computer based on color centers in diamond. *Appl. Phys. Rev.*, 8(1):011308, February 2021. ISSN 1931-9401. doi: 10.1063/5.0007444.
- [65] Colin D. Bruzewicz, John Chiaverini, Robert McConnell, and Jeremy M. Sage. Trapped-ion quantum computing: Progress and challenges. *Appl. Phys. Rev.*, 6(2):021314, May 2019. ISSN 1931-9401. doi: 10.1063/1.5088164.
- [66] Loïc Henriët, Lucas Beguin, Adrien Signoles, Thierry Lahaye, Antoine Browaeys, Georges-Olivier Reymond, and Christophe Jurczak. Quantum computing with neutral atoms. *Quantum*, 4:327, September 2020. doi: 10.22331/q-2020-09-21-327.



- [67] C. S. Adams, J. D. Pritchard, and J. P. Shaffer. Rydberg atom quantum technologies. *J. Phys. B: At. Mol. Opt. Phys.*, 53(1):012002, December 2019. ISSN 0953-4075. doi: 10.1088/1361-6455/ab52ef.
- [68] Yasuhiko Arakawa and Mark J. Holmes. Progress in quantum-dot single photon sources for quantum information technologies: A broad spectrum overview. *Appl. Phys. Rev.*, 7(2): 021309, June 2020. ISSN 1931-9401. doi: 10.1063/5.0010193.
- [69] David P. DiVincenzo. The Physical Implementation of Quantum Computation. *Fortschritte Phys.*, 48(9-11):771–783, 2000. ISSN 1521-3978. doi: 10.1002/1521-3978(200009)48:9/11<771::AID-PROP771>3.0.CO;2-E.
- [70] Chris Boesch. Nobel prizes for nuclear magnetic resonance: 2003 and Historical perspectives. *J. Magn. Reson. Imaging*, 20(2):177–179, 2004. ISSN 1522-2586. doi: 10.1002/jmri.20120.
- [71] Neil A. Gershenfeld and Isaac L. Chuang. Bulk Spin-Resonance Quantum Computation. *Science*, 275(5298):350–356, January 1997. doi: 10.1126/science.275.5298.350.
- [72] David G. Cory, Amr F. Fahmy, and Timothy F. Havel. Ensemble quantum computing by NMR spectroscopy. *Proc. Natl. Acad. Sci.*, 94(5):1634–1639, March 1997. doi: 10.1073/pnas.94.5.1634.
- [73] M. A. Nielsen, E. Knill, and R. Laflamme. Complete quantum teleportation using nuclear magnetic resonance. *Nature*, 396(6706):52–55, November 1998. ISSN 1476-4687. doi: 10.1038/23891.
- [74] John Cavanagh, Wayne J. Fairbrother, Arthur G. Palmer III, and Nicholas J. Skelton. *Protein NMR Spectroscopy: Principles and Practice*. Elsevier, November 1995. ISBN 978-0-08-051529-8.
- [75] Malcolm H. Levitt. *Spin Dynamics: Basics of Nuclear Magnetic Resonance*. John Wiley & Sons, May 2013. ISBN 978-1-118-68184-8.
- [76] James Keeler. *Understanding NMR Spectroscopy*. John Wiley & Sons, September 2011. ISBN 978-1-119-96493-3.

- [77] David G. Cory, Mark D. Price, and Timothy F. Havel. Nuclear magnetic resonance spectroscopy: An experimentally accessible paradigm for quantum computing. *Physica D: Nonlinear Phenomena*, 120(1):82–101, September 1998. ISSN 0167-2789. doi: 10.1016/S0167-2789(98)00046-3.
- [78] John C. Doyle, Bruce A. Francis, and Allen R. Tannenbaum. *Feedback Control Theory*. Courier Corporation, April 2013. ISBN 978-0-486-31833-2.
- [79] Steven A. Frank. *Control Theory Tutorial: Basic Concepts Illustrated by Software Examples*. Springer, May 2018. ISBN 978-3-319-91707-8.
- [80] Jerzy Zabczyk. *Mathematical Control Theory: An Introduction*. Systems & Control: Foundations & Applications. Springer International Publishing, Cham, 2020. ISBN 978-3-030-44776-2 978-3-030-44778-6. doi: 10.1007/978-3-030-44778-6.
- [81] John Bechhoefer. *Control Theory for Physicists*. Cambridge University Press, April 2021. ISBN 978-1-107-00118-3.
- [82] Roland Burns. *Advanced Control Engineering*. Elsevier, October 2001. ISBN 978-0-08-049878-2.
- [83] Moshe Shapiro and Paul Brumer. Coherent control of molecular dynamics. *Rep. Prog. Phys.*, 66(6):859, May 2003. ISSN 0034-4885. doi: 10.1088/0034-4885/66/6/201.
- [84] H. Rabitz, null de Vivie-Riedle R, M. Motzkus, and K. Kompa. Whither the future of controlling quantum phenomena? *Science*, 288(5467):824–828, May 2000. ISSN 1095-9203. doi: 10.1126/science.288.5467.824.
- [85] Marcos Dantus and Vadim V. Lozovoy. Experimental Coherent Laser Control of Physicochemical Processes. *Chem. Rev.*, 104(4):1813–1860, April 2004. ISSN 0009-2665. doi: 10.1021/cr020668r.
- [86] J. Werschnik and E. K. U. Gross. Quantum optimal control theory. *J. Phys. B: At. Mol. Opt. Phys.*, 40(18):R175, September 2007. ISSN 0953-4075. doi: 10.1088/0953-4075/40/18/R01.

- [87] Steffen J. Glaser, Ugo Boscain, Tommaso Calarco, Christiane P. Koch, Walter Köckenberger, Ronnie Kosloff, Ilya Kuprov, Burkhard Luy, Sophie Schirmer, Thomas Schulte-Herbrüggen, Dominique Sugny, and Frank K. Wilhelm. Training Schrödinger’s cat: Quantum optimal control. *Eur. Phys. J. D*, 69(12):279, December 2015. ISSN 1434-6079. doi: 10.1140/epjd/e2015-60464-1.
- [88] Domenico D’Alessandro. *Introduction to Quantum Control and Dynamics*. CRC Press, July 2021. ISBN 978-1-00-039499-3.
- [89] Christiane P. Koch, Ugo Boscain, Tommaso Calarco, Gunther Dirr, Stefan Filipp, Steffen J. Glaser, Ronnie Kosloff, Simone Montangero, Thomas Schulte-Herbrüggen, Dominique Sugny, and Frank K. Wilhelm. Quantum optimal control in quantum technologies. Strategic report on current status, visions and goals for research in Europe. *EPJ Quantum Technol.*, 9(1):19, December 2022. ISSN 2662-4400, 2196-0763. doi: 10.1140/epjqt/s40507-022-00138-x.
- [90] T. S. Mahesh, Priya Batra, and M. Harshanth Ram. Quantum Optimal Control: Practical Aspects and Diverse Methods. *J Indian Inst Sci*, 103(2):591–607, April 2023. ISSN 0019-4964. doi: 10.1007/s41745-022-00311-2.
- [91] Eric W. Weisstein. Lyapunov Function.
- [92] Alberto Isidori. *Nonlinear Control Systems*. Communications and Control Engineering. Springer, London, 1995. ISBN 978-1-4471-3909-6 978-1-84628-615-5. doi: 10.1007/978-1-84628-615-5.
- [93] Paolo Vettori. On the convergence of a feedback control strategy for multilevel quantum systems. In *Proc. MTNS Conf.*, pages 1–6. Citeseer, 2002.
- [94] Symeon Grivopoulos and Bassam Bamieh. Lyapunov-based control of quantum systems. In *42nd IEEE Int. Conf. Decis. Control IEEE Cat No 03CH37475*, volume 1, pages 434–438. IEEE, 2003.
- [95] Mazyar Mirrahimi, Pierre Rouchon, and Gabriel Turinici. Lyapunov control of bilinear

- Schrödinger equations. *Automatica*, 41(11):1987–1994, November 2005. ISSN 0005-1098. doi: 10.1016/j.automatica.2005.05.018.
- [96] Jean-Michel Coron, Andreea Grigoriu, Cătălin Lefter, and Gabriel Turinici. Quantum control design by Lyapunov trajectory tracking for dipole and polarizability coupling. *New J. Phys.*, 11(10):105034, October 2009. ISSN 1367-2630. doi: 10.1088/1367-2630/11/10/105034.
- [97] Xiaoting Wang and S. G. Schirmer. Entanglement generation between distant atoms by Lyapunov control. *Phys. Rev. A*, 80(4):042305, October 2009. doi: 10.1103/PhysRevA.80.042305.
- [98] S. C. Hou, M. A. Khan, X. X. Yi, Daoyi Dong, and Ian R. Petersen. Optimal Lyapunov-based quantum control for quantum systems. *Phys. Rev. A*, 86(2):022321, August 2012. doi: 10.1103/PhysRevA.86.022321.
- [99] Sen Kuang, Daoyi Dong, and Ian R. Petersen. Rapid Lyapunov control of finite-dimensional quantum systems. *Automatica*, 81:164–175, July 2017. ISSN 0005-1098. doi: 10.1016/j.automatica.2017.02.041.
- [100] Alexander Pechen and Herschel Rabitz. Teaching the environment to control quantum systems. *Phys. Rev. A*, 73(6):062102, June 2006. doi: 10.1103/PhysRevA.73.062102.
- [101] Raffaele Romano and Domenico D’Alessandro. Environment-Mediated Control of a Quantum System. *Phys. Rev. Lett.*, 97(8):080402, August 2006. doi: 10.1103/PhysRevLett.97.080402.
- [102] Evan M. Fortunato, Marco A. Pravia, Nicolas Boulant, Grum Teklemariam, Timothy F. Havel, and David G. Cory. Design of strongly modulating pulses to implement precise effective Hamiltonians for quantum information processing. *J. Chem. Phys.*, 116(17):7599–7606, April 2002. ISSN 0021-9606. doi: 10.1063/1.1465412.
- [103] Navin Khaneja, Roger Brockett, and Steffen J. Glaser. Time optimal control in spin systems. *Phys. Rev. A*, 63(3):032308, February 2001. doi: 10.1103/PhysRevA.63.032308.

- [104] Ugo Boscain, Grégoire Charlot, Jean-Paul Gauthier, Stéphane Guérin, and Hans-Rudolf Jauslin. Optimal control in laser-induced population transfer for two- and three-level quantum systems. *J. Math. Phys.*, 43(5):2107–2132, April 2002. ISSN 0022-2488. doi: 10.1063/1.1465516.
- [105] Ugo Boscain and Paolo Mason. Time minimal trajectories for a spin 1/2 particle in a magnetic field. *J. Math. Phys.*, 47(6):062101, June 2006. ISSN 0022-2488. doi: 10.1063/1.2203236.
- [106] Navin Khaneja, Timo Reiss, Cindie Kehlet, Thomas Schulte-Herbrüggen, and Steffen J. Glaser. Optimal control of coupled spin dynamics: Design of NMR pulse sequences by gradient ascent algorithms. *J. Magn. Reson.*, 172(2):296–305, February 2005. ISSN 1090-7807. doi: 10.1016/j.jmr.2004.11.004.
- [107] Colm Ryan. *Characterization and Control in Large Hilbert Spaces*. Doctoral Thesis, University of Waterloo, December 2008. Accepted: 2008-12-03T16:45:25Z  
Accepted: 2008-12-03T16:45:25Z.
- [108] P. de Fouquieres, S. G. Schirmer, S. J. Glaser, and Ilya Kuprov. Second order gradient ascent pulse engineering. *J. Magn. Reson.*, 212(2):412–417, October 2011. ISSN 1090-7807. doi: 10.1016/j.jmr.2011.07.023.
- [109] D. L. Goodwin and Ilya Kuprov. Modified Newton-Raphson GRAPE methods for optimal control of spin systems. *J. Chem. Phys.*, 144(20):204107, May 2016. ISSN 0021-9606. doi: 10.1063/1.4949534.
- [110] Priya Batra, V. R. Krithika, and T. S. Mahesh. Push-pull optimization of quantum controls. *Phys. Rev. Research*, 2(1):013314, March 2020. ISSN 2643-1564. doi: 10.1103/PhysRevResearch.2.013314.
- [111] Vadim Krotov. *Global Methods in Optimal Control Theory*. CRC Press, October 1995. ISBN 978-0-8247-9329-6.
- [112] Ivan I. Maximov, Zdeněk Tošner, and Niels Chr. Nielsen. Optimal control design of NMR

- and dynamic nuclear polarization experiments using monotonically convergent algorithms. *J. Chem. Phys.*, 128(18):184505, May 2008. ISSN 0021-9606. doi: 10.1063/1.2903458.
- [113] Mads S. Vinding, Ivan I. Maximov, Zdeněk Tošner, and Niels Chr. Nielsen. Fast numerical design of spatial-selective rf pulses in MRI using Krotov and quasi-Newton based optimal control methods. *J. Chem. Phys.*, 137(5):054203, August 2012. ISSN 0021-9606. doi: 10.1063/1.4739755.
- [114] Xiangzhen Zhou, Sanjiang Li, and Yuan Feng. Quantum Circuit Transformation Based on Simulated Annealing and Heuristic Search. *IEEE Trans. Comput.-Aided Des. Integr. Circuits Syst.*, 39(12):4683–4694, December 2020. ISSN 1937-4151. doi: 10.1109/TCAD.2020.2969647.
- [115] Haozhen Situ and Zhimin He. Using simulated annealing to learn the SDC quantum protocol. *Eur. Phys. J. Plus*, 137(1):98, January 2022. ISSN 2190-5444. doi: 10.1140/epjp/s13360-021-02336-5.
- [116] M. Harshanth Ram, V. R. Krithika, Priya Batra, and T. S. Mahesh. Robust quantum control using hybrid pulse engineering. *Phys. Rev. A*, 105(4):042437, April 2022. doi: 10.1103/PhysRevA.105.042437.
- [117] Ehsan Zahedinejad, Sophie Schirmer, and Barry C. Sanders. Evolutionary algorithms for hard quantum control. *Phys. Rev. A*, 90(3):032310, September 2014. doi: 10.1103/PhysRevA.90.032310.
- [118] Gaurav Bhole, V. S. Anjusha, and T. S. Mahesh. Steering quantum dynamics via bang-bang control: Implementing optimal fixed-point quantum search algorithm. *Phys. Rev. A*, 93(4):042339, April 2016. doi: 10.1103/PhysRevA.93.042339.
- [119] Deepak Khurana and T. S. Mahesh. Bang-bang optimal control of large spin systems: Enhancement of  $^{13}\text{C}$ – $^{13}\text{C}$  singlet-order at natural abundance. *J. Magn. Reson.*, 284:8–14, November 2017. ISSN 1090-7807. doi: 10.1016/j.jmr.2017.09.006.
- [120] Hailan Ma, Chunlin Chen, and Daoyi Dong. Differential Evolution with Equally-Mixed

- Strategies for Robust Control of Open Quantum Systems. In *2015 IEEE Int. Conf. Syst. Man Cybern.*, pages 2055–2060, October 2015. doi: 10.1109/SMC.2015.359.
- [121] Patrick Doria, Tommaso Calarco, and Simone Montangero. Optimal Control Technique for Many-Body Quantum Dynamics. *Phys. Rev. Lett.*, 106(19):190501, May 2011. doi: 10.1103/PhysRevLett.106.190501.
- [122] Tommaso Caneva, Tommaso Calarco, and Simone Montangero. Chopped random-basis quantum optimization. *Phys. Rev. A*, 84(2):022326, August 2011. doi: 10.1103/PhysRevA.84.022326.
- [123] N. Rach, M. M. Müller, T. Calarco, and S. Montangero. Dressing the chopped-random-basis optimization: A bandwidth-limited access to the trap-free landscape. *Phys. Rev. A*, 92(6):062343, December 2015. doi: 10.1103/PhysRevA.92.062343.
- [124] J. J. W. H. Sørensen, M. O. Aramburu, T. Heinzl, and J. F. Sherson. Quantum optimal control in a chopped basis: Applications in control of Bose-Einstein condensates. *Phys. Rev. A*, 98(2):022119, August 2018. doi: 10.1103/PhysRevA.98.022119.
- [125] Re-Bing Wu, Haijin Ding, Daoyi Dong, and Xiaoting Wang. Learning robust and high-precision quantum controls. *Phys. Rev. A*, 99(4):042327, April 2019. doi: 10.1103/PhysRevA.99.042327.
- [126] Shai Machnes, Elie Assémat, David Tannor, and Frank K. Wilhelm. Tunable, Flexible, and Efficient Optimization of Control Pulses for Practical Qubits. *Phys. Rev. Lett.*, 120(15):150401, April 2018. doi: 10.1103/PhysRevLett.120.150401.
- [127] David Silver, Aja Huang, Chris J. Maddison, Arthur Guez, Laurent Sifre, George van den Driessche, Julian Schrittwieser, Ioannis Antonoglou, Veda Panneershelvam, Marc Lanctot, Sander Dieleman, Dominik Grewe, John Nham, Nal Kalchbrenner, Ilya Sutskever, Timothy Lillicrap, Madeleine Leach, Koray Kavukcuoglu, Thore Graepel, and Demis Hassabis. Mastering the game of Go with deep neural networks and tree search. *Nature*, 529(7587):484–489, January 2016. ISSN 1476-4687. doi: 10.1038/nature16961.

- [128] Marin Bukov, Alexandre G. R. Day, Dries Sels, Phillip Weinberg, Anatoli Polkovnikov, and Pankaj Mehta. Reinforcement Learning in Different Phases of Quantum Control. *Phys. Rev. X*, 8(3):031086, September 2018. doi: 10.1103/PhysRevX.8.031086.
- [129] Murphy Yuezhen Niu, Sergio Boixo, Vadim N. Smelyanskiy, and Hartmut Neven. Universal quantum control through deep reinforcement learning. *npj Quantum Inf*, 5(1):1–8, April 2019. ISSN 2056-6387. doi: 10.1038/s41534-019-0141-3.
- [130] Zheng An and D. L. Zhou. Deep reinforcement learning for quantum gate control. *EPL*, 126(6):60002, July 2019. ISSN 0295-5075. doi: 10.1209/0295-5075/126/60002.
- [131] Xiao-Ming Zhang, Zezhu Wei, Raza Asad, Xu-Chen Yang, and Xin Wang. When does reinforcement learning stand out in quantum control? A comparative study on state preparation. *npj Quantum Inf*, 5(1):1–7, October 2019. ISSN 2056-6387. doi: 10.1038/s41534-019-0201-8.
- [132] Utkan Güngördü and J. P. Kestner. Robust quantum gates using smooth pulses and physics-informed neural networks. *Phys. Rev. Res.*, 4(2):023155, May 2022. doi: 10.1103/PhysRevResearch.4.023155.
- [133] Ariel Norambuena, Marios Mattheakis, Francisco J. González, and Raúl Coto. Physics-informed neural networks for quantum control, June 2022. Comment: 14 pages, 9 figures  
Comment: 14 pages, 9 figures.
- [134] Frank Schäfer, Michal Kloc, Christoph Bruder, and Niels Lörch. A differentiable programming method for quantum control. *Mach. Learn.: Sci. Technol.*, 1(3):035009, August 2020. ISSN 2632-2153. doi: 10.1088/2632-2153/ab9802.
- [135] Ilia Khait, Juan Carrasquilla, and Dvira Segal. Optimal control of quantum thermal machines using machine learning. *Phys. Rev. Research*, 4(1):L012029, March 2022. ISSN 2643-1564. doi: 10.1103/PhysRevResearch.4.L012029.
- [136] S. Machnes, U. Sander, S. J. Glaser, P. de Fouquières, A. Gruslys, S. Schirmer, and T. Schulte-Herbrüggen. Comparing, optimizing, and benchmarking quantum-control algo-



- rithms in a unifying programming framework. *Phys. Rev. A*, 84(2):022305, August 2011. doi: 10.1103/PhysRevA.84.022305.
- [137] Reuven Eitan, Michael Mundt, and David J. Tannor. Optimal control with accelerated convergence: Combining the Krotov and quasi-Newton methods. *Phys. Rev. A*, 83(5): 053426, May 2011. doi: 10.1103/PhysRevA.83.053426.
- [138] Anthony Kiely and Steve Campbell. Fast and robust magnon transport in a spin chain. *New J. Phys.*, 23(3):033033, March 2021. ISSN 1367-2630. doi: 10.1088/1367-2630/abea43.
- [139] Priya Batra, M. Harshanth Ram, and T. S. Mahesh. Recommender system expedited quantum control optimization. *Phys. Open*, 14:100127, February 2023. ISSN 2666-0326. doi: 10.1016/j.physo.2022.100127.
- [140] Andriy Burkov. *The Hundred-page Machine Learning Book*. Andriy Burkov, 2019. ISBN 978-1-9995795-0-0.
- [141] Drew Conway and John Myles White. *Machine Learning for Hackers: Case Studies and Algorithms to Get You Started*. "O'Reilly Media, Inc.", February 2012. ISBN 978-1-4493-3053-8.
- [142] Ian Goodfellow, Yoshua Bengio, and Aaron Courville. *Deep Learning*. MIT Press, November 2016. ISBN 978-0-262-03561-3.
- [143] Dastan Maulud and Adnan M. Abdulazeez. A Review on Linear Regression Comprehensive in Machine Learning. *J. Appl. Sci. Technol. Trends*, 1(4):140–147, December 2020. ISSN 2708-0757. doi: 10.38094/jastt1457.
- [144] Jonathon Shlens. A Tutorial on Principal Component Analysis, April 2014.
- [145] Sreerama K. Murthy. Automatic Construction of Decision Trees from Data: A Multi-Disciplinary Survey. *Data Min. Knowl. Discov.*, 2(4):345–389, December 1998. ISSN 1573-756X. doi: 10.1023/A:1009744630224.
- [146] Jeannette Lawrence. *Introduction to Neural Networks*. California Scientific Software, USA, 1993. ISBN 978-1-883157-00-5.

- [147] M. Arif Wani, Mehmed Kantardzic, and Moamar Sayed-Mouchaweh. *Deep Learning Applications*. Springer Nature, February 2020. ISBN 9789811518164.
- [148] Juan Carrasquilla and Roger G. Melko. Machine learning phases of matter. *Nat. Phys*, 13(5):431–434, May 2017. ISSN 1745-2481. doi: 10.1038/nphys4035.
- [149] Giacomo Torlai, Guglielmo Mazzola, Juan Carrasquilla, Matthias Troyer, Roger Melko, and Giuseppe Carleo. Neural-network quantum state tomography. *Nat. Phys*, 14(5):447–450, May 2018. ISSN 1745-2481. doi: 10.1038/s41567-018-0048-5.
- [150] Giuseppe Carleo and Matthias Troyer. Solving the quantum many-body problem with artificial neural networks. *Science*, 355(6325):602–606, February 2017. doi: 10.1126/science.aag2302.
- [151] Zhaokai Li, Xiaomei Liu, Nanyang Xu, and Jiangfeng Du. Experimental Realization of a Quantum Support Vector Machine. *Phys. Rev. Lett.*, 114(14):140504, April 2015. doi: 10.1103/PhysRevLett.114.140504.
- [152] Vasil S. Denchev, Nan Ding, S. V. N. Vishwanathan, and Hartmut Neven. Robust classification with adiabatic quantum optimization. In *Proc. 29th Int. Conference Int. Conf. Mach. Learn.*, ICML’12, pages 1003–1010, Madison, WI, USA, June 2012. Omnipress. ISBN 978-1-4503-1285-1.
- [153] Iordanis Kerenidis and Anupam Prakash. Quantum Recommendation Systems. In Christos H. Papadimitriou, editor, *8th Innov. Theor. Comput. Sci. Conf. ITCS 2017*, volume 67 of *Leibniz International Proceedings in Informatics (LIPIcs)*, pages 49:1–49:21, Dagstuhl, Germany, 2017. Schloss Dagstuhl–Leibniz-Zentrum fuer Informatik. ISBN 978-3-95977-029-3. doi: 10.4230/LIPIcs.ITCS.2017.49.
- [154] Adam Smith, M. S. Kim, Frank Pollmann, and Johannes Knolle. Simulating quantum many-body dynamics on a current digital quantum computer. *npj Quantum Inf*, 5(1):1–13, November 2019. ISSN 2056-6387. doi: 10.1038/s41534-019-0217-0.
- [155] Sepehr Ebadi, Tout T. Wang, Harry Levine, Alexander Keesling, Giulia Semeghini, Ahmed Omran, Dolev Bluvstein, Rhine Samajdar, Hannes Pichler, Wen Wei Ho, Soonwon Choi,

- Subir Sachdev, Markus Greiner, Vladan Vuletić, and Mikhail D. Lukin. Quantum phases of matter on a 256-Atom programmable quantum simulator. *Nature*, 595(7866):227–232, July 2021. ISSN 1476-4687. doi: 10.1038/s41586-021-03582-4.
- [156] C. Monroe, W. C. Campbell, L.-M. Duan, Z.-X. Gong, A. V. Gorshkov, P. W. Hess, R. Islam, K. Kim, N. M. Linke, G. Pagano, P. Richerme, C. Senko, and N. Y. Yao. Programmable quantum simulations of spin systems with trapped ions. *Rev. Mod. Phys.*, 93(2):025001, April 2021. doi: 10.1103/RevModPhys.93.025001.
- [157] Nathan Wiebe, Christopher Granade, Christopher Ferrie, and D. G. Cory. Hamiltonian Learning and Certification Using Quantum Resources. *Phys. Rev. Lett.*, 112(19):190501, May 2014. doi: 10.1103/PhysRevLett.112.190501.
- [158] Nathan Wiebe, Christopher Granade, and D. G. Cory. Quantum bootstrapping via compressed quantum Hamiltonian learning. *New J. Phys.*, 17(2):022005, February 2015. ISSN 1367-2630. doi: 10.1088/1367-2630/17/2/022005.
- [159] Mária Kieferová and Nathan Wiebe. Tomography and generative training with quantum Boltzmann machines. *Phys. Rev. A*, 96(6):062327, December 2017. doi: 10.1103/PhysRevA.96.062327.
- [160] Iris Cong, Soonwon Choi, and Mikhail D. Lukin. Quantum convolutional neural networks. *Nat. Phys.*, 15(12):1273–1278, December 2019. ISSN 1745-2481. doi: 10.1038/s41567-019-0648-8.
- [161] G. Linden, B. Smith, and J. York. Amazon.Com recommendations: Item-to-item collaborative filtering. *IEEE Internet Comput.*, 7(1):76–80, January 2003. ISSN 1941-0131. doi: 10.1109/MIC.2003.1167344.
- [162] Simon Funk. Netflix update: Try this at home, 2006.
- [163] J Ben Schafer, Joseph A Konstan, and John Riedl. E-commerce recommendation applications. *Data Min. Knowl. Discov.*, 5(1-2):115–153, 2001.
- [164] Henry Lieberman. Autonomous interface agents. In *Proc. ACM SIGCHI Conf. Hum. Factors Comput. Syst.*, pages 67–74, 1997.

- [165] Pattie Maes. Agents that reduce work and information overload. In *Readings in Human–Computer Interaction*, pages 811–821. Elsevier, 1995.
- [166] Robin Burke. Knowledge-based recommender systems. *Encycl. Libr. Inf. Syst.*, 69 (Supplement 32):175–186, 2000.
- [167] David Goldberg, David Nichols, Brian M Oki, and Douglas Terry. Using collaborative filtering to weave an information tapestry. *Commun. ACM*, 35(12):61–70, 1992.
- [168] J Ben Schafer, Dan Frankowski, Jon Herlocker, and Shilad Sen. Collaborative filtering recommender systems. In *The Adaptive Web*, pages 291–324. Springer, 2007.
- [169] Yehuda Koren, Robert Bell, and Chris Volinsky. Matrix factorization techniques for recommender systems. *Computer*, 42(8):30–37, 2009.
- [170] Mária Kieferová and Nathan Wiebe. Tomography and generative training with quantum Boltzmann machines. *Phys. Rev. A*, 96(6):062327, 2017.
- [171] Giacomo Torlai and Roger G Melko. Neural decoder for topological codes. *Phys. Rev. Lett.*, 119(3):030501, 2017.
- [172] Moritz August and Xiaotong Ni. Using recurrent neural networks to optimize dynamical decoupling for quantum memory. *Phys. Rev. A*, 95(1):012335, 2017.
- [173] Askery Canabarro, Felipe Fernandes Fanchini, André Luiz Malvezzi, Rodrigo Pereira, and Rafael Chaves. Unveiling phase transitions with machine learning. *Phys. Rev. B*, 100(4):045129, 2019.
- [174] Xun Gao and Lu-Ming Duan. Efficient representation of quantum many-body states with deep neural networks. *Nat. Commun.*, 8(1):1–6, 2017.
- [175] Xiao-Ming Lu, Jian Ma, Zhengjun Xi, and Xiaoguang Wang. Optimal measurements to access classical correlations of two-qubit states. *Phys. Rev. A*, 83(1):012327, 2011.
- [176] Yue-Chi Ma and Man-Hong Yung. Transforming bell’s inequalities into state classifiers with machine learning. *Npj Quantum Inf.*, 4(1):1–10, 2018.

- [177] Jun Gao, Lu-Feng Qiao, Zhi-Qiang Jiao, Yue-Chi Ma, Cheng-Qiu Hu, Ruo-Jing Ren, Ai-Lin Yang, Hao Tang, Man-Hong Yung, and Xian-Min Jin. Experimental machine learning of quantum states. *Phys. Rev. Lett.*, 120(24):240501, 2018.
- [178] Mu Yang, Chang-liang Ren, Yue-chi Ma, Ya Xiao, Xiang-Jun Ye, Lu-Lu Song, Jin-Shi Xu, Man-Hong Yung, Chuan-Feng Li, and Guang-Can Guo. Experimental simultaneous learning of multiple nonclassical correlations. *Phys. Rev. Lett.*, 123(19):190401, 2019.
- [179] Valeria Cimini, Marco Barbieri, Nicolas Treps, Mattia Walschaers, and Valentina Parigi. Neural Networks for Detecting Multimode Wigner Negativity. *Phys. Rev. Lett.*, 125(16):160504, October 2020. doi: 10.1103/PhysRevLett.125.160504.
- [180] Xiao-Yu Li, Qin-Sheng Zhu, Ming-Zheng Zhu, Yi-Ming Huang, Hao Wu, and Shao-Yi Wu. Machine learning study of the relationship between the geometric and entropy discord. *EPL Europhys. Lett.*, 127(2):20009, 2019.
- [181] Wikipedia contributors. Matrix factorization (recommender systems) — Wikipedia, the free encyclopedia, 2020.
- [182] Andrew Ng, Stanford Machine Learning Course.
- [183] V. Al Osipov, H.-J. Sommers, and K. Życzkowski. Random Bures mixed states and the distribution of their purity. *J. Phys. A: Math. Theor.*, 43(5):055302, January 2010. ISSN 1751-8121. doi: 10.1088/1751-8113/43/5/055302.
- [184] Jonas Maziero. Random sampling of quantum states: A survey of methods. *Braz. J. Phys.*, 45(6):575–583, 2015.
- [185] Martin B. Plenio and Shashank S. Virmani. An Introduction to Entanglement Theory. In Erika Andersson and Patrik Öhberg, editors, *Quantum Information and Coherence*, Scottish Graduate Series, pages 173–209. Springer International Publishing, Cham, 2014. ISBN 978-3-319-04063-9. doi: 10.1007/978-3-319-04063-9\_8.
- [186] Hemant Katiyar, Soumya Singha Roy, TS Mahesh, and Apoorva Patel. Evolution of quantum discord and its stability in two-qubit NMR systems. *Phys. Rev. A*, 86(1):012309, 2012.

- [187] Yichen Huang. Computing quantum discord is NP-complete. *New J. Phys.*, 16(3):033027, 2014.
- [188] Xiao-Ming Lu, Jian Ma, Zhengjun Xi, and Xiaoguang Wang. Optimal measurements to access classical correlations of two-qubit states. *Phys. Rev. A*, 83(1):012327, January 2011. doi: 10.1103/PhysRevA.83.012327.
- [189] Michael A Nielsen and Isaac Chuang. Quantum computation and quantum information, 2002.
- [190] B. Georgeot and D. L. Shepelyansky. Emergence of quantum chaos in the quantum computer core and how to manage it. *Phys. Rev. E*, 62(5):6366–6375, November 2000. doi: 10.1103/PhysRevE.62.6366.
- [191] Philipp Hauke, Fernando M Cucchietti, Luca Tagliacozzo, Ivan Deutsch, and Maciej Lewenstein. Can one trust quantum simulators? *Rep. Prog. Phys.*, 75(8):082401, 2012.
- [192] Fritz Haake, M Kuś, and Rainer Scharf. Classical and quantum chaos for a kicked top. *Z. Für Phys. B Condens. Matter*, 65(3):381–395, 1987.
- [193] Vaibhav Madhok, Vibhu Gupta, Denis-Alexandre Trottier, and Shohini Ghose. Signatures of chaos in the dynamics of quantum discord. *Phys. Rev. E*, 91(3):032906, March 2015. doi: 10.1103/PhysRevE.91.032906.
- [194] V. R. Krithika, V. S. Anjusha, Udaysinh T. Bhosale, and T. S. Mahesh. NMR studies of quantum chaos in a two-qubit kicked top. *Phys. Rev. E*, 99(3):032219, March 2019. doi: 10.1103/PhysRevE.99.032219.
- [195] J. F. Poyatos, J. I. Cirac, and P. Zoller. Complete characterization of a quantum process: The two-bit quantum gate. *Phys. Rev. Lett.*, 78(2):390–393, January 1997. doi: 10.1103/PhysRevLett.78.390.
- [196] Phila Rembold, Nimba Oshnik, Matthias M. Müller, Simone Montangero, Tommaso Calarco, and Elke Neu. Introduction to quantum optimal control for quantum sensing with nitrogen-vacancy centers in diamond. *AVS Quantum Sci.*, 2(2):024701, 2020. doi: 10.1116/5.0006785.

- [197] Florian Dolde, Ville Bergholm, Ya Wang, Ingmar Jakobi, Boris Naydenov, Sébastien Pezagna, Jan Meijer, Fedor Jelezko, Philipp Neumann, Thomas Schulte-Herbrüggen, et al. High-fidelity spin entanglement using optimal control. *Nat. Commun.*, 5(1):1–9, 2014.
- [198] I. M. Georgescu, S. Ashhab, and Franco Nori. Quantum simulation. *Rev. Mod. Phys.*, 86(1):153–185, March 2014. doi: 10.1103/RevModPhys.86.153.
- [199] Vasco Cavina, Andrea Mari, Alberto Carlini, and Vittorio Giovannetti. Optimal thermodynamic control in open quantum systems. *Phys. Rev. A*, 98(1):012139, July 2018. doi: 10.1103/PhysRevA.98.012139.
- [200] Pavel Sekatski, Michalis Skotiniotis, Janek Kołodzyński, and Wolfgang Dür. Quantum metrology with full and fast quantum control. *Quantum*, 1:27, September 2017. ISSN 2521-327X. doi: 10.22331/q-2017-09-06-27.
- [201] Constantin Brif, Raj Chakrabarti, and Herschel Rabitz. Control of quantum phenomena: Past, present and future. *New J. Phys.*, 12(7):075008, 2010.
- [202] Domenico d’Alessandro. *Introduction to Quantum Control and Dynamics*. Chapman and hall/CRC, 2021.
- [203] Steffen J Glaser, Ugo Boscain, Tommaso Calarco, Christiane P Koch, Walter Köckenberger, Ronnie Kosloff, Ilya Kuprov, Burkhard Luy, Sophie Schirmer, Thomas Schulte-Herbrüggen, et al. Training Schrödinger’s cat: Quantum optimal control. *Eur. Phys. J. D*, 69(12):1–24, 2015.
- [204] Jing Liu, Haidong Yuan, Xiao-Ming Lu, and Xiaoguang Wang. Quantum Fisher information matrix and multiparameter estimation. *J. Phys. Math. Theor.*, 53(2):023001, 2019.
- [205] Navin Khaneja, Timo Reiss, Cindie Kehlet, Thomas Schulte-Herbrüggen, and Steffen J Glaser. Optimal control of coupled spin dynamics: Design of NMR pulse sequences by gradient ascent algorithms. *J. Magn. Reson.*, 172(2):296–305, 2005.
- [206] Shai Machnes, Elie Assémat, David Tannor, and Frank K. Wilhelm. Tunable, flexible, and efficient optimization of control pulses for practical qubits. *Phys. Rev. Lett.*, 120(15):150401, April 2018. doi: 10.1103/PhysRevLett.120.150401.

- [207] José P. Palao and Ronnie Kosloff. Optimal control theory for unitary transformations. *Phys. Rev. A*, 68(6):062308, December 2003. doi: 10.1103/PhysRevA.68.062308.
- [208] Daniel M Reich, Mamadou Ndong, and Christiane P Koch. Monotonically convergent optimization in quantum control using Krotov’s method. *J. Chem. Phys.*, 136(10):104103, 2012.
- [209] Patrick Doria, Tommaso Calarco, and Simone Montangero. Optimal control technique for many-body quantum dynamics. *Phys. Rev. Lett.*, 106(19):190501, May 2011. doi: 10.1103/PhysRevLett.106.190501.
- [210] D. J. Egger and F. K. Wilhelm. Adaptive hybrid optimal quantum control for imprecisely characterized systems. *Phys. Rev. Lett.*, 112(24):240503, June 2014. doi: 10.1103/PhysRevLett.112.240503.
- [211] Evan M Fortunato, Marco A Pravia, Nicolas Boulant, Grum Teklemariam, Timothy F Havel, and David G Cory. Design of strongly modulating pulses to implement precise effective Hamiltonians for quantum information processing. *J. Chem. Phys.*, 116(17):7599–7606, 2002.
- [212] Ehsan Zahedinejad, Sophie Schirmer, and Barry C. Sanders. Evolutionary algorithms for hard quantum control. *Phys. Rev. A*, 90(3):032310, September 2014. doi: 10.1103/PhysRevA.90.032310.
- [213] Zheng An and DL Zhou. Deep reinforcement learning for quantum gate control. *EPL Europhys. Lett.*, 126(6):60002, 2019.
- [214] Xiao-Ming Zhang, Zezhu Wei, Raza Asad, Xu-Chen Yang, and Xin Wang. When does reinforcement learning stand out in quantum control? A comparative study on state preparation. *Npj Quantum Inf.*, 5(1):1–7, 2019.
- [215] Murphy Yuezhen Niu, Sergio Boixo, Vadim N Smelyanskiy, and Hartmut Neven. Universal quantum control through deep reinforcement learning. *Npj Quantum Inf.*, 5(1):1–8, 2019.



- [216] Marin Bukov, Alexandre G. R. Day, Dries Sels, Phillip Weinberg, Anatoli Polkovnikov, and Pankaj Mehta. Reinforcement learning in different phases of quantum control. *Phys. Rev. X*, 8(3):031086, September 2018. doi: 10.1103/PhysRevX.8.031086.
- [217] Ilia Khait, Juan Carrasquilla, and Dvira Segal. Optimal control of quantum thermal machines using machine learning. *Phys. Rev. Research*, 4(1):L012029, March 2022. doi: 10.1103/PhysRevResearch.4.L012029.
- [218] TS Mahesh, Priya Batra, and M Harshanth Ram. Quantum optimal control: Practical aspects and diverse methods. *J. Indian Inst. Sci.*, pages 1–17, 2022.
- [219] Christiane P Koch, Ugo Boscain, Tommaso Calarco, Gunther Dirr, Stefan Filipp, Steffen J Glaser, Ronnie Kosloff, Simone Montangero, Thomas Schulte-Herbrüggen, Dominique Sugny, et al. Quantum optimal control in quantum technologies. Strategic report on current status, visions and goals for research in Europe. *EPJ Quantum Technol.*, 9(1):19, 2022.
- [220] P. de Fouquieres, S.G. Schirmer, S.J. Glaser, and Ilya Kuprov. Second order gradient ascent pulse engineering. *J. Magn. Reson.*, 212(2):412–417, 2011. ISSN 1090-7807. doi: 10.1016/j.jmr.2011.07.023.
- [221] Priya Batra, V. R. Krithika, and T. S. Mahesh. Push-pull optimization of quantum controls. *Phys. Rev. Research*, 2(1):013314, March 2020. doi: 10.1103/PhysRevResearch.2.013314.
- [222] Gaurav Bhole, V. S. Anjusha, and T. S. Mahesh. Steering quantum dynamics via bang-bang control: Implementing optimal fixed-point quantum search algorithm. *Phys. Rev. A*, 93(4):042339, April 2016. doi: 10.1103/PhysRevA.93.042339.
- [223] Michael Garwood and Lance DelaBarre. The return of the frequency sweep: Designing adiabatic pulses for contemporary NMR. *J. Magn. Reson.*, 153(2):155–177, 2001.
- [224] M. Harshanth Ram, V. R. Krithika, Priya Batra, and T. S. Mahesh. Robust quantum control using hybrid pulse engineering. *Phys. Rev. A*, 105(4):042437, April 2022. doi: 10.1103/PhysRevA.105.042437.
- [225] N. Boulant, K. Edmonds, J. Yang, M. A. Pravia, and D. G. Cory. Experimental demonstration of an entanglement swapping operation and improved control in NMR

- quantum-information processing. *Phys. Rev. A*, 68(3):032305, September 2003. doi: 10.1103/PhysRevA.68.032305.
- [226] Dennis Lucarelli. Quantum optimal control via gradient ascent in function space and the time-bandwidth quantum speed limit. *Phys. Rev. A*, 97(6):062346, June 2018. doi: 10.1103/PhysRevA.97.062346.
- [227] Yao Song, Junning Li, Yong-Ju Hai, Qihao Guo, and Xiu-Hao Deng. Optimizing quantum control pulses with complex constraints and few variables through autodifferentiation. *Phys. Rev. A*, 105(1):012616, January 2022. doi: 10.1103/PhysRevA.105.012616.
- [228] Mao Zhang, Huai-Ming Yu, Haidong Yuan, Xiaoguang Wang, Rafał Demkowicz-Dobrzański, and Jing Liu. QuanEstimation: An open-source toolkit for quantum parameter estimation. *Phys. Rev. Research*, 4(4):043057, October 2022. doi: 10.1103/PhysRevResearch.4.043057.
- [229] D. A. Lidar, I. L. Chuang, and K. B. Whaley. Decoherence-free subspaces for quantum computation. *Phys. Rev. Lett.*, 81(12):2594–2597, September 1998. doi: 10.1103/PhysRevLett.81.2594.
- [230] Lorenza Viola, Emanuel Knill, and Seth Lloyd. Dynamical decoupling of open quantum systems. *Phys. Rev. Lett.*, 82(12):2417–2421, March 1999. doi: 10.1103/PhysRevLett.82.2417.
- [231] Katharine W. Moore Tibbetts, Constantin Brif, Matthew D. Grace, Ashley Donovan, David L. Hocker, Tak-San Ho, Re-Bing Wu, and Herschel Rabitz. Exploring the trade-off between fidelity and time optimal control of quantum unitary transformations. *Phys. Rev. A*, 86(6):062309, December 2012. doi: 10.1103/PhysRevA.86.062309.
- [232] Reuven Eitan, Michael Mundt, and David J. Tannor. Optimal control with accelerated convergence: Combining the Krotov and quasi-Newton methods. *Phys. Rev. A*, 83(5):053426, May 2011. doi: 10.1103/PhysRevA.83.053426.
- [233] S. Machnes, U. Sander, S. J. Glaser, P. de Fouquières, A. Gruslys, S. Schirmer, and T. Schulte-Herbrüggen. Comparing, optimizing, and benchmarking quantum-control algo-

- rithms in a unifying programming framework. *Phys. Rev. A*, 84(2):022305, August 2011. doi: 10.1103/PhysRevA.84.022305.
- [234] T. S. Mahesh and Dieter Suter. Quantum-information processing using strongly dipolar coupled nuclear spins. *Phys. Rev. A*, 74(6):062312, December 2006. doi: 10.1103/PhysRevA.74.062312.
- [235] Gaurav Bhole and Jonathan A Jones. Practical pulse engineering: Gradient ascent without matrix exponentiation. *Front. Phys.*, 13(3):1–6, 2018.
- [236] Linyuan Lü, Matúš Medo, Chi Ho Yeung, Yi-Cheng Zhang, Zi-Ke Zhang, and Tao Zhou. Recommender systems. *Phys. Rep.*, 519(1):1–49, 2012.
- [237] Jesús Bobadilla, Fernando Ortega, Antonio Hernando, and Abraham Gutiérrez. Recommender systems survey. *Knowl.-Based Syst.*, 46:109–132, 2013.
- [238] Jeffrey L. Krause, David H. Reitze, Gary D. Sanders, Alex V. Kuznetsov, and Christopher J. Stanton. Quantum control in quantum wells. *Phys. Rev. B*, 57(15):9024–9034, April 1998. doi: 10.1103/PhysRevB.57.9024.
- [239] Ehsan Zahedinejad, Joydip Ghosh, and Barry C. Sanders. High-fidelity single-shot toffoli gate via quantum control. *Phys. Rev. Lett.*, 114(20):200502, May 2015. doi: 10.1103/PhysRevLett.114.200502.
- [240] Emile HL Aarts and Peter JM van Laarhoven. Simulated annealing: A pedestrian review of the theory and some applications. In *Pattern Recognition Theory and Applications*, pages 179–192. Springer, 1987.
- [241] Dimitris Bertsimas and John Tsitsiklis. Simulated annealing. *Stat. Sci.*, 8(1):10–15, 1993.
- [242] Jonathan L Herlocker, Joseph A Konstan, Loren G Terveen, and John T Riedl. Evaluating collaborative filtering recommender systems. *ACM Trans. Inf. Syst. TOIS*, 22(1):5–53, 2004.
- [243] Xiaoyuan Su and Taghi M Khoshgoftaar. A survey of collaborative filtering techniques. *Adv. Artif. Intell.*, 2009, 2009.

- [244] Ajit P Singh and Geoffrey J Gordon. A unified view of matrix factorization models. In *Jt. Eur. Conf. Mach. Learn. Knowl. Discov. Databases*, pages 358–373. Springer, 2008.
- [245] Priya Batra, Anukriti Singh, and T. S. Mahesh. Efficient Characterization of Quantum Evolutions via a Recommender System. *Quantum*, 5:598, December 2021. ISSN 2521-327X. doi: 10.22331/q-2021-12-06-598.
- [246] Polak, E. and Ribiere, G. Note sur la convergence de méthodes de directions conjuguées. *R.I.R.O.*, 3(16):35–43, 1969. doi: 10.1051/m2an/196903R100351.
- [247] William H Press, Saul A Teukolsky, William T Vetterling, and Brian P Flannery. *Numerical Recipes in FORTRAN 77 Macintosh Diskette Version 2.0: The Art of Scientific Computing*, volume 1. Cambridge university press, 1992.
- [248] Arthur Earl Bryson. *Applied Optimal Control: Optimization, Estimation and Control*. Routledge, 2018.
- [249] Lev Semenovich Pontryagin. *Mathematical Theory of Optimal Processes*. Routledge, 2018.
- [250] J Werschnik and EKH Gross. Quantum optimal control theory. *J. Phys. B At. Mol. Opt. Phys.*, 40(18):R175, 2007.
- [251] Daoyi Dong and Ian R Petersen. Quantum control theory and applications: A survey. *IET Control Theory Appl.*, 4(12):2651–2671, 2010.
- [252] Paul Brumer and Moshe Shapiro. Coherence chemistry: Controlling chemical reactions [with lasers]. *Acc. Chem. Res.*, 22(12):407–413, 1989.
- [253] Linda Petzold and Wenjie Zhu. Model reduction for chemical kinetics: An optimization approach. *AIChE J.*, 45(4):869–886, 1999.
- [254] David J Tannor and Stuart A Rice. Control of selectivity of chemical reaction via control of wave packet evolution. *J. Chem. Phys.*, 83(10):5013–5018, 1985.
- [255] Wusheng Zhu, Jair Botina, and Herschel Rabitz. Rapidly convergent iteration methods for quantum optimal control of population. *J. Chem. Phys.*, 108(5):1953–1963, 1998.

- [256] Niels Chr Nielsen, Cindie Kehlet, Steffen J Glaser, and Navin Khaneja. Optimal control methods in NMR spectroscopy. *eMagRes*, 2007.
- [257] José P Palao and Ronnie Kosloff. Quantum computing by an optimal control algorithm for unitary transformations. *Phys. Rev. Lett.*, 89(18):188301, 2002.
- [258] Patrick Doria, Tommaso Calarco, and Simone Montangero. Optimal control technique for many-body quantum dynamics. *Phys. Rev. Lett.*, 106(19):190501, 2011.
- [259] P De Fouquieres, SG Schirmer, SJ Glaser, and Ilya Kuprov. Second order gradient ascent pulse engineering. *J. Magn. Reson.*, 212(2):412–417, 2011.
- [260] Shai Machnes, Elie Assémat, David Tannor, and Frank K Wilhelm. Tunable, flexible, and efficient optimization of control pulses for practical qubits. *Phys. Rev. Lett.*, 120(15):150401, 2018.
- [261] VF Krotov. Quantum system control optimization. In *Dokl. Math.*, volume 78, pages 949–952. Springer, 2008.
- [262] Ivan I Maximov, Zdeněk Tošner, and Niels Chr Nielsen. Optimal control design of NMR and dynamic nuclear polarization experiments using monotonically convergent algorithms. *J. Chem. Phys.*, 128(18):05B609, 2008.
- [263] Tommaso Caneva, Tommaso Calarco, and Simone Montangero. Chopped random-basis quantum optimization. *Phys. Rev. A*, 84(2):022326, 2011.
- [264] J. J. W. H Sørensen, M. O Aranburu, Till Heinzl, and J. F Sherson. Quantum optimal control in a chopped basis: Applications in control of Bose-Einstein condensates. *Phys. Rev. A*, 98(2):022119, 2018.
- [265] Gaurav Bhole, V. S Anjusha, and T. S Mahesh. Steering quantum dynamics via bang-bang control: Implementing optimal fixed-point quantum search algorithm. *Phys. Rev. A*, 93(4):042339, 2016.
- [266] Deepak Khurana and T. S Mahesh. Bang-bang optimal control of large spin systems: Enhancement of  $^{13}\text{C}$ – $^{13}\text{C}$  singlet-order at natural abundance. *J. Magn. Reson.*, 284:8–14, 2017.

- [267] Chunlin Chen, Daoyi Dong, Han-Xiong Li, Jian Chu, and Tzyh-Jong Tarn. Fidelity-based probabilistic Q-learning for control of quantum systems. *IEEE Trans. Neural Netw. Learn. Syst.*, 25(5):920–933, 2013.
- [268] Xiao-Ming Zhang, Zezhu Wei, Raza Asad, Xu-Chen Yang, and Xin Wang. When reinforcement learning stands out in quantum control? A comparative study on state preparation. *ArXiv Prepr. ArXiv190202157*, 2019.
- [269] Lieven MK Vandersypen and Isaac L Chuang. NMR techniques for quantum control and computation. *Rev. Mod. Phys.*, 76(4):1037, 2005.
- [270] Kilian Singer, Ulrich Poschinger, Michael Murphy, Peter Ivanov, Frank Ziesel, Tommaso Calarco, and Ferdinand Schmidt-Kaler. Colloquium: Trapped ions as quantum bits: Essential numerical tools. *Rev. Mod. Phys.*, 82(3):2609, 2010.
- [271] Yun-Pil Shim and Charles Tahan. Semiconductor-inspired design principles for superconducting quantum computing. *Nat. Commun.*, 7:11059, 2016.
- [272] Mads S Vinding, Ivan I Maximov, Zdeněk Tošner, and Niels Chr Nielsen. Fast numerical design of spatial-selective rf pulses in MRI using Krotov and quasi-Newton based optimal control methods. *J. Chem. Phys.*, 137(5):054203, 2012.
- [273] Raj Chakrabarti and Herschel Rabitz. Quantum control landscapes. *Int. Rev. Phys. Chem.*, 26(4):671–735, 2007.
- [274] Alexander N Pechen and David J Tannor. Are there traps in quantum control landscapes? *Phys. Rev. Lett.*, 106(12):120402, 2011.
- [275] Ramamurti Shankar. *Principles of Quantum Mechanics*. Springer Science & Business Media, 2012.
- [276] Vadim Krotov. *Global Methods in Optimal Control Theory*, volume 195. CRC Press, 1995.
- [277] Jonathan Richard Shewchuk et al. An introduction to the conjugate gradient method without the agonizing pain, 1994.

- [278] Marina Carravetta, Ole G Johannessen, and Malcolm H Levitt. Beyond the T<sub>1</sub> limit: Singlet nuclear spin states in low magnetic fields. *Phys. Rev. Lett.*, 92(15):153003, 2004.
- [279] Marina Carravetta and Malcolm H Levitt. Long-lived nuclear spin states in high-field solution NMR. *J. Am. Chem. Soc.*, 126(20):6228–6229, 2004.
- [280] Giuseppe Pileio. Singlet NMR methodology in two-spin-1/2 systems. *Prog. Nucl. Magn. Reson. Spectrosc.*, 98:1–19, 2017.
- [281] S. Pancharatnam. Generalized theory of interference, and its applications. *Proc. Indian Acad. Sci.*, 44(5):247–262, November 1956. ISSN 0370-0089. doi: 10.1007/BF03046050.
- [282] MV Berry. *Proc. R. Soc. London. A*, 392:45, 1984.
- [283] Y. Aharonov and J. Anandan. Phase change during a cyclic quantum evolution. *Phys. Rev. Lett.*, 58(16):1593–1596, April 1987. doi: 10.1103/PhysRevLett.58.1593.
- [284] Frank Wilczek and A. Zee. Appearance of gauge structure in simple dynamical systems. *Phys. Rev. Lett.*, 52(24):2111–2114, June 1984. doi: 10.1103/PhysRevLett.52.2111.
- [285] J. Anandan. Non-adiabatic non-abelian geometric phase. *Phys. Lett. A*, 133(4):171–175, 1988. ISSN 0375-9601. doi: 10.1016/0375-9601(88)91010-9.
- [286] Erik Sjöqvist, Vahid Azimi Mousolou, and Carlo M. Canali. Conceptual aspects of geometric quantum computation. *Quantum Inf. Process.*, 15(10):3995–4011, October 2016. ISSN 1573-1332. doi: 10.1007/s11128-016-1381-1.
- [287] Jiang Zhang, Thi Ha Kyaw, Stefan Filipp, Leong-Chuan Kwek, Erik Sjöqvist, and Dianmin Tong. Geometric and holonomic quantum computation. *arXiv e-prints*, (arXiv:2110.03602):arXiv:2110.03602, October 2021. doi: 10.48550/arXiv.2110.03602.
- [288] Jonathan A. Jones, Vlatko Vedral, Artur Ekert, and Giuseppe Castagnoli. Geometric quantum computation using nuclear magnetic resonance. *Nature*, 403(6772):869–871, February 2000. ISSN 1476-4687. doi: 10.1038/35002528.

- [289] Wang Xiang-Bin and Matsumoto Keiji. Nonadiabatic Conditional Geometric Phase Shift with NMR. *Phys. Rev. Lett.*, 87(9):097901, August 2001. doi: 10.1103/PhysRevLett.87.097901.
- [290] Shi-Liang Zhu and Z. D. Wang. Implementation of Universal Quantum Gates Based on Nonadiabatic Geometric Phases. *Phys. Rev. Lett.*, 89(9):097902, August 2002. doi: 10.1103/PhysRevLett.89.097902.
- [291] Zhennan Zhu, Tao Chen, Xiaodong Yang, Ji Bian, Zheng-Yuan Xue, and Xinhua Peng. Single-Loop and Composite-Loop Realization of Nonadiabatic Holonomic Quantum Gates in a Decoherence-Free Subspace. *Phys. Rev. Appl.*, 12(2):024024, August 2019. doi: 10.1103/PhysRevApplied.12.024024.
- [292] Tongxing Yan, Bao-Jie Liu, Kai Xu, Chao Song, Song Liu, Zhensheng Zhang, Hui Deng, Zhiguang Yan, Hao Rong, Keqiang Huang, Man-Hong Yung, Yuanzhen Chen, and Dapeng Yu. Experimental Realization of Nonadiabatic Shortcut to Non-Abelian Geometric Gates. *Phys. Rev. Lett.*, 122(8):080501, February 2019. doi: 10.1103/PhysRevLett.122.080501.
- [293] T.-Q. Cai, J.-H. Wang, Z.-L. Wang, X.-Y. Han, Y.-K. Wu, Y.-P. Song, and L.-M. Duan. All-microwave nonadiabatic multiqubit geometric phase gate for superconducting qubits. *Phys. Rev. Res.*, 3(4):043071, October 2021. doi: 10.1103/PhysRevResearch.3.043071.
- [294] Yan Liang, Pu Shen, Li-Na Ji, and Zheng-Yuan Xue. State-Independent Nonadiabatic Geometric Quantum Gates. *Phys. Rev. Appl.*, 19(2):024051, February 2023. doi: 10.1103/PhysRevApplied.19.024051.
- [295] J.-F. Wei, F.-Q. Guo, D.-Y. Wang, Y. Jia, L.-L. Yan, M. Feng, and S.-L. Su. Fast multiqubit Rydberg geometric fan-out gates with optimal control technology. *Phys. Rev. A*, 105(4):042404, April 2022. doi: 10.1103/PhysRevA.105.042404.
- [296] Bao-Jie Liu, Xue-Ke Song, Zheng-Yuan Xue, Xin Wang, and Man-Hong Yung. Plug-and-Play Approach to Nonadiabatic Geometric Quantum Gates. *Phys. Rev. Lett.*, 123(10):100501, September 2019. doi: 10.1103/PhysRevLett.123.100501.



- [297] K. Z. Li, P. Z. Zhao, and D. M. Tong. Approach to realizing nonadiabatic geometric gates with prescribed evolution paths. *Phys. Rev. Res.*, 2(2):023295, June 2020. doi: 10.1103/PhysRevResearch.2.023295.
- [298] K. Z. Li, G. F. Xu, and D. M. Tong. Coherence-protected nonadiabatic geometric quantum computation. *Phys. Rev. Res.*, 3(2):023104, May 2021. doi: 10.1103/PhysRevResearch.3.023104.
- [299] Pankaj Mehta, Marin Bukov, Ching-Hao Wang, Alexandre G. R. Day, Clint Richardson, Charles K. Fisher, and David J. Schwab. A high-bias, low-variance introduction to Machine Learning for physicists. *Phys. Rep.*, 810:1–124, May 2019. ISSN 0370-1573. doi: 10.1016/j.physrep.2019.03.001.
- [300] Mario Krenn, Jonas Landgraf, Thomas Foesel, and Florian Marquardt. Artificial intelligence and machine learning for quantum technologies. *Phys. Rev. A*, 107(1):010101, January 2023. doi: 10.1103/PhysRevA.107.010101. Publisher: American Physical Society.
- [301] Maziar Raissi, Alireza Yazdani, and George Em Karniadakis. Hidden Fluid Mechanics: A Navier-Stokes Informed Deep Learning Framework for Assimilating Flow Visualization Data, August 2018.
- [302] Maziar Raissi, Alireza Yazdani, and George Em Karniadakis. Hidden fluid mechanics: Learning velocity and pressure fields from flow visualizations. *Science*, 367(6481):1026, February 2020. doi: 10.1126/science.aaw4741.
- [303] Maziar Raissi, Paris Perdikaris, and George Em Karniadakis. Physics Informed Deep Learning (Part I): Data-driven Solutions of Nonlinear Partial Differential Equations, November 2017. arXiv:1711.10561.
- [304] M. Raissi, P. Perdikaris, and G. E. Karniadakis. Physics-informed neural networks: A deep learning framework for solving forward and inverse problems involving nonlinear partial differential equations. *J. Comput. Phys.*, 378:686–707, February 2019. ISSN 0021-9991. doi: 10.1016/j.jcp.2018.10.045.

- [305] Kurt Hornik, Maxwell Stinchcombe, and Halbert White. Multilayer feedforward networks are universal approximators. *Neural Networks*, 2(5):359–366, January 1989. ISSN 0893-6080. doi: 10.1016/0893-6080(89)90020-8.
- [306] Igor Babuschkin, Kate Baumli, Alison Bell, Surya Bhupatiraju, Jake Bruce, Peter Buchlovsky, David Budden, Trevor Cai, Aidan Clark, Ivo Danihelka, Antoine Dedieu, Claudio Fantacci, Jonathan Godwin, Chris Jones, Ross Hemsley, Tom Hennigan, Matteo Hessel, Shaobo Hou, Steven Kapturowski, Thomas Keck, Iurii Kemaev, Michael King, Markus Kunesch, Lena Martens, Hamza Merzic, Vladimir Mikulik, Tamara Norman, George Papamakarios, John Quan, Roman Ring, Francisco Ruiz, Alvaro Sanchez, Rosalia Schneider, Eren Sezener, Stephen Spencer, Srivatsan Srinivasan, Wojciech Stokowiec, Luyu Wang, Guangyao Zhou, and Fabio Viola. *The DeepMind JAX Ecosystem*, 2020.
- [307] Tom Hennigan, Trevor Cai, Tamara Norman, and Igor Babuschkin. *Haiku: Sonnet for JAX*, 2020.
- [308] Atılım Günes Baydin, Barak A. Pearlmutter, Alexey Andreyevich Radul, and Jeffrey Mark Siskind. Automatic differentiation in machine learning: A survey. *J. Mach. Learn. Res.*, 18(1):5595–5637, January 2017. ISSN 1532-4435.